GEOLOGICAL SURVEY OF CANADA

OPEN FILE 2418

DETERMINATION OF CREEP PROPERTIES OF FROZEN SOILS BY MEANS OF THE BOREHOLE DILATOMETER

1991

DETERMINATION OF CREEP PROPERTIES OF FROZEN SOILS BY MEANS OF THE BOREHOLE DILATOMETER RELAXATION TEST

FINAL REPORT

prepared for

Science Branch
SUPPLY AND SERVICES CANADA
12C1, Phase II, Place du Portage
11 Laurier Street
Hull (Québec) K1A 0S5
DSS File No. 50SS.23233-7-1125

30 June 1991 C.D.T.PROJECT P1233

C.D.T. Project P1233

DETERMINATION OF CREEP PROPERTIES OF FROZEN SOILS BY MEANS OF THE BOREHOLE DILATOMETER RELAXATION TEST

FINAL REPORT

prepared for:

Science Branch
SUPPLY AND SERVICES CANADA
12C1, Phase III, Place du Portage
11 Laurier Street
Hull (Québec) K1A 0S5
DSS File No. 50SS.23233-7-1125

by:

Branko Ladanyi, P.Eng., Ph.D.
Professor of Civil Engineering
Director, Northern Engineering Centre (CINEP)
ECOLE POLYTECHNIQUE DE MONTREAL

submitted by:

LE CENTRE DE DEVELOPPEMENT TECHNOLOGIQUE
DE L'ECOLE POLYTECHNIQUE DE MONTREAL
Campus de l'Université de Montréal
Case postale 6079, Succursale A
Montréal, Québec, H3C 3A7

30 June 1991

Branko Ladanyi,
Project Director

TABLE OF CONTENTS

DETERMINATION OF CREEP PROPERTIES OF FROZEN SOILS BY MEANS OF THE BOREHOLE DILATOMETER RELAXATION TEST

Branko Ladanyi

Ecole Polytechnique, Montreal

Background: The Geological Survey of Canada, as part of its contribution to the Energy Research and Development Program, is undertaking research into various aspects of environmental constraints on energy transportation in northern Canada posed by permafrost terrain. A component of this research includes interest in the mechanical properties of permafrost soils, and in improved methods for determining those properties in the field and in the laboratory.

Objectives: As stated in the Contract No. 50SS.23233-7-1125 of 01-09- 87, this study has the objective: "To investigate the usefulness of the borehole dilatometer relaxation test (BDRT) as a method for in place determination of creep properties of frozen soils".

Method: The study was required to include:

- An experimental portion, consisting of a series of full-scale borehole relaxation tests in a test chamber, under well-controlled cold room conditions, to be carried out with an artificially prepared frozen soil, such as frozen sand. The purposes of the experimental portion were:

1. To investigate and develop the most efficient testing method for medium- and long-term creep parameter determination;
2. To modify, or propose modifications and improvements to the commercially available dilatometer equipment, with a special reference to the automatic recording system and the computer processing of data;
3. To compare the deduced creep parameters with those obtained from triaxial compression and borehole dilatometer creep tests.

- A theoretical portion, that would contain:
- A critical review of the available test interpretation methods;
- Application of these methods to the experimental data and the comparison of the parameters obtained;
- Discussion of the effects on the parameters of the following: loading rate in step-loaded tests, strain history, relaxation time, and lateral confining pressure.

Deliverables: Semi-annual progress reports and a final report, containing:

- A review of previously published data on the subject;
- A detailed description of equipment, testing procedures and interpretation methods;
- Discussion on all subjects described previously, and
- Recommendations for future research, if appropriate.

1.0 INTRODUCTION

The understanding of permafrost phenomena and the design of structures in permafrost regions requires an adequate knowledge of the mechanical properties of frozen soils and ice under field conditions. A conventional way of getting this information consists in taking samples of frozen soils and testing them, preferably in a field laboratory. Although it is in principle relatively easy to obtain good undisturbed samples from most frozen soils, except from those containing coarse gravel and rock debris, the field tests are often favoured relative to the laboratory tests, because 1. the preservation of frozen samples and their transport to specialized laboratories, which are still rather scarce, are difficult and expensive, and 2. most of ice-rich permafrost soils have a complex large-scale structure of ice lenses and inclusions that can much better be investigated by large-scale field tests than by testing samples in the laboratory.

For these reasons, several attempts have been made in the last twenty years to find appropriate field methods for testing frozen soils, either by adapting known methods used in unfrozen soils, or by developing new ones, able to furnish certain basic frozen soil parameters needed in the design.

Most field methods, developed originally for testing unfrozen soils, can also be used in frozen soils, provided the equipment is sufficiently strong to deform and fail the more resistant frozen soil. However, although the equipment may be of the same type as in unfrozen soils, different test procedures and data processing methods are usually needed to obtain the frozen soil parameters. For example, in field tests in unfrozen soils, mostly only short-term strength and deformation properties, including compressibility, may be required. In frozen soils, in turn, attention is concentrated on long-term creep behaviour and the sensitivity of properties to temperature variation.

Although various geophysical methods are able to furnish valuable information on the state and the extent of permafrost in situ, the present investigation is limited only to the geotechnical field methods, designed to measure in-situ mechanical properties of such soils. At present, there are two such field methods that have been in use or under development for testing frozen soils: the borehole dilatometer (or pressuremeter) test, and the deep static cone penetrometer test.

This investigation deals exclusively with the former type of test, and in particular when such a test is performed in the stress-relaxation mode. Although the test equipment used in the study was essentially a version of the "Menard Pressuremeter", the test has been called the Borehole Dilatometer Relaxation Test, or BDRT. This clarification is necessary to avoid a confusion with the Flat Dilatometer Test used in unfrozen soils mechanics.

2.0 REVIEW OF PREVIOUS WORK

In the last 20 years, several field studies, as well as cold room investigations with the original field equipment, have been carried out by the author and his collaborators. Until recently, these studies consisted essentially in performing borehole short-term and creep tests with the Menard pressuremeter equipment, with the purpose of deducing from them certain basic short-term and creep parameters of frozen soils. The procedure used in these studies remained basically the same as that described by Ladanyi & Johnston (1973, 1978).

The experience gained in this period has shown that the borehole dilatometer (pressuremeter) test offers a good possibility for determining the creep parameters of materials whose creep behaviour can be described by a generalized power law, such as ice, frozen soil, rock salt and potash. However, the same experience has shown also that, because of the total injected fluid volume limitation of the pressuremeter cell, stage-loaded creep tests, with several stages as required for test interpretation, could furnish creep data only for relatively short creep times and for a medium stress range. In addition, it was also realized that the results of such stage-loaded tests with up to 1 hour creep period per stage, can be seriously affected by the stress redistribution problem, i.e., by the fact that at the end of each new loading stage, the stress-redistribution from the previous stage is not yet complete. This subject was dealt with by Murat et al.(1989), who showed that a special data processing and interpretation procedure is necessary for taking into account this effect.

On the other hand, a borehole relaxation test does not suffer from the aforementioned disadvantages. Firstly, in such tests, it is the strain which is controlled, while the stress variation with time is observed, so that the volume capacity of the cell is never inadvertendly exceeded, and, secondly, a borehole relaxation test is basically a stress-redistribution test and its interpretation is straightforward.

The first such tests were performed by Ladanyi et al. (1978) in ice, followed by a series of such tests in a frozen silt at Inuvik, NWT (Ladanyi, 1982), and in a frozen sand in cold room (Eckardt & Ladanyi, 1983). More recently, such borehole relaxation tests were carried out in the CRREL Permafrost Tunnel in Alaska (Ladanyi et al. 1991 a) and at a Norwegian Geotechnical Institute test site at Longyearbyen, Svalbard, (Ladanyi et al. 1991 b). Theoretical treatment of the BDRT-s was presented in Ladanyi et al. (1978) and in Ladanyi (1979) and Ladanyi & Huneault (1987). No literature record on performing such tests in either frozen soils or ice, or in any other earth material, has been found to date.

The results of the borehole dilatometer relaxation tests carried out for the present study in a frozen sand under cold room conditions, will be shown and discussed in the subsequent sections.

3.0 RELAXATION TESTING AND THEORIES

3.1 General

Relaxation testing is an important alternative for investigating the creep properties of a material. Quite generally, stress relaxation is a fundamental process by which an effective measure of the state of stress within a solid can be seen to decrease in time due to the conversion of elastic into inelstic strain. A relaxation test can generally be viewed as the inverse of a creep test: instead of maintaining a constant load and recording strain variation with time, an initial strain level is maintained and the decaying stress is monitored over time. The importance of relaxation testing lies essentially in the potential it offers for verifying experimentally and independently a material flow rule, based originally on creep testing.

Figure 3.1.1 (after Gangi, 1981) shows a general constitutive surface, $f(\epsilon, \dot{\epsilon}, \sigma) = 0$, containing all typical stress, strain and strain-rate paths used

in the tests. In the following, some typical relaxation solutions will be reviewed, mainly for illustration purposes.

3.2 Uniaxial relaxation of a linear Maxwell material (after Findley et al. 1966)

The Maxwell material can be represented by a two-element rheological model, consisting of a linear spring element and a linear- viscous dashpot element, connected in series, as shown in Fig. 3.2 a. The stress-strain relations of spring and dashpot are described respectively by

[3.2.1] $$\sigma = E\epsilon_s$$

[3.2.2] $$\sigma = \eta\dot{\epsilon}_d$$

where E is the Young's modulus and η is the coefficient of viscosity.

Since both elements are connected in series, the total strain is

[3.2.3] $$\epsilon = \epsilon_s + \epsilon_d$$

or the strain rate is

[3.2.4] $$\dot{\epsilon} = \dot{\epsilon}_s + \dot{\epsilon}_d$$

With [3.2.1] and [3.2.2] this becomes

[3.2.5] $$\dot{\epsilon} = \dot{\sigma}/E + \sigma/\eta$$

If the Maxwell model is subjected to a constant strain, ϵ_o, at time t = 0, for which the initial value of stress is σ_o, the stress response can be obtained by integrating [3.2.5] for these initial conditions with the following result:

[3.2.6] $\sigma(t) = \sigma_o \exp(-Et/\eta) = E\,\epsilon_o \exp(-Et/\eta)$

where ϵ_o is the initial strain at t = 0+, which refers to the time just after application of the strain. Eq. [3.2.6] describes the stress relaxation phenomenon for a linear Maxwell model under constant strain. This phenomenon is shown in Fig. 3.2 c. The rate of stress change is given by the derivative of [3.2.6]:

[3.2.7] $\dot{\sigma} = -(\sigma_o\, E/\eta) \exp(-Et/\eta)$

Thus, the initial rate of change in stress at t = 0+ is $\dot{\sigma} = -\sigma_o/t_R$, where the term $t_R = \eta/E$ is called the relaxation time of the linear Maxwell model.

3.3 Uniaxial relaxation of a non-linear Maxwell material

Relaxation solutions for a non-linear Maxwell model, which is considered to be able to properly represent the creep behaviour of ice and frozen soils, depend on the type of the non-linear creep function selected, and on whether the time-hardening or the strain-hardening concept is assumed.

When a power-law form, both in stress and in time, is selected as the non-linear creep function, and the time-hardening concept is adopted, one obtains the solution shown by Eq. A(12) in Appendix A. On the other hand, a solution based on the strain-hardening concept, but based on the same power law, has been obtained by Huneault, and is shown by Eq. 37 in App. B.

In addition, Appendix B presents also relaxation solutions for time-hardening creep laws, where the non-linearity in stress is expressed by a hyperbolic sine function (Eq. 43 to 47 in App.B), and for an exponential function (Eq. 52 in App. B).

For properly interpreting the results of relaxation tests performed in a borehole drilled in a visco-elastic material, it is necessary to develop a

solution for relaxation of a thick-walled visco-elastic cylinder under internal pressure. Such a solution was developed by Ladanyi (1979) in connection with borehole relaxation tests in ice. The solution was later further extended by Ladanyi & Huneault (1987) to include an instantaneous non-linear response of the material. The theory is valid for any material which shows a non-linear Maxwell-type of creep response, defined by a power law of stress, but it has a linear-elastic response during elastic unloading in relaxation. The complete theory of borehole relaxation is shown in Appendix A. The same theory will be used in this report as a basis of an advanced method for interpretation of borehole relaxation tests, called the "Reference Stress Method", which will be described in the following.

3.4 Borehole relaxation data processing by the Reference Stress Method

The purpose of the borehole relaxation method described in this report is to find the basic creep parameters in the creep portion of the total strain equation (Eq. A3 in App. A).

[3.4.1] $$\epsilon_{e,c} = (\dot{\epsilon}_c/B)^B \ (\sigma_e/\sigma_c)^n \ t^B$$

where the subscript "e" denotes the von Mises equivalent stress and strain measure, and t is the time. The creep parameters to be determined from the relaxation tests are the two exponents, B and n, and the creep modulus, σ_c, valid for an arbitrary strain rate, $\dot{\epsilon}_c$.

Clearly, the same creep parameters can also be determined by performing a series of borehole creep tests, as shown by Ladanyi & Johnston (1973). However, based on the experience since that time, it is considered now that the borehole creep tests present some definite disadvantages from both a theoretical and a practical point of view.

The output of any stage-strained relaxation test, performed with a sufficiently rigid dilatometer system (or corrected for finite rigidity), represents a set of stress relaxation curves, each of them starting from a different applied borehole expansion strain $(\Delta a/a)_o$. For hydraulic-type dilatometers, like the Texam pressuremeter used in this study, where the volume expansion of the probe is recorded, the value of $\Delta a/a$ is related to the specific volume expansion $\Delta V/V$ by the relation, valid for large strain

[3.4.2] $$\Delta a/a = 1 - (1 - \Delta V/V)^{1/2}$$

For small strains, $\Delta a/a \approx 0.5 \ \Delta V/V$.

For each experimental relaxation curve, the relaxing stress, p_{it}, at the cavity wall starts from its initial value, p_{io}, given by Eq. A20, which, with $k = 1$ and $\sigma_k/\epsilon_k = E$, becomes

[3.4.3] $p_{io} = (2/3)E(\Delta a/a)_o \approx G_p(\Delta V/V)_o$

where G_p is the pressuremeter shear modulus determined from the loading slope of a rapid loading pressuremeter curve (Fig. 3.4.1)

[3.4.4] $G_p = \Delta p_{io}/\Delta(\Delta V/V)_o$

For data processing, Eq. A36 can be written as

[3.4.5] $(\bar{p}_{io}/\bar{p}_{it})^{n-1} - 1 = Dt^B$, where

[3.4.6] $D = [(n-1)/n^n](\bar{p}_{io}\sqrt{3})^{n-1} A E$

Here, $\bar{p}_{io}$ (Eq. A22) is the net pressure

[3.4.7] $\bar{p}_{io} = p_{io} - p_o$

E is the Young's modulus of the material in unloading, and

[3.4.8] $A = (\dot{\epsilon}_c/B)^B \sigma_c^{-n}$

The unloading modulus, E, should be determined by performing, in a short-term pressuremeter test, several loading-unloading cycles within the region of relaxation strains covered by the relaxation test.

For finding the creep parameters, B, n, and σ_c, from the results of a stage strained relaxation test (Fig.3.4.2), the method suggested in [Ladanyi, 1979] consists in plotting first the term on the left hand side of Eq.[3.4.5] against

time in a log-log plot, as shown in Fig.3.4.3. This yields a family of nearly straight ascending lines, whose slope is equal to B. However, for making this plot, one must know, or guess in advance, the values of the total far-field stress p_o and of the stress exponent n. The former can be determined by putting it approximately equal to the total overburden pressure (in the case of field tests in permafrost). As for the value of n, one can take for the first trial n = 2 or 3, to be improved in the next step.

In this first plot (fig.3.4.3), the values of D in Eq.(3.4.5) can be read from the intersections of the lines with the ordinate at t = 1. When these D-values are plotted against the corresponding initial stresses, $\bar{p}_{io}$ (shown superimposed in Fig.3.4.3), it is found that the new line has the slope

$$[3.4.9] \quad n - 1 = \Delta(\log D)/\Delta(\log \bar{p}_{io})$$

which makes it possible to find an improved value of n.

Finally, when B and n have been determined in such a manner, the value of the creep modulus, σ_c, for an arbitrary value of $\dot{\epsilon}_c$, can be calculated from the coordinates of any point S on the $(D, \bar{p}_{io})$-line, using Eq.3.4.6, giving (Eq. A40 with k=1):

$$[3.4.10] \quad \sigma_c^n = [(n-1)/n^n](\bar{p}_{io,s}\sqrt{3})^{n-1}(E/D_s)(\dot{\epsilon}_c/B)^B$$

This makes it possible to write the creep portion, Eq. A3, of the total strain equation A1. The instantaneous loading portion, Eq. A2 of Eq. A1 is determined from the p_{io} vs. $(\Delta a/a)_o$ relationship found in the same pressuremeter test.

3.5 Borehole relaxation in a thick-walled cylinder

As the cold-room relaxation tests described in this study were made in thick cylinders of frozen sand, some corrections had to be introduced into the foregoing formulas, in order to take into account the finite outside radius of the cylinder.

It can be shown (Ladanyi, 1979) that, for a thick hollow cylinder with an inside radius a and an ouside radius b, the following formulas apply.

The initial stress p_{io} corresponding to an applied elastic strain $(\Delta a/a)_o$, should be calculated from:

[3.5.1] $$p_{io} = (2G/\lambda)(\Delta a/a)_o \approx (G/\lambda)(\Delta V/V)_o$$

where the shear modulus

[3.5.2] $$G = E/2(1+\nu) \approx \lambda \Delta p_{io} / \Delta (\Delta V/V)_o$$

is obtained from the first straight-line portion of the pressuremeter curve, corresponding to a quasi-instantaneous loading. Herein, for a plane strain case

[3.5.3] $$\lambda = [1 + (1- 2\nu)(a/b)^2]/[1 - (a/b)^2]$$

In the relaxation domain, it is found that, for a finite thick-walled cylinder, the dimensionless time unit, t^* (Eq. A24) becomes

[3.5.4] $$t^* = E[(\sqrt{3}/\alpha)(\bar{p}_{io})^{n-1} A\, t^B, \text{ where}$$

[3.5.5] $$\alpha = 1 - (a/b)^2$$

In addition, in that case, the factor 2/k preceding the integral sign in Eq. A21, should be replaced by $2/\alpha k$, which implies that all the four exact solutions shown in App. A, to be valid for a thickwalled cylinder, should also be divided by α.

If the Reference Stress Method is used, it is found that for a finite cylinder, the reference stress σ_R has the value (with k = 1):

[3.5.6] $$\sigma_R = \sqrt{3}\, n^{-n/(n-1)} (p_i - p_o)\, \Omega \alpha^{1-n}$$

where α is given by [3.5.5], and

[3.5.7] $$\Omega = \alpha^n / [1 - (a/b)^{2/n}]^n$$

Eq. A34 then becomes (with k = 1):

[3.5.8] $$\bar{p}_{it}/\bar{p}_{io} = \{1 + [(n-1)/n^n]\, t^*\, \Omega\}^{-1/(n-1)}$$

where t^* is given by Eq.3.5.4.

Eq.3.5.8 gives a good approximation for all values of n between $1 < n < 1.7$, when $b/a > 5$, as well as for any n-value, when $b/a \leq 5$. When $b/a > 5$ and $n > 2$, it is found (Ladanyi, 1979) that a better approximation to the exact solution is obtained if in Eq.3.5.8 the term in square brackets is replaced by $[(n-1)/n^{1.7}]$, but this was not used in this report.

In the same manner, for interpretation of a relaxation test in a thick-walled cylinder, D in Eq.3.4.5 becomes:

[3.5.9] $$D = [(n-1)/n^n]\, \Omega (\bar{p}_{io}\, \sqrt{3}/\alpha)^{n-1}\, A\, E$$

and the value of σ_c is then found from

[3.5.10] $$\sigma_c^n = [(n-1)/n^n]\ \Omega(E/D_s)(\bar{p}_{io,s}\sqrt{3}/\alpha)^{n-1}(\dot{\epsilon}_c/B)^B$$

with the same remark about the n-term in square brackets as before.

4.0 SOME APPROXIMATE METHODS FOR BOREHOLE RELAXATION DATA PROCESSING

4.1 Method based on the isochronous pressuremeter curves

Figure 4.1.1 shows the result of a step-strained borehole relaxation test, carried out in a thick block of ice (Ladanyi et al., 1978). The test consisted of 12 equal-volume-increment steps, each of them followed by a 16 min long stress relaxation interval, with stress readings taken after 0.25, 0.5, 1, 2, 4 8, and 16 min. A very simple, but grossly approximate, method for interpreting such borehole relaxation test results is by considering the curves in Fig.4.1.1 as a set of isochronous pressure vs. borehole expansion curves that can be treated in the same manner as ordinary pressuremeter curves. By using the interpretation method for short-term tests described by Ladanyi & Johnston (1973, 1978), one can then easily deduce from each of these curves: (a) the initial modulus of deformation, E_p (from the slope of the tangent passing through the true origin O', and the whole stress- strain curve up and beyond the peak point.

Figure 4.1.2 shows the resulting isochronous stress-strain curves. The curves have a peak ($q = q_f$) at about $\epsilon_1 = 1.5\%$, while the total failure of the block occurred at about $\epsilon_1 = 2.6\%$. The resulting values of E_p and q_f are plotted in Fig.4.1.3 as functions of time.

A similar method was also used for interpreting the borehole relaxation tests carried out in frozen silt at Inuvik, NWT (Ladanyi, 1982, Figs. 4 & 5).

It is noted that this method does not furnish the creep parameters, but only the effect of time on the deformability and strength of the tested material.

4.2 Method based on the aging theory of creep

Another simple, but not necessarily the best, way for deducing from borehole relaxation test results the time-dependent deformation and strength parameters of the material, is by considering that there is a unique and continuous surface in space, relating stress with strain and time (Fig. 4.2.1). This assumption is known as the basis of the simplest type of the aging theory of creep based on total strains. Although not very accurate, the theory is considered to be able to furnish predictions which do not severely disagree with practice (Rabotnov,1966).

In borehole relaxation testing, the aging theory can be used in two different manners. In the first one, a step-strained borehole relaxation test is used to generate a series of time-dependent pressure-expansion curves, from which the time-dependent moduli and strength parameters can be deduced by means of a conventional pressuremeter curve interpretation method (e.g., Ladanyi, 1979). The second one consists in using the observed borehole relaxation curves for finding the numerical values of some basic creep parameters of the soil. In the aging theory, it is assumed that creep and relaxation are closely related, so that a relaxation curve is nothing else but a creep curve under a continuously decreasing stress, resulting in a constant value of strain. In other words, according to this assumption, any constitutive creep equation can be transformed directly into a relaxation equation by making the creep strain constant and equal to the applied initial strain. In that theory, no consideration is given to the fact that the applied strain may be partially elastic and that the material may have a different behaviour in loading and in unloading. Nevertheless, in spite of these drawbacks, the theory has been found many times in the past to be a useful tool for generalizing the results of stress relaxation tests. For example, in unfrozen soil mechanics literature, this method was used with success by Lacerda and Houston (1973) for describing the results of relaxation tests, carried out on three types of unfrozen soils in triaxial apparatus.

The following method for interpretation of borehole relaxation tests in ice-rich frozen soils, which was first shown by Ladanyi et al. (1978), has been found to be simple and easy to use in practice.

According to the aging creep theory, a creep process can be expressed by a family of isocurves (Rabotnov, 1966), given by

[4.2.1] $$\phi(\epsilon) = \sigma.\Psi(t)$$

where $\phi(\epsilon)$ is a strain function, σ is stress and $\Psi(t)$ is a time function. For including the instantaneous response, it is required that $\Psi(0) = 1$. According to this creep theory, the stress relaxation is then given by

[4.2.2] $$\sigma = \phi(\epsilon)/\Psi(t)$$

If, however, one wants to retain the same form of the time function as that contained in Eq. 3.4.1 the condition $\Psi(0) = 1$ cannot be satisfied, but should be replaced by $\Psi(t') = \text{const}$, where t' is a very short time interval in which the response of the structure is taken to be non-linear elastic. This assumption implies that, at any point and time, the total strain is equal to the sum of a pseudo-elastic strain, corresponding to t', and a creep strain, corresponding to t', where t' is the real time. Adopting a similar strain measure as in Ladanyi and Johnston (19730, one can then write for an expanding cylindrical cavity (Ladanyi et al., 1978):

[4.2.3] $$[\ln(V/V_o)]^{1/n} = M^{1/n}\,[(p_i - p_o)/\sigma_c](t' + t)^{B/n}$$

For small strains, say for $\Delta V/V < 5\%$, and for plane strain, the large strain measure $\ln(V/V_o)$ may be replaced by $\ln(V/V_o) \approx \Delta V/V \approx \gamma \approx 2\,\epsilon_1$, where γ is the engineering shear strain). From Eq. 4.2.3 it follows that the family of relaxation curves is defined by

$$[4.2.4] \qquad (p_i - p_o) = \sigma_c \left[\frac{\ln(V/V_o)}{M(t'+t)^B}\right]^{1/n}, \text{where}$$

$$[4.2.5] \qquad M = 2(\sqrt{3}/2)^{n+1}(2/n)^n(\dot{e}_c/B)^B$$

If the relaxation curves are plotted against the real time t instead of (t' + t), as in Fig. 4.2.2, they come close to Eq. 4.2.4 only when $t \ll t'$. For example, if one takes $t' = 0.1$ min, at the end of any 15 min interval, t' is less than 0.7% of t, and the curves are sufficiently accurate for parameter determination.

It will be seen from Eq . 4.2.4 that, when such relaxation curves are plotted in a log $(p_i - p_o)$ vs log t plot with the strain $\ln (V/V_o)$ as the parameter, their slope at the end of interval gives the ratio

$$[4.2.6] \qquad \frac{B}{n} = -\frac{\Delta \log (p_i - p_o)}{\Delta \log t} = \frac{v}{h} \text{ in Fig. 4.2.2.}$$

On the other hand, if at the same end of interval, where $t = t_i = \text{const.}$, one plots log $[\ln(V/V_o)]$ vs log $(p_i - p_o)$, as shown superimposed in Fig. 4.2.2, the slope of the line gives:

$$[4.2.7] \qquad n = \frac{\Delta \log [\ln (V/V_o)]}{\Delta \log (p_i - p_o)} = \frac{h_1}{v_1} \text{ in Fig. 4.2.2.}$$

When B and n are known, the value of σ_c (for a given $\dot{\epsilon}_c$) can be determined from any point k on the line $\ln (V/V_o)$ vs $(p_i - p_o)$, by using Eq. 4.2.4

$$[4.2.8] \qquad \sigma_c = (p_i - p_o)_k \left[\frac{M\, t_i^B}{\ln(V/V_o)_k} \right]^{1/n}$$

4.3 A graphical method based on the flow theory of creep

As mentioned in the foregoing, a relaxation test consists in rapidly increasing the strain in the sample to a given level, and then keeping it constant while letting the mobilized stress relax with time. In a uniaxial compression test, this condition can be expressed by

$$[4.3.1] \qquad \epsilon_1 = \epsilon_{1,pi} + \epsilon_{1,cr}$$

where ϵ_1 is the total strain, while $\epsilon_{1,pi}$ and $\epsilon_{1,cr}$ are the pseudo-instantaneous (elastic + plastic) and the creep strain, respectively. As, during relaxation, ϵ_1 = const., the time rate form of Eq.4.3.1 is

$$[4.3.2] \qquad \dot{\epsilon}_{1,pi} + \dot{\epsilon}_{1,cr} = 0$$

Since, for a linear-elastic material,

$$[4.3.3] \qquad \dot{\epsilon}_{1,pi} = \dot{\epsilon}_{1,el} = \dot{\sigma}_1/E,$$

it follows that $\dot{\epsilon}_{1,cr}$ can be determined from

$$[4.3.4] \qquad \dot{\epsilon}_{1,cr} = -\dot{\epsilon}_{1,pi} = -\dot{\sigma}_1/E.$$

In other words, this relationship makes it possible to determine from a set of relaxation curves [$\sigma_1 = f(t)$ with ϵ_1 as parameter], a set of corresponding curves [$\sigma_1 = f(\dot{\epsilon}_{1,cr})$ with ϵ_1 as parameter], from which one can determine a set of rate-dependent stress-strain curves [$\sigma_1 = f(\epsilon_1)$ with $\dot{\epsilon}_{1,cr}$ as parameter] by means of a simple graphical construction. The method is based on the flow theory of creep, and is directly related to Fig. 3.1.1.

The interpretation method consists in first plotting the set of experimental stress-relaxation curves, each of them corresponding to a different initial constant strain ϵ_1. By determining the slope, $\dot{\sigma}_1 = d\sigma_1/dt$, at different points of each relaxation curve, one gets from [4.3.4] the relationship $\sigma_1 = f(\dot{\epsilon}_{1,cr}, \epsilon_1)$, which represents a family of curves in a $\dot{\epsilon}_{1,cr}$ vs. σ_1 plot, with ϵ_1 as parameter. By intersecting these latter curves with $\sigma_1 = \text{const.}$ lines, makes it possible to deduce the corresponding $\dot{\epsilon}_{1,cr}$ vs. ϵ_1 curves, with σ_1 as parameter. Any given section of the last curves with a line $\dot{\epsilon}_{1,cr} = \text{const.}$, yields a rate-dependent stress-strain curve of the material.

The method, which is theoretically equivalent to the exact solution shown earlier, does not require a knowledge of the analytical form of relaxation curves, but its use is easier if the experimental relaxation curves are expressed by simple analytical expressions.

If the same method is applied to an expanding cylindrical cavity, the following replacements of terms in the preceding equations should be made:

[4.3.5] $\sigma_1 \longrightarrow p_i$

[4.3.6] $\epsilon_1 \longrightarrow (u/a) = -(1/2)\ \Delta V/V$

[4.3.7] $\dot{\epsilon}_{1,cr} \longrightarrow (\dot{u}/a)_{cr} = -\dot{p}_i/2G_p$,

and the resulting curves are not stress-strain curves, but constant- strain-rate pressuremeter curves, from which the stress-strain curves can readily be determined by the conventional pressuremeter interpretation method (e.g., Ladanyi & Johnston, 1973, 1978).

It is noted, nevertheless, that the above described application of the uniaxial compression method to the case of a borehole relaxation test, is only an approximation, because, at the wall, there is also some stress redistribution occurring during relaxation, which is not taken into account in the application.

4.4 Correction for loading system rigidity

If the loading system of the dilatometer (e.g., Texam Pressuremeter System) is not completely rigid, but extends slightly during a borehole relaxation period, this should be taken into account in the evaluation of test results.

The correction for system rigidity can be made similarly as that described by Bressers (1978) for a uniaxial relaxation test. The basic borehole relaxation equation for a completely rigid system can approximately be written as

$$[4.4.1] \quad (\dot{u}_i/a)_{el} + (\dot{u}_i/a)_{cr} = 0$$

(which is actually strictly valid only for a skeletal point located at a distance of about 2a from the borehole axis, inside the material.) If the system is not completely rigid, Eq.4.4.1 becomes

$$[4.4.2] \quad (\dot{u}_i/a)_{el} + (\dot{u}_i/a)_{cr} = -(\dot{u}_i/a)_{system}$$

For the dilatometer cell of length L and diameter 2a, the volume increase corresponding to u_i is

$$[4.4.3] \quad \Delta V_i = 2\pi a \, L \, u_i$$

By performing a calibration test, which consists in inflating the cell in a thick-walled steel tube, one can find from the slope of the line of injected fluid volume, V_i vs. the applied pressure, p_i, the system rigidity, s

$$[4.4.4] \quad s = \Delta V_i / \Delta p_i, \text{ from which}$$

$$[4.4.5] \quad \Delta \dot{V}_i = \dot{p}_i / s, \text{ and}$$

$$[4.4.6] \quad \dot{u}_i = \Delta \dot{V}_i / 2\pi a \, L = \dot{p}_i / 2\pi a \, L \, s$$

Since, $(\dot{u}_i/a)_{el} = \dot{p}_i/2G$, Eq.4.4.2 can be written as

[4.4.7] $(\dot{u}_i/a)_{cr} = -(\dot{p}_i/2)(1/G + 1/ALs) = -(\dot{p}_i/2G')$

where $A = a^2\pi$ is the cross-sectional area of the borehole. The effective unloading shear modulus is then

[4.4.8] $G' = G/(1 + G/ALS)$

Noting that $G \approx E/3$, one gets the corresponding effective Young's modulus:

[4.4.9] $E' = E(1 + E/3ALs)$

The corrected modulus E' should be used in Eq.3.4.4 instead of the measured unloading modulus E.

When using the Texam Pressuremeter System, one finds that $s = 6.5$ cm^3/MPa, and AL 2025 cm^3, which gives: 3ALS = 39485.5 MPa. For a typical unloading modulus E = 600 MPa, this gives a correction of about 4.5%, i.e., E' = 591 MPa instead of 600 MPa.

5.0 BOREHOLE RELAXATION TESTING

5.1 Introduction

Although only cold-room borehole relaxation testing was included in this contract, it happened that during the contract period two field studies of the same test were also made independently, one of them in a frozen silt in the CRREL Permafrost Tunnel at Fox, near Fairbanks, Alaska, and another in a frozen silty sand at Longyearbyen, Svalbard (Spitsbergen). It is noted that the former was financed by a strategic NSERC grant, and the latter partly by an individual NSERC grant, and partly by the Norwegian Geotechnical Institute, Oslo.

As these two field studies had a great value in investigating the practical side of the testing procedure, a brief report on their performance and results will be presented here, in addition to the results of cold-room tests made specially for this study.

5.2 Description of equipment and testing procedure in the field

The pressuremeter used in this investigation was the TEXAM monocell pressuremeter equiped with an NX-type probe (Fig.5.2.1). It consists of a pressure-volume control unit connected to the probe by a reinforced plastic tubing. The system has a volumetric capacity of 1200 cm^3, whereas admissible pressures range from 0 to 10 MPa.

The probe consists of a steel cylindrical core over which rubber membrane sleeve is fitted. The membrane is protected by an extensible jacket made of overlapping metal strips. The assembly is made leakproof by 0 rings and plastic vulcolan collars which are held in place by two end-nuts. The probe has a deflated diameter of approximately 7 cm and an active length of 45 cm. In a tight borehole the pressuremeter can increase the borehole radius by 40%.

For low-temperature testing, a mixture of ethylene-glycol and water for filling the probe and the hydraulic circuits is normally used.

The standard control unit contains precise pressure gauges, while the volume of injected fluid is controlled by monitoring the displacement of the pressuremeter piston head by means of a displacement gauge.

In field tests, the boreholes are drilled by a compressed air drill rig, able to drill 3 inch (76 mm) diameter holes.

After insertion of the probe into the borehole, a quantity of fluid is injected until initial contact between the probe and the borehole wall is established. If the tests performed are volume (or strain) controlled, no compressed gas supply is necessary. Usually, only two types of tests are made: Fast (or short-term) tests with equal volume injection at each stage every 2 min, and slow (or relaxation) tests in which, after an equal volume injection, the system is closed and the pressure is allowed to relax during a certain period of time.

5.2.1 Short-term tests, preceding relaxation tests

The main purpose of short-term dilatometer (or pressuremeter) tests is the determination of the whole stress-strain curve of the soil (which can be done by using, e.g., the method described by Ladanyi & Johnston, 1973, 1978), necessary to serve as a basis for planning and performing the subsequent stage-strained relaxation tests.

In this study, the short-term strain-controlled tests, consisted in injecting into the probe a fluid volume of 19.3 cm^3 every 2 min and taking readings at 0.5, 1 and 2 min. This corresponds to a shear strain rate of about $5x10^{-3}$ min^{-1}. In a multi-stage borehole relaxation test, the aveargе loading rate is clearly much slower, depending on the length and number of stages.

In order to determine the short-term data, the raw pressuremeter test results have to be processed in a well-defined manner, described also in Ladanyi & Johnston, 1973, 1978.. The procedure consists of the following steps.

1. A short-term pressuremeter test gives as a result a relationship of the form (Fig.5.2.2):

[5.2.1] $V_m = f(p_c)$

where V_m is the injected fluid volume, and p_c is the corrected pressure, calculated from

[5.2.2] $p_c = p_m - q_i(V_m) + q_{pz}$

where p_m is the recorded pressure, q_i is the membrane resistance correction, and q_{pz} is the piezometric pressure, equal to the hydrostatic pressure of the column of water between the probe and the measuring system at the ground surface. The value of q_i is determined by a calibration test in the open air at the surface, and at the test temperature.

2. The pressuremeter curve $V_m = f(p_c)$ is then plotted, and its true origin is determined, by considering (Fig.5.2.2) the value of the original lateral ground pressure to be $p_o = \gamma D$, where D is the depth of the probe below the ground surface, and γ is the total unit weight of the soil. This method clearly implies that the value of K_o(total) = 1, which is usually assumed in the case of tests in frozen soils, because of the creep behaviour of pore ice. Usually, the true value of K_o is of only a minor importance in the tests, performed at a relatively shallow depth because of the high strength of the tested frozen soil.

The origin of the pressuremeter curve at $p_c = p_o$, gives also the value of $V_m = V_{mo}$, i.e., the volume that had to be injected before the membrane started expanding the borehole (Fig.5.2.2). The initial volume of the hole is then

[5.2.3] $V_o = V_{emp} + V_{mo}$

where $V_{emp} = 1270\ cm^3$ for the probe used in the tests. The current volume of the hole is

[5.2.4] $V = V_o + \Delta V$

where ΔV denotes the volume increase of the hole, given by

[5.2.5] $\Delta V = V_m - V_{mo}$

The true pressuremeter curve represents then the relationship $\Delta V = f(p)$ between the volume increase of the hole ΔV, and the corresponding net applied pressure

[5.2.6] $p = p_c - p_o$

As shown in Ladanyi & Johnston (1973, 1978), from any two consecutive points on such a pressuremeter curve it is possible to determine the coordinates of a point on the plane-strain stress-strain curve of the tested frozen soil, by using the expressions:

[5.2.7] $$q_{i,i+1} = (\sigma_1 - \sigma_3)_{i,i+1} = \frac{2(p_i - p_{i+1})}{\ln\{(\Delta V/V)_i / (\Delta V/V)_{i+1}\}}$$

[5.2.8] $$\gamma_{i,i+1} = (\varepsilon_1 - \varepsilon_3)_{i,i+1} = \tfrac{1}{2}\{(\Delta V/V)_i + (\Delta V/V)_{i+1})\}$$

In addition, one can also calculate the values of total principal stresses

[5.2.9] $$\sigma_1 = \tfrac{1}{2}(p_{c,i} + p_{c,i+1})$$

[5.2.10] $\sigma_3 = \sigma_1 - q_{i,i+1}$

from which a portion of the failure envelope and eventually the tensile strength of the soil can be determined. (Note: for getting a regular stress-strain curve, it is recommended to smooth-up the pressuremeter curve by plotting it in a (p, log $\Delta V/V$) plot).

As mentioned, all pressuremeter results are considered to be valid for plane-strain conditions. For transforming them into the axial symmetry case, the von Mises flow law is assumed to apply, giving data equivalent to triaxial test conditions,

[5.2.11] $(\sigma_1 - \sigma_3)_a = (\sqrt{3}/2)\ q_{i,i+1}$

[5.2.12] $\varepsilon_{1,a} = (1/\sqrt{3})\ \gamma_{i,1+1}$

As a result, the pressuremeter shear modulus, calculated from

[5.2.13] $G_p = \Delta p / \Delta(\Delta V/V)$

is related to the axial symmetry modulus of deformation, E_a (with $\nu = 0.5$) by

[5.2.14] $E_a = 1.5\ G_p$

Figure 5.2.2 shows a set of typical isochronous pressuremeter curves obtained in connection with a multi-stage borehole relaxation test, carried out in the CRREL pressuremeter tunnel in Alaska (Ladanyi et al., 1991). The calculation and plotting of these pressuremeter curves, and the corresponding initial stress-strain curve (Fig.5.2.3) is essential as a starting point for the interpretation of borehole relaxation results. The location of subsequent

relaxation stages on the stress-strain curve has certain important consequences for relaxation tests interpretation. Figure 5.2.4 shows a set of relaxation curves obtained in the same test, the interpretation of which will be described later.

5.3 Description of the cold-room test set-up

5.3.1 Test container

The relaxation tests in cold room were carried out in a cylindrical tank, 89 cm diam. and 46 cm deep. To prevent frozen soil from adhering to the container wall, the latter was greased and covered with an air- bubble plastic membrane. Another role of the compressible plastic membrane was to prevent a build-up of lateral pressure both during freezing and during borehole relaxation testing, simulating the effect of an infinite medium.

In order to keep open the hole into which the pressuremeter probe had to be introduced, a steel tube 7.3 cm diam. and 76.5 cm long was installed in the container centre. To prevent its adhering to the soil, and to facilitate its extraction after freezing, the tube was previously greased and covered with a thin plastic sheet.

The experimental set-up is shown schematically in Fig. 5.3.1.

5.3.2 Preparation of frozen sand

The sand used in the tests was an angular quartz sand, originating from the region of Joliette on the North Shore of St.Lawrence River, about 150 km east of Montreal. After a mechanical sieving for eliminating its coarse-grained portion, the sand was poored into the tank, with taking care to keep it in a relatively loose state. Figure 5.3.2 shows a typical grain-size distribution range of the tested sand.

The sand mass in the tank was then saturated from below through a vertical copper tube, perforated at its lower end (Fig.5.3.3). The saturation was achieved by repeatedly inserting the tube into the sand at several places. The saturation proceeded slowly in the upward direction, so that the air could escape without

driving up fine sand particles. The water used for saturation was previously distilled and de-aerated.

After the sand saturation, the container was insulated from outside and from above by a thick glass-wool cover and envelope. The central steel tube sticking out from the sand was also insulated, in order to limit the heat transfer. During freezing, the freezing front remained horizontal and propagated vertically from below upwards, which eliminated the formation of ice lenses and the build-up of internal freezing pressures.

The container was then placed in the cold room at a temperature of -5°C, and was left to freeze. A complete freezing of the sand sample was generally achieved in about a week. After freezing, the tube serving to prepare the central hole for the test was pulled out carefully, taking care not to damage the hole walls.

The relaxation tests were then carried out following the usual procedure, to be described later. At the end of each test, measurements of water content and density of frozen sand were carried out on samples taken from the container. Their average values in the tests were:

Water content: $w = 20$ %

Bulk density: $\rho = 1870$ kg/m^3

Dry density: $\rho_d = 1560$ kg/m^3.

5.4 Relaxation test results in cold room

In this testing program, six separate dilatometer tests, each containing 8 relaxation stages were carried out, with the length of each stage varying between 40 min and over 24 hours. In order to investigate the effect of the method of loading on the results, each of the six multi-stage relaxation tests was performed in a slightly different manner. The following gives a brief description of the performance of each test.

Test R1

In this test, with 8 relaxation stages, it was attempted to control the initial stress, p_{io}, so that in each successive stage, the p_{io} value would be about 1 MPa higher than that in the preceding one. This required clearly the injection of increasing volumes of fluid at each successive stage. Also, the length of stages was varied from about 1 hour at low pressures to 8 hours at higher pressures. In this test, the loading time was as short as possible, i.e., the loading rate as fast as allowed by the Texam Pressuremeter loading system.

Table 5.4.1 presents the general loading sequence of this test, and Fig. 5.4.1 the test results in a linear plot. The test took about 7 days to perform.

Table 5.4.1. Test R1: Loading sequence

Stage	Total injected volume	Time of relaxation
	cm^3	min
R11	320.76	60
R12	353.96	60
R13	379.63	120
R14	411.28	368
R15	454.14	284
R16	495.05	490
R17	542.33	490
R18	585.98	490

Test R2

This test was carried out in a manner similar to the preceding on (R1), i.e., by attempting to control the initial pressure at each stage. Table 5.4.2 shows the loading sequence in this test, and Fig. 5.4.2 the obtained relaxation curves in a linear scale. The test lasted about 7 days.

Table 5.4.2. Test R2: Loading sequence

Stage	Total injected volume	Injection time	Relaxation time
	cm^3	min	min
R21	566.45	2	4320
R22	586.13	1.33	219
R23	603.5	2	270
R24	626.27	2.33	941
R25	662.37	3	272
R26	703.86	5	1176
R27	756.76	5	1456
R28	828.56	6	480

Test R3

In this test, with 8 stages, instead of initial pressure, the injected volume was controlled, by injecting at each stage an additional amount of 60 cm^3. At the same time, the rate of injection was kept as constant as possible, varying only between 2 and 3 min, as allowed by the loading system. Table 5.4.3 shows for this test the loading sequence, and Fig. 5.4.3 the observed relaxation curves. This test lasted about 4 days.

Table 5.4.3. Test R3: Loading sequence

Stage	Total injected volume	Injection time	Relaxation time
	cm^3	min	min
R31	660	2.5	976
R32	720	2	180
R33	780	3	180
R34	840	3	1424
R35	900	2.5	180
R35	960	2.5	960
R37	1020	2	204
R38	1080	2	150

Test R4

In this test, with 7 relaxation stages, the fluid injection was controlled in such a manner that 120 cm^3 was injected at each of the first two stages, and 60 cm^3 per stage for the rest of the stages. The loading injection rate varied from 2 to 4 min. The test lasted about 3 days. Table 5.4.4. shows the loading sequence, and Fig. 5.4.4 the resulting relaxation curves.

Table 5.4.4. Test R4: Loading sequence

Stage	Total injected volume	Injection time	Relaxation time
	cm^3	min	min
R41	400	2	40
R42	520	3	1156
R43	640	4	100
R44	700	2.3	100
R45	760	2.5	1112
R47	880	2.5	120

Test R5

When calculating the results of previous tests, it was found that most relaxation stages were performed in the region of large initial strains, i.e., close to the peak and beyond the peak of the stress- strain curve of the soil. For that reason, it was decided to limit in this test the initial strains, so that all the relaxation stages would remain within the ascending portion of the stress-strain curve. This was achieved by increasing the strain in much smaller steps of only 20 cm^3 per stage. Table 5.4.5 shows the loading sequence in this test, and Fig. 5.4.5 the resulting relaxation curves.

Table 5.4.5. Test R5: Loading sequence.

Stage	Total injected volume	Injection time	Relaxation time
	cm^3	min	min
R51	560	-	1114
R52	580	0.67	80
R53	600	1	90
R54	620	1	90
R55	640	1	80
R56	660	1	90
R57	670	1	1037
R58	700	1	80

Test R6

This test was made in the same manner as Test R5, i.e., by injecting 20 cm^3 of fluid per stage. The loading rate in each stage was 60 sec, and the length of each relaxation period was 30 min. The purpose of this loading sequence was to simulate the method used currently in the field borehole relaxation tests. Figure 5.4.6 shows the resulting relaxation curves.

5.5 Relaxation tests interpretation by the Aging Theory of Creep

In order to determine from the relaxation test results shown in Section 5.4 the corresponding creep parameters in the general creep equation 3.4.1, two previously described methods will be used and their results compared.

The first one is the approximate method based on the "Aging Theory of Creep", described in Section 4.2. As mentioned there, this method consists in plotting in a log-log plot all the relaxation lines in a given stage-loaded test. Then, the value of the ratio B/n is found from the average slope of the curves, and the values of n and σ_c are deduced by replotting on the same graph the relationship: $\log(p_i - p_o)$ vs. $\log(\ln V/V_o)$ at a selected time, t_i.

Since in the majority of both borehole creep and relaxation tests performed until now (e.g., Ladanyi & Eckardt, 1983) it was found that the creep behaviour at small strains differs from that at large strains, (or, in other terms, before

and after the soil has attained its peak strength), it was decided to determine separately the creep parameters for these two regions of strain.

The following Tables 5.5.1 to 5.5.6 present the results of calculation by this method for six performed multi-stage tests, R1 to R6. For each test, and for each relaxation stage, the following values are shown:

For each test:

- The value of V_{mo}, determined as in Fig.5.2.2, by assuming that $p_o = 0$.

For each relaxation stage:

- The value of the initial strain $\Delta V/V \approx \ln(V/V_o)$.
- The values of A and B/n in the equation

[5.5.1] $$p_i - p_o = A\, t^{-B/n}$$

which is a simplified form of Eq.4.2.4.

Finally, Table 5.5.7 shows, for the six series of relaxation tests, the deduced creep parameters, n, B and σ_c. Figures 5.5.1 to 5.5.6 show the corrected relaxation lines, used for the determination of creep parameters.

Table 5.5.1: Test R1. Aging Creep Theory interpretation. (V_{mo} = 310 cm^3)

Stage	$\Delta V/V$ %	A (kPa, min)	B/n
R11	0.68		0.081
R12	2.71		0.122
R13	4.22		0.141
R14	6.02		0.162
R15	8.36		0.151
R16	10.48		0.153
R17	12.82		0.144
R18	14.82		0.142

Table 5.5.2: Test R2. Aging Creep Theory interpretation. (V_{mo} = 515 cm^3)

Stage	ΔV/V %	A (kPa, min)	B/n
R21	2.80	1887.35	0.08234
R22	3.83	2922.22	0.10014
R23	4.74	3745.70	0.11540
R24	5.87	4534.78	0.13745
R25	7.62	5254.24	0.14459
R26	9.56	5868.55	0.15280
R27	11.93	6499.80	0.15839
R28	14.94	7048.55	0.15809

Table 5.5.3: Test R3. Aging Creep Theory interpretation. (V_{mo} = 640 cm^3)

Stage	ΔV/V %	A (kPa, min)	B/n
R31	1.03	2244.40	0.04270
R32	4.02	2936.97	0.10355
R33	6.83	5220.23	0.17199
R34	9.48	6351.65	0.19297
R35	1198	6451.61	0.17736
R36	14.35	6648.14	0.17212
R37	16.59	6856.93	0.16505
R38	18.72	6998.42	0.16107

Table 5.5.4: Test R4. Aging Creep Theory interpretation. (V_{mo} = 490 cm^3).

Stage	ΔV/V %	A (kPa, min)	B/n
R41	(Not used. Contact with soil uncertain)		
R42	1.67	1154.25	0.19790
R43	7.65	6007.58	0.18686
R44	10.66	6523.23	0.17466
R45	13.30	6966.84	0.16817
R46	15.79	7319.31	0.16364
R47	18.14	7526.79	0.15280

Table 5.5.5: Test R5. Aging Creep Theory interpretation. (V_{mo} = 540 cm^3)

Stage	ΔV/V %	A (kPa, min)	B/n
R51	1.09	547.02	0.07746
R52	2.16	1240.47	0.04890
R53	3.21	1851.17	0.06155
R54	4.23	2357.05	0.07418
R55	5.23	2791.30	0.08456
R56	6.22	3113.26	0.08622
R57	7.78	3395.47	0.08880
R58	8.12	3429.26	0.07670

Table 5.5.6: Test R6. Aging Creep Theory interpretation. (V_{mo} = 430 cm^3)

Stage	ΔV/V %	A (kPa, min)	B/n
R61	0.58	888.67	0.09032
R62	1.73	1600.06	0.07173
R63	2.86	2800.85	0.10695
R64	3.95	3810.13	0.13076
R65	5.03	4437.56	0.14158
R66	6.08	4798.35	0.14435

Table 5.5.7: Tests R1 to R6. Average creep parameters deduced from the tests by means of the Aging Creep Theory interpretation method.

Test	ΔV/V %	n	B	σ_c (MPa, for $\dot{\varepsilon}_c = 10^{-5}$ min^{-1})
R1	<6.00	1.50	0.21	10.36
	>6.00	2.19	0.32	3.29
R2	<5.00	0.86	0.086	186
	>5.00	2.47	0.37	3.06
R3	<6.83	1.30	0.18	64.12
	>6.83	4.24	0.73	1.00
R4	<7.85	0.94	0.18	44.85
	>7.85	2.95	0.50	1.87
R5	<5.23	1.22	0.08	36.75
	>5.23	1.96	0.16	7.02
R6	<3.95	1.13	0.113	61.11
	>3.95	2.18	0.305	1.18

5.6 Relaxation tests interpretation by the Reference Stress Method

As mentioned in Section 3.4, the Reference Stress Method, which is derived from the exact solution of the thick-walled cylinder relaxation problem, is theoretically much more advanced than the preceding Aging Creep Theory. The main difference between the two is that the Aging Creep Theory lumps together all strains in a total strain formulation, while the Reference Stress Method separates properly the instantaneous from delayed (or creep) strains. Because of these two different concepts, the two interpretation methods will necessarily furnish different values for the creep parameters. However, in application to practical problems, any of them may be able to lead to satisfactory predictions, provided they are applied in a logical manner, taking into account their basic assumptions.

The use of the Aging Creep Theory for relaxation test interpretation, as described in Section 3.4, requires the knowledge of both the loading and the unloading deformation modulus. The loading shear modulus, G_p, can be obtained from the initial linear portion of the pressuremeter curve by means of Eq. 5.3.3, but for finding the unloading Young's modulus, E, a separate short-term pressuremeter test with one or more loading-unloading cycles should be performed in the same material.

The experience from previous pressuremeter tests and from laboratory triaxial test results with the same frozen Joliette Sand, shows that the unloading modulus is approximately 2.5 times higher that the loading modulus, leading to the conclusion that E should be equal to about 600 MPa.

The value of the initial stress, p_{io}, necessary in the theory, can be obtained in two different ways, i.e., either from Eq.5.3.3., or by extrapolating each relaxation line back to a very short time, say, 0.01 min. Generally, the second method is found to be more reliable, facilitating considerably the test interpretation. As explained in Section 3.4, the test interpretation by this

method cannot proceed directly, but requires a trial and error approach. The procedure proceeds as follows:

(a) A probable initial value of n is assumed, e.g., n = 2 or 3.
(b) For each relaxation stage, the relationship (Eq.3.4.5):

[5.6.1] $(\bar{p}_{io}/\bar{p}_{it})^{n-1} - 1 = f(t)$

is calculated and represented in a log-log plot against time, as shown in Fig.5.6.1 for Test R2. From the slope of the resulting ascending lines, an average value of B is determined.
(c) At a fixed time t, the value of $D = f[(\bar{p}_{io}/\bar{p}_{it})^{n-1} - 1]$ is calculated or read directly from the plot, (as in Fig.3.4.3), and plotted on the same graph as a function of $\bar{p}_{io}$. The slope of this new line gives a calculated value of (n-1).
(d) The previous calculation steps are repeated with this new value of n, until a satisfactory agrement between the assumed and the calculated n-value is reached.
(e) Using the n and B values so determined, and after selecting a convenient value of $\dot{\epsilon}_c$ (e.g., 10^{-5} min^{-1} in this study), the value of the creep modulus σ_c can be calculated from the coordinates of any point S on the line $D = f(\bar{p}_{io})$. This is achieved by means of Eq.3.4.10, which is repeated below:

[3.4.10] $\sigma_c^n = [(n-1)/n^n](\bar{p}_{io,s}\sqrt{3})^{n-1}(E/D_s)(\dot{\epsilon}_c/B)^B$

(f) As all the tests were made in a thick-walled cylinder and not in an infinite medium, the corrected value of σ_c can be obtained from Eq.3.5.10, or

[5.6.2] $\sigma_{c,corr}^n = \sigma_c^n (\Omega/\alpha^{n-1})$

where α and Ω are defined by Eqs. 3.5.5 and 3.5.7, respectively.

The results of such a semi-graphical calculation are shown in Table 5.6.1 and in Figs. 5.6.1 to 5.6.9.

Table 5.6.1: Tests R2 to R6. Creep parameters determination by means of the Reference Stress Method

Tests	$\Delta V/V$ %	n	B	σ_c MPa (for $\dot{\varepsilon}_c = 10^{-5}$ min^{-1})
R2	<4.74	1.44	0.168	58.21
	>5.87	2.83	0.379	7.00
R3	<6.83	1.24	0.220	18.53
	>9.48	4.36	0.620	2.79
R4	>7.85	3.03	0.420	5.90
R5	<5.23	1.59	0.152	35.90
	>5.23	1.23	0.155	92.32
R6	<3.95	1.60	0.193	37.32
	>3.95	1.39	0.191	55.97

5.7 Comparison of results obtained by two different interpretation methods

As mentioned in the foregoing, the two selected interpretation methods differ in their basic principles and assumptions, so that they are not expected to furnish closely similar values of creep parameters. However, as it will be seen in Table 5.7.1, they nevertheless show a similar trend as for the difference in the parameters between small and large strain domains.

Table 5.7.1: Tests R2 to R6. Comparison of creep parameters obtained respectivement by:

1: Aging Creep Theory, and 2: Reference Stress Method

Tests	Strains	n		B		σ_c, MPa (for $\dot{\epsilon}_c = 10^{-5}$ min^{-1})	
		1	2	1	2	1	2
R2	Small	0.86	1.44	0.086	0.168	186	58.21
	Large	2.47	2.83	0.37	0.379	3.06	7.00
R3	Small	1.30	1.24	0.18	0.22	64.12	18.53
	Large	4.24	4.36	0.73	0.62	1.0	2.79
R4	Large	2.95	3.03	0.50	0.42	1.87	5.90
R5	Small	1.22	1.59	0.082	0.152	36.75	35.90
	Large	1.96	1.23	0.16	0.155	7.02	92.32
R6	Small	1.13	1.60	0.113	0.193	61.11	37.32
	Large	2.18	1.39	0.305	0.191	1.18	55.97

If only the average values of the parameters are compared according to the two methods, one gets from Table 5.7.1:

Table 5.7.2: Average values of parameters obtained in this study at T = -5 °C

A. Aging Creep Theory: (Tests R2 to R6)

	n	B	σ_c, MPa
Small strains:	1.09	0.128	78.57
Large strains:	2.76	0.413	2.83

B. Reference Stress Method: (Tests R2 to R6)

	n	B	σ_c, MPa
Small strains:	1.47	0.173	37.49
Large strains:	2.57	0.353	32.80

6.0 DISCUSSION AND COMPARISON WITH PREVIOUS RESULTS

In the list of objectives at the beginning of this report, it is stated that this study should "compare the deduced creep parameters with those obtained from triaxial compression and borehole dilatometer creep tests".

Although the experimental program of this investigation has been limited only to the performance of borehole relaxation tests under cold- room conditions, some other independent previous studies have made it possible to compare the results obtained with the same (or similar) frozen sand, when using different testing methods.

For example, it is noted that the same frozen sand (Joliette Sand) was used previously in a series of triaxial compression tests by Lauzon (1985), while a complete series of pressuremeter creep tests was carried out with the same frozen sand under cold-room conditions by Eckardt during 1980/80 (Reported in: Eckardt, 1981, 1982, Eckardt & Ladanyi, 1983, Ladanyi & Eckardt, 1983).

In other words, there exists a very good basis for the comparison for the same testing material and conditions.

On the other hand, there are also some very good data in the literature on the creep behaviour of various other frozen sands (e.g., Sayles, 1968, Meissner & Eckardt, 1976), which can be used to compare certain creep parameters.

Finally, the field study in Longyearbyen, described briefly in Appendix D, which was made in a dense frozen silty sand, can also be used as a basis for comparison under field conditions.

It is clear, however, that any comparison has a sense only if it takes into account the sand density, the degree of ice saturation, and the testing temperature. Although one cannot do much about the first two effects, the

temperature effect can be taken into account approximately in the comparison, by making the usual assumption that the creep exponents n and B are not sensibly affected by temperature in the considered temperature range, while the value of the creep modulus can be reduced to the same temperature range by using the empirical formula (e.g., Ladanyi, 1972):

$$[6.1] \qquad \sigma_{c\theta} = \sigma_{co}(1 + \theta/\theta_o)^w$$

where $\sigma_{c\theta}$ and σ_{co} are the values of the creep modulus at temperatures of $\theta = -T°C$ and extrapolated to $\theta = 0°C$, respectively, and w is an empirical exponent, usually equal to 1 for frozen sands.

As a start for the comparison, the average values of creep parameters obtained in this study, at a temperature of -5°C, and shown in Table 5.7.2.A, are repeated below.

Table 6.1. Creep parameters obtained in this study (Joliette Sand, -5°C)

	n	B	σ_c, MPa
Small strains:	1.09	0.128	78.57
Large strains:	2.76	0.413	2.83

(Note: For creep modulus: $\dot{\epsilon}_c = 10^{-5}$ min^{-1}, everywhere)

Tests by Eckardt (1981)

During 1980/81, Eckardt (in a 1-year post-doc study) carried out in the same sand in cold room a series of borehole creep and relaxaton tests using the Menard pressuremeter. The sand was prepared essentially in the same manner as in this study, but the tests were made at a temperature of about -2.0 to -2.5 °C, and there was also a provision for applying in the test tank a lateral pressure of up to 300 kPa. The results of that study were presented in an internal report (Eckardt, 1981), two papers (Eckardt & Ladanyi, 1983, Ladanyi & Eckardt, 1983),

and a discussion (Eckardt, 1982). The investigation included short-term tests and stage-loaded creep and relaxation tests.

Three important conclusions were drawn from that study: First, that creep behaviour of frozen sand differs at small and at large strains (see Ladanyi & Eckardt, 1983, Figs. 3 & 4), Second that stress-redistribution affects the stage-loaded creep test results (see Ladanyi & Eckardt, 1983), and Third, that the effect on the creep rate of the lateral confining pressure of up to 300 kPa may be considered as negligible (Eckardt, 1982, Fig.4). The average value of creep parameters, deduced from stage-loaded borehole creep tests with 30 min per stage, are shown below.

Table 6.2. Creep parameters obtained by Eckardt(1981) (Joliette Sand, temperature correction made from T = -2.1°C to -5°C)

	n	B	σ_c, MPa
Small strain	1.0	0.52	22.51
Large strain	3.2	0.90	1.70

Compared with the values in Table 6.1, the latter values show clearly a very similar trend in all the three creep parameters. As for their absolute values, it is well known in the metal creep literature, that, because of very different test conditions in creep and relaxation tests, they usually do not give exactly the same values of creep parameters. (See also a comparison in Ladanyi, 1982).

Tests at Longyearbyen, 1990

In the Summer of 1990, the author carried out at Longyearbyen, Svalbard, a series of borehole dilatometer relaxation tests with the same Texam Pressuremeter System as in this study. The tests were made in boreholes drilled into a dense frozen silty sand at depths varying from 3 to 5 m, and at temperatures between -2.3°C and -3.2°C (For more details, see Appendix D).

Average values of creep parameters obtained in such a manner for that frozen material are listed below.

Table 6.3. Creep parameters for Svalbard Silty Sand (Temperature correction made from -2.725°C to -5°C)

	n	B	σ_c, MPa
Small strains	1.15	0.140	32.1
Large strains	2.15	0.305	3.7

Again, although the sand was different, one can see that the trend and the values of creep parameters are very similar to those found in the present study.

Finally, it may be of some interest to compare the creep parameters obtained by borehole creep and relaxation tests with those deduced from triaxial testing of frozen sand specimens by various authors. (In this case, only the values of creep exponents can be compared). Table 6.4 shows some typical results of such studies.

Table 6.4. Creep parameters deduced from triaxial compression tests, carried out on some frozen sands

	n	B
Ottawa Sand (Sayles, 1968)	1.28	0.45
Manchester Fine Sand (Sayles, 1968)	2.63	0.63
Karlsruhe Silty Sand (Meissner & Eckardt, 1976)	2.00	0.40

Again a similar trend and similar values of creep exponents are found for different frozen sands, when compared with the results of the present study.

7.0 CONCLUSIONS

The objective of this project was "To investigate the usefulness of the borehole dilatometer relaxation test (BDRT) as a method for in place determination of creep properties of frozen soils". In general, it is considered that this objective has been attained, because, as shown in this report:

(1) A series of borehole relaxation tests under cold-room conditions, together with two independent field studies with the same method and equipment, has made it possible to examine the performance of the available testing equipment (Texam Pressuremeter System), and to develop an optimum testing method, requiring a minimum loss of time for getting all necessary information.

(2) A comparison of several theoretical approaches and interpretation methods, some of which specially developed for this project, has made it possible to select two most promising ones, and to compare their results.

(3) The values of creep parameters found by the borehole dilatometer relaxation tests, compare very well with those found by some other testing methods, including triaxial compression and borehole creep testing.

(4) No particular modification of the Texam Pressuremeter System has been found necessary, but an electronic system for monitoring of pressures and volume variation of the probe during the test has been developed, realized and tested in the field and in the laboratory.

(5) When the BDRT-s are performed as described in this study, which is considered to be an optimal practical method, the results are found not to be seriously affected by loading rate, strain history and relaxation time. However, the effect of the lateral confining pressure, especially in tests in frozen sands, may require some additional theoretical and experimental investigations.

Finally, this report has presented a review of the most important findings made during this investigation. However, additional information, such as details on the monitoring system and the related computer programs are available on request.

ACKNOWLEDGEMENTS

During the period of this contract, 1988-1991, several collaborators have made important contributions to the realization of this project. In particular, Mr.Paul Huneault, Research Associate, has developed several alternative theoretical solutions for the relaxation problem (App. A), and has also devised and realized a field and laboratory system for long-term monitoring of creep and stress- relaxation tests. The cold-room borehole relaxation tests were organized and carried out by the graduate students: Mr. Bachir Touileb and Mr. Jamel Sgaoula, with the help of the laboratory technician, Mr. Andre Ducharme. The final calculation and processing of test results was performed by the graduate student, Mr. Moha Melouki. The author of this report wishes to express to all of them his sincere thanks and appreciation for their valuable help.

REFERENCES

1. Bressers, J. 1978. Testing in creep research. In"Creep of Engineering Materials and Structures" (G. Bernasconi & G. Piatti, eds.), Applied Science Publishers, London.

2. Eckardt, H. 1981. Laboratory and creep and relaxation tests in thick- walled cylinders of frozen sand. Int.Report, Northern Engrg Centre, Ecole Polytechnique, 125 p.

Eckardt, H. 1982. Discussion, 4th Canadian Permafrost Conf, Calgary, 1981, pp. 416-418.

4. Eckardt, H. & Ladanyi, B. 1983. Dilatometer-Laborversuche mit gefrorenem Sand. Die Bautechnik, v. 60, pp. 56-65.

5. Findley, W.N. 1951. derivation of a stress-strain equation from creep data on plastics. Proc. First Congress on Appl. Mechanics, ASME, pp. 595-602.

6. Findley, W.N., Lai, J.S. & Onaran, K. 1976. Creep and Relaxation of Nonlinear Viscoelastic Materials. North-Holland Publ.Co.,Amsterdam, 367p.

7. Gangi, A.F. 1981. A constitutive equation for one-dimensional transient and steady-state flow of rocks. In "Mechanical Behavior of Crustal Rocks", (N.L.Carter et al., eds), AGU Monograph, 24, pp. 275-285.

8. Lacerda, W.A. & Houston, W.N. 1973. Stress relaxation in soils. Proc 8th ICSMFE, Moscow, V. 1, pp. 221-227.

9. Ladanyi, B. 1972. An engineering theory of creep of frozen soils. Canad.Geotech.J., V.9, pp. 63-80.

10. Ladanyi, B. 1979. Borehole relaxation test as a means for determining the creep properties of ice covers. Proc. 5th POAC Conf., Trondheim, V.1, pp.757-770.

11. Ladanyi, B. 1982. Borehole creep and relaxation tests in ice-rich permafrost. Proc. 4th Canad. Permafrost Conf., Calgary, R.J.E.Brown Mem.Vol, NRCC-ACGR, Ottawa, pp. 406-415.

12. Ladanyi, B. & Johnston, G.H. 1973. Evaluation of in situ creep properties of frozen soils with the pressuremeter. Proc. 2nd Int. Permafrost Conf., Yakutsk, North Amer.Contrib.Vol., NAS, Washington, pp. 310-318.

13. Ladanyi, B. & Johnston, G.H. 1978. Field investigations in frozen ground. Chap.9 in "Geotech. Engrg. for Cold Regions (Andersland & Anderson, eds.), McGraw-Hill, pp. 459-504.

14. Ladanyi, B., Barthelemy, E. & Saint-pierre, R. 1978. In situ determination of creep properties of ice covers by means of borehole creep and relaxation tests. Proc. Workshop on Bearing Cap. of Ice Covers, Winnipeg, NRCC-ACGR Tech, Memo. no.123, 1979, pp. 44-64.

15. Ladanyi, B. & Eckardt. H. 1983. Dilatometer testing in thick cylinders of frozen sand. Proc. 4th Int. Permafrost Conf., Fairbanks, Nat.Acad.Press, Washington, V.1, pp. 677-682.

16. Ladanyi, B. & Huneault, P. 1987. Use of the borehole stress- relaxation test for determining the creep properties of ice. Proc. 6th Annual OMAE Symp., Houston, Vol.IV, pp. 253-259.

17. Ladanyi,B., Lunne, T. & Vergobbi, P. 1990. Predicting creep settlements for foundations in permafrost: Results of in situ tests at Longyearbyen, Svalbard, Report No. 527040-9, Norwegian Geotech.Inst., Oslo.

18. Ladanyi, B. Touileb, B. & Huneault, P. 1991. Pressuremeter stress relaxation testing in a permafrost tunnel. Proc. Geotech. Engrg. Congress, Boulder, CO, June 9-12, 1991.

Lauzon, M. 1985. Comportement mecanique de trois sols geles. M.Sc.A. Thesis, Civil Engrg. Dept., Ecole Polytechnique, Montreal.

20. Meissner, H. & Eckardt, H.1976. Deflection of frozen soil beams under constant temperature gradient. (In German). Proc. 6th European Conf. on SMFE, Vienna, pp. 251-256.

21. Murat, J.R., Ladanyi, B. & Huneault, P. 1989. In-situ determination of creep properties of sea ice with the pressuremeter. Canad.Geotech.J., V.26, pp. 575-594.

22. Rabotnov. Y.N. 1966. Creep Problems in Structural Members. (Transl.from Russian). North-Holland Publ.Co., 1969.

23. Sayles, F.H. 1968. Creep of Frozen sands. Tech. Rep.190, A.S.Army CRREL, Hanover, NH, 31 p.

FIGURES

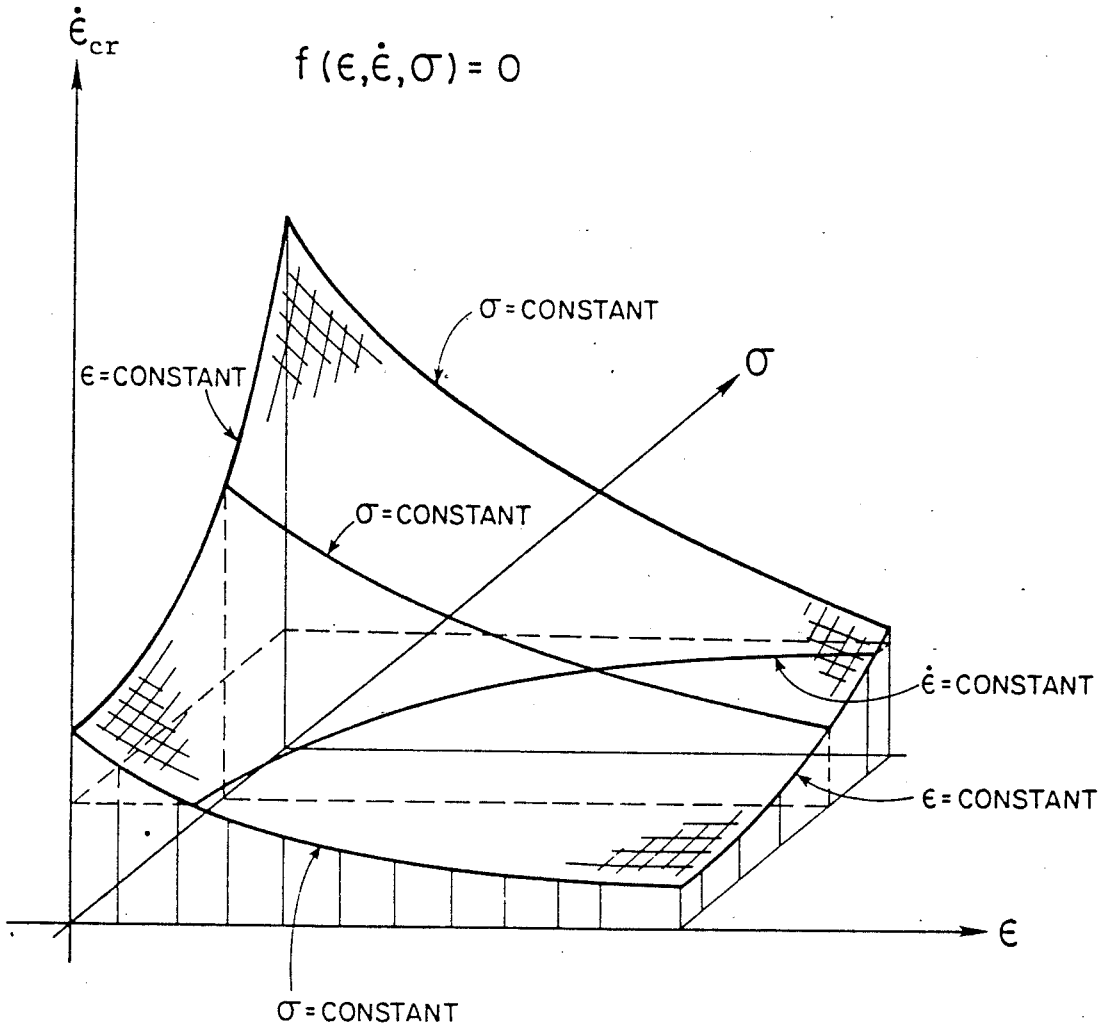

Fig. 3.1.1 Reduced-dimensional constitutive surface, showing the different paths of constant strain-rate, creep, and relaxation tests at constant temperature (after Gangi, 1981, Figure 1).

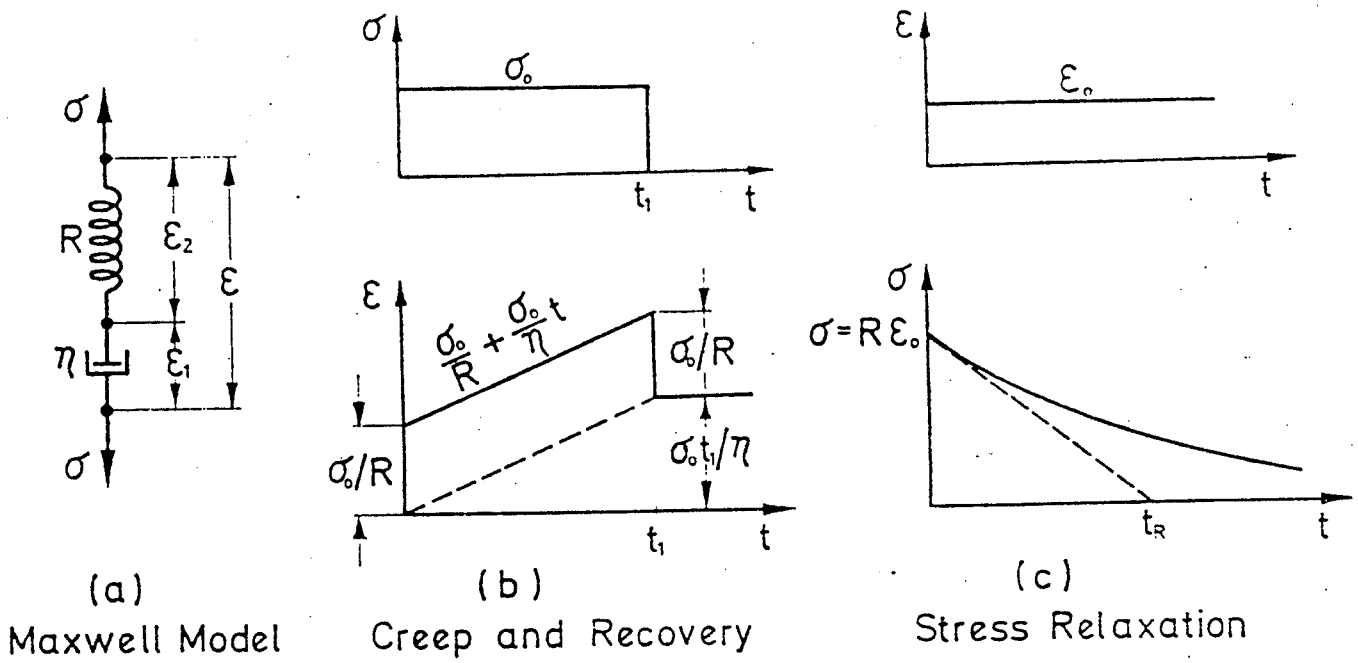

Fig.3.2.1. Behaviour of a linear Marwell Model.
(After Findlay et al., 1976)

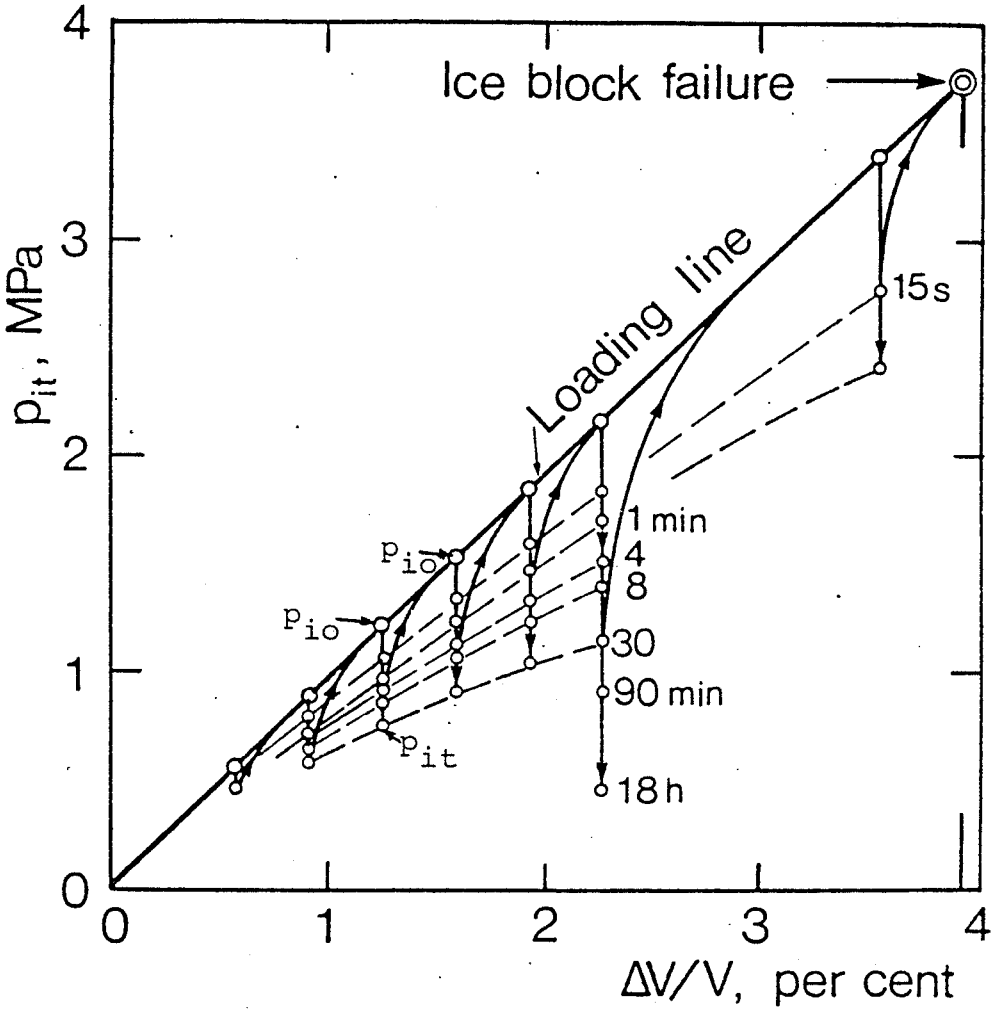

Fig.3.4.1 Pressure versus volume dilation curves from a stage-strained borehole relaxation test in ice at -5°C. (after Ladanyi, 1979)

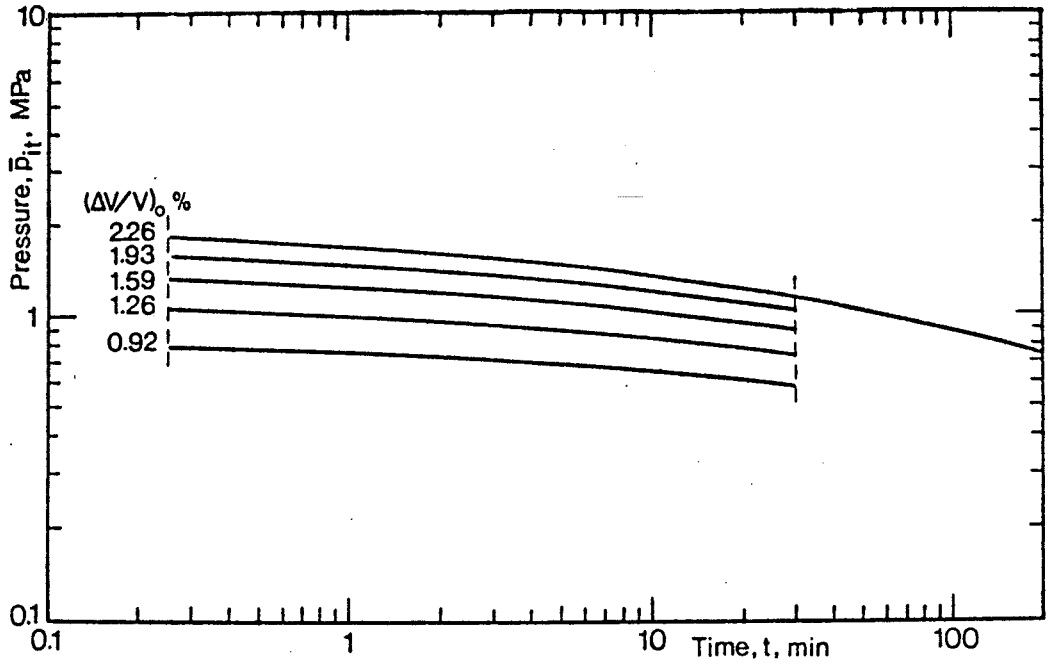

Fig. 3.4.2 Relaxation curves obtained in a stage-strained borehole relaxation test in ice at -5°C.
(after Ladanyi, 1979)

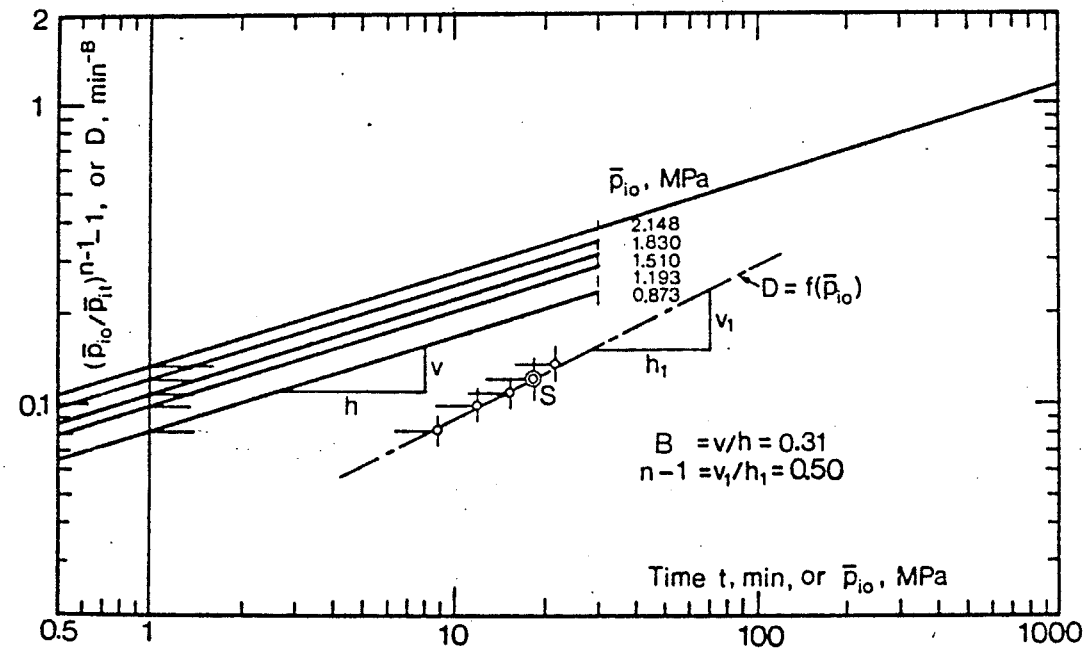

Fig. 3.4.3 Determination of creep parameters from a stage-strained borehole relaxation test.
(after Ladanyi, 1979)

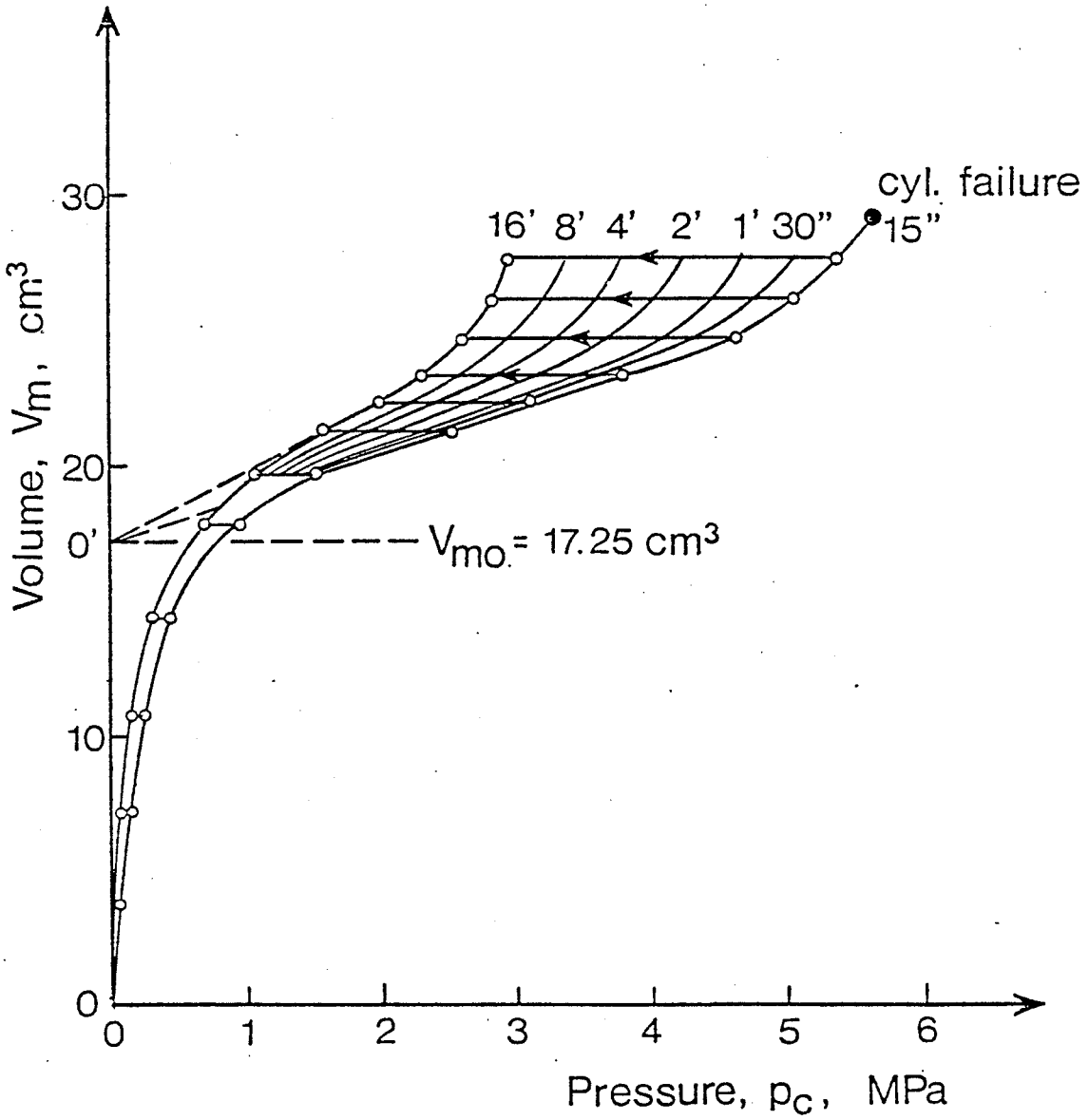

Fig.4.1.1. Results of a borehole dilatometer relaxation test in fresh-water ice: Pressuremeter curves at constant relaxation times. T = -5^{0}C. (From: Ladanyi et al., 1978)

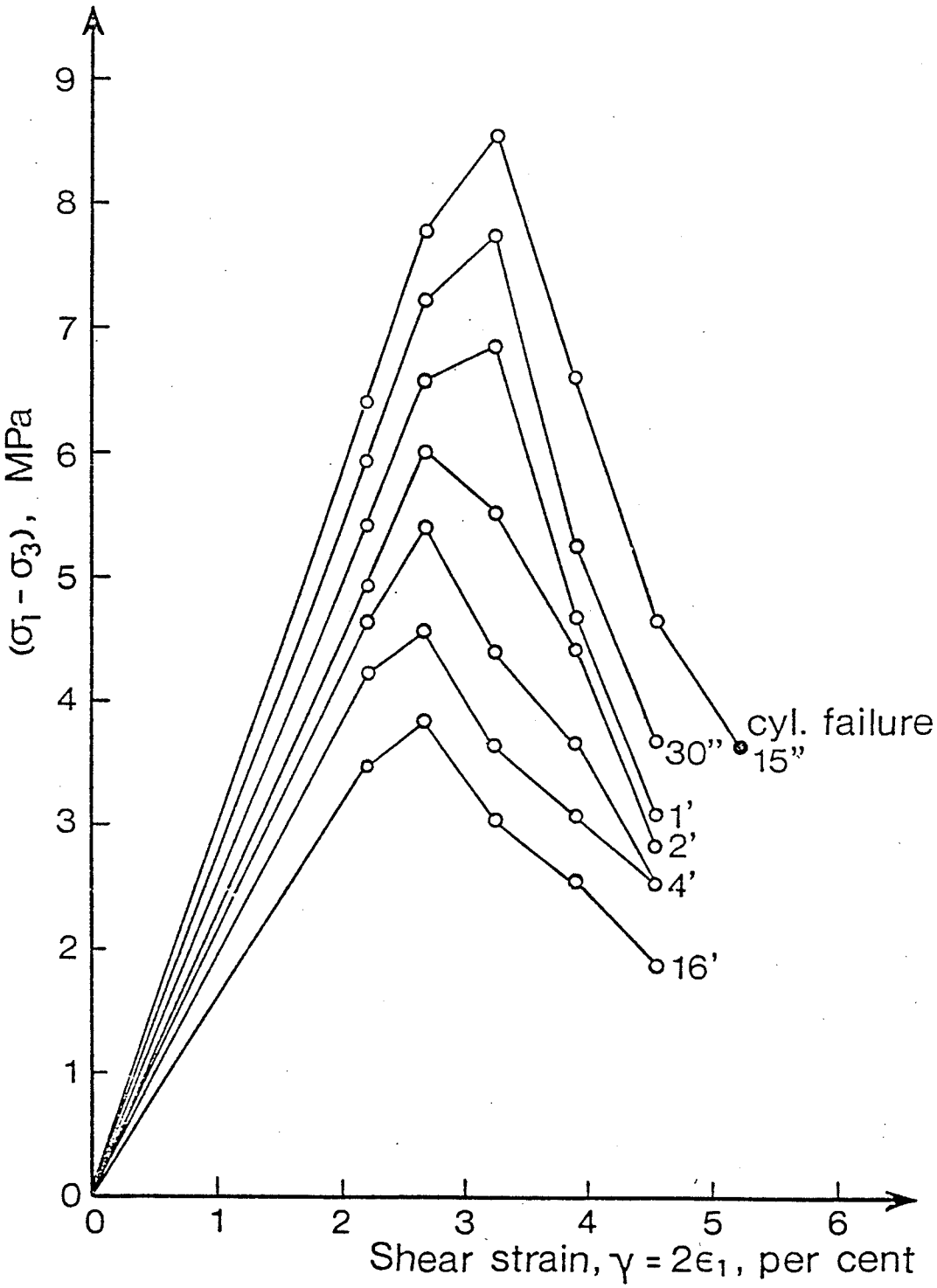

Fig.4.1.2. Result of a borehole dilatometer relaxation test in fresh-water ice: Stress-strain curves at constant relaxation times. (From: Ladanyi et al., 1978)

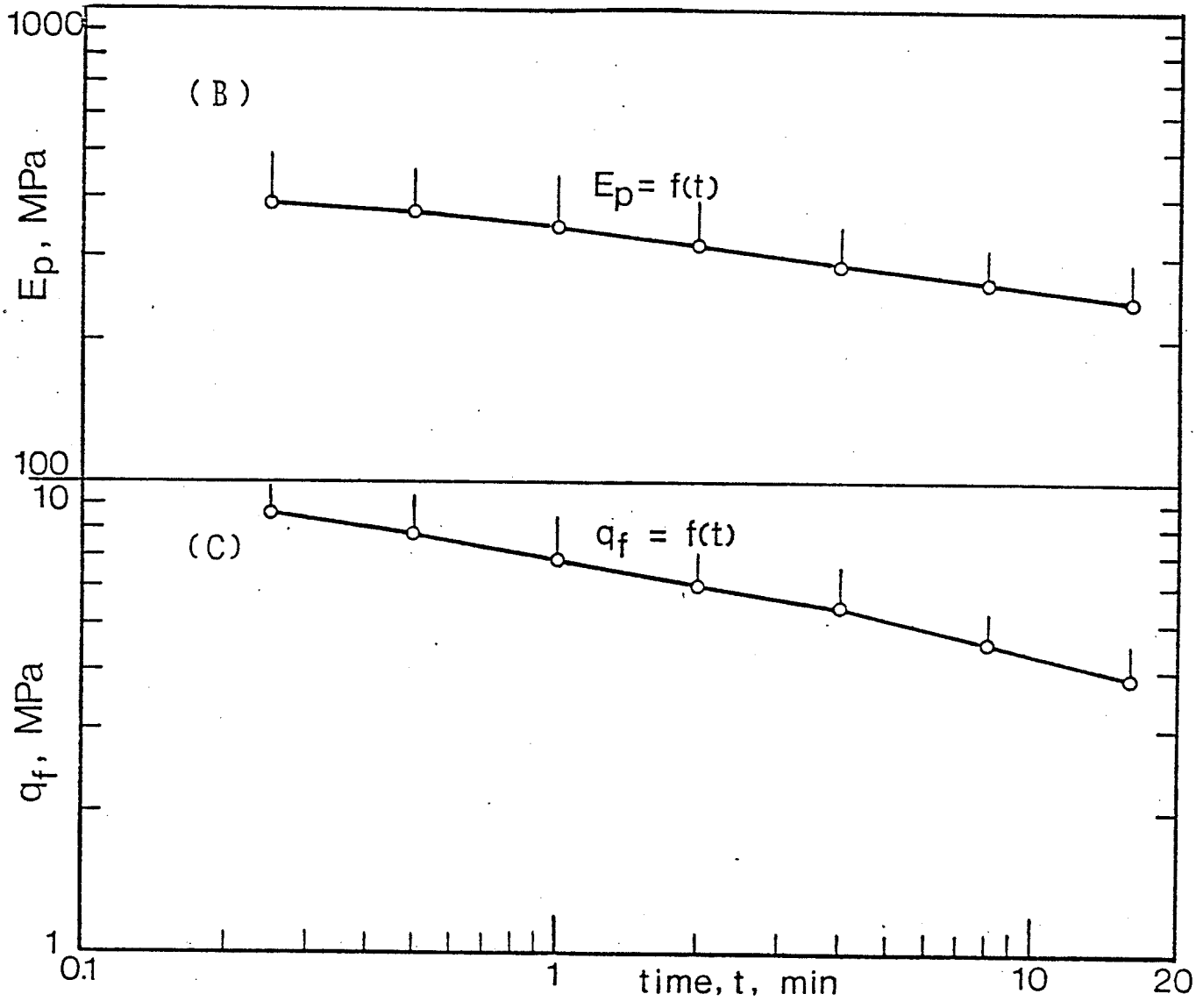

Fig.4.1.3. Results of borehole dilatometer relaxation tests in a fresh-water ice cylinder. Variation of deformation modulus and compression strength with time. (From: Ladanyi et al., 1978)

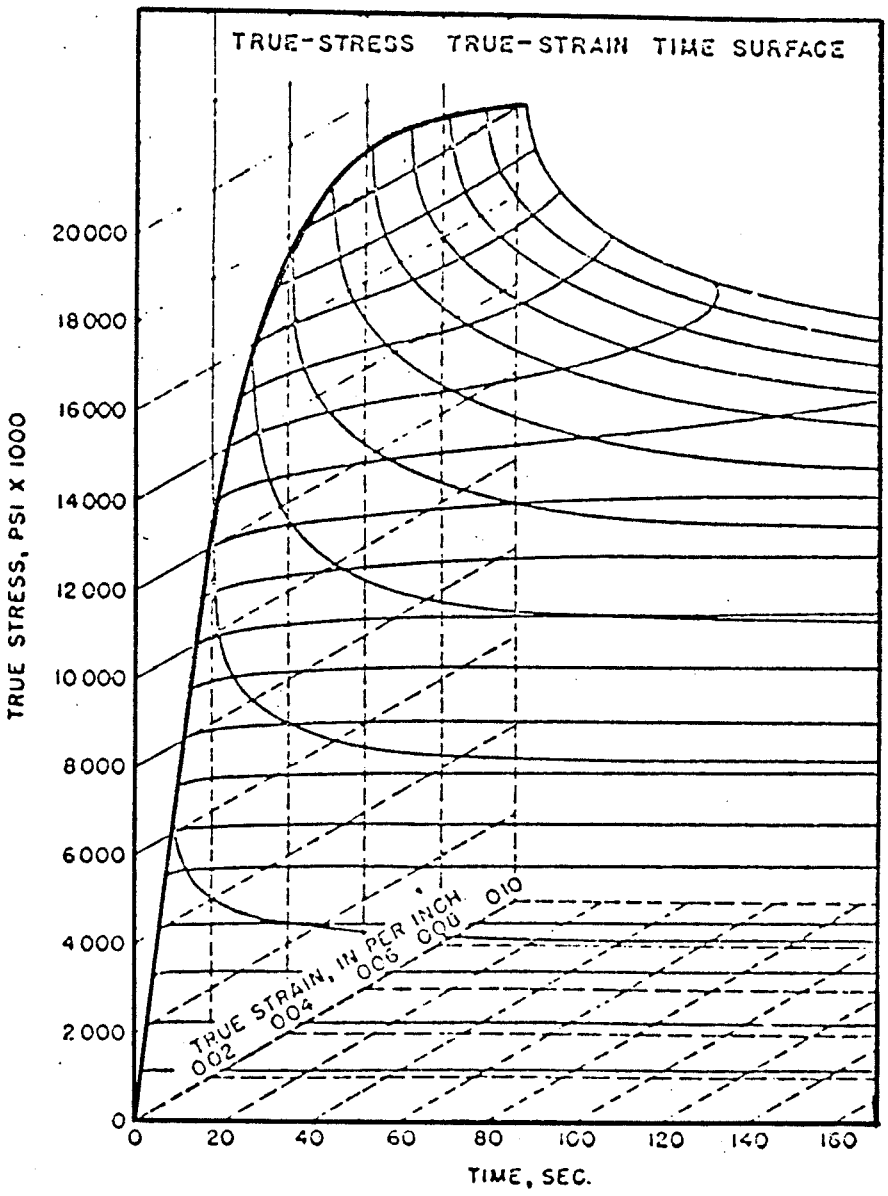

Fig.4.2.1. Total strain method: Stress-strain-time surface. (After Findlay, 1951)

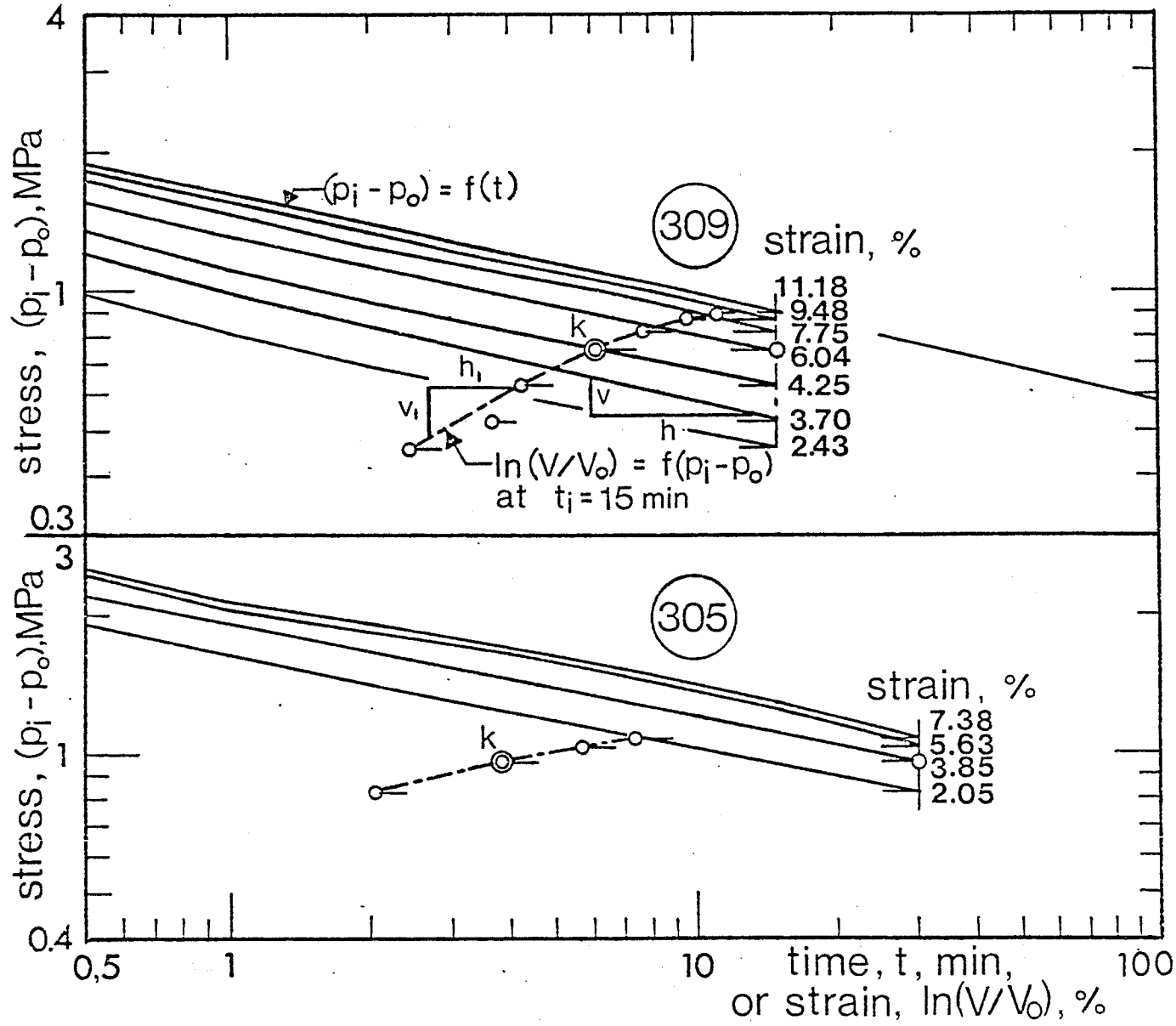

Fig.4.2.2. Relaxation curves from stage-loaded borehole relaxation tests. (from: Ladanyi, 1982)

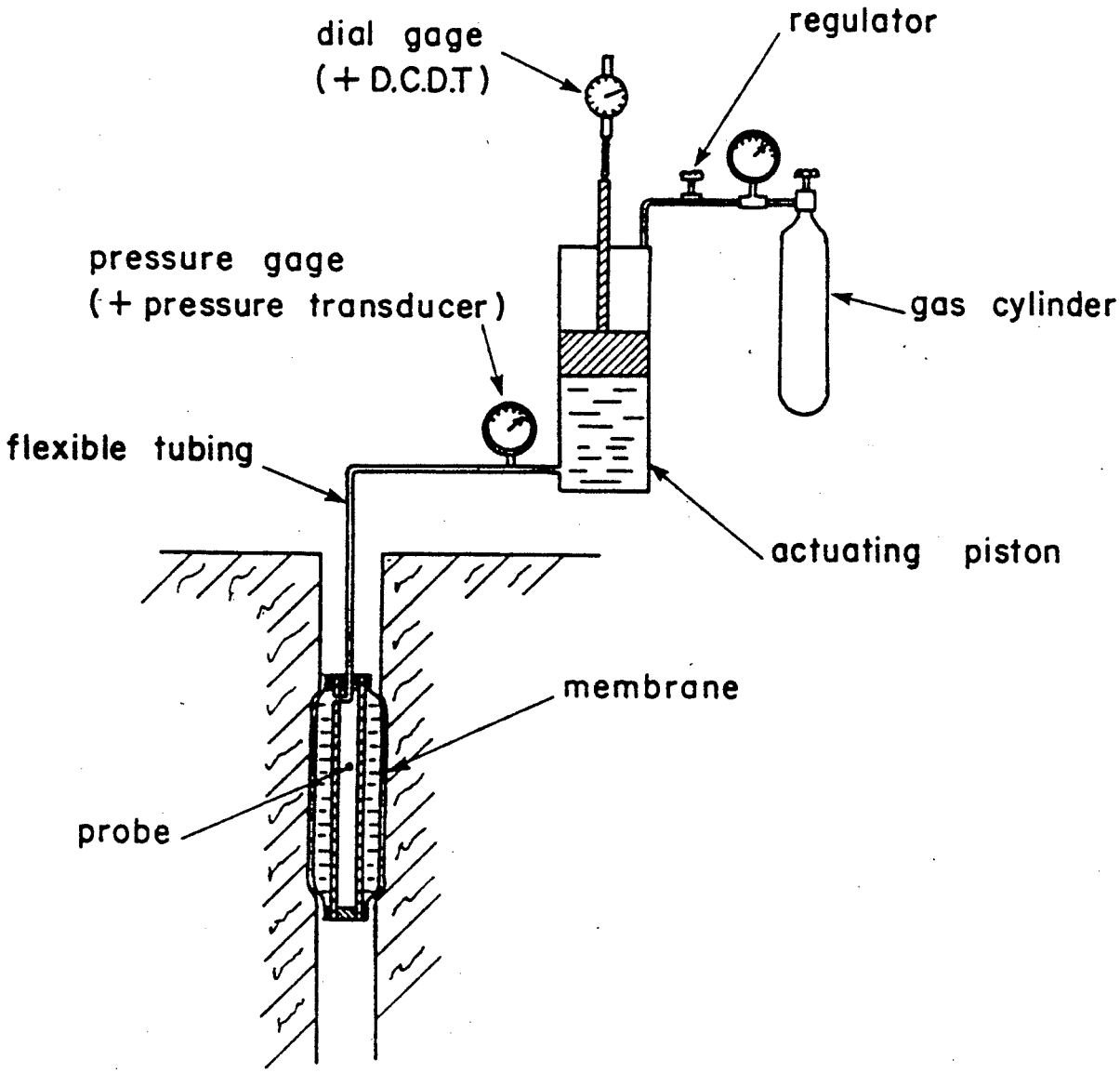

Fig.5.2.1. Schematic of the TEXAM PRESSUREMETER SYSTEM.

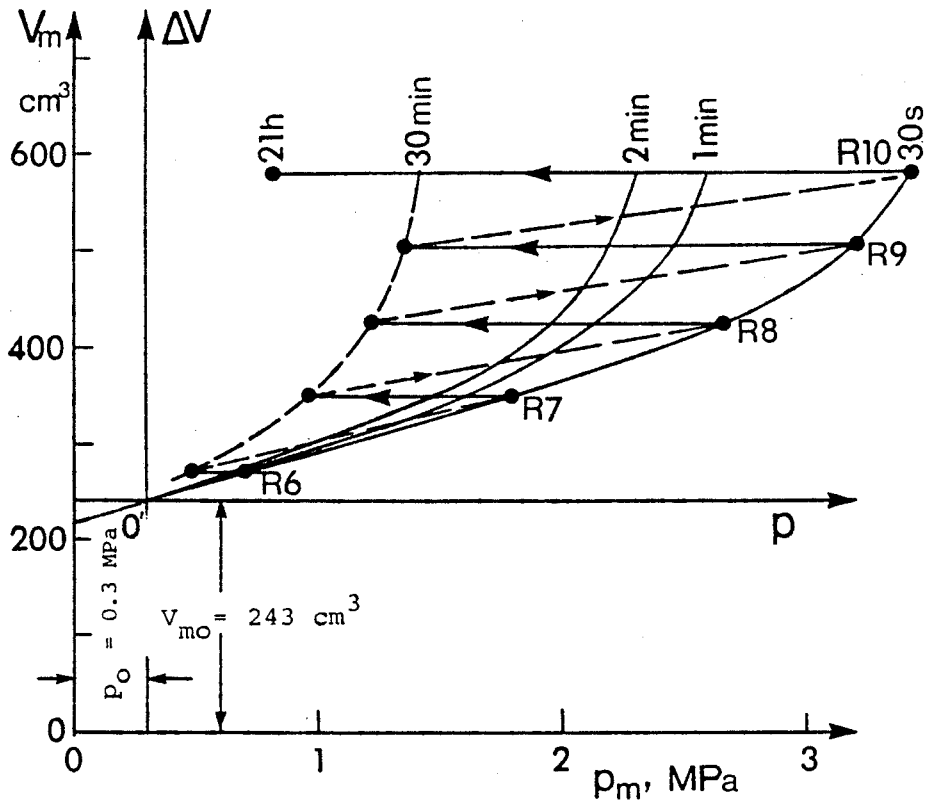

Fig.5.2.2. Isochronous pressuremeter curves and the levels of relaxation tests (Test PRF6, from Ladanyi et al., 1991)

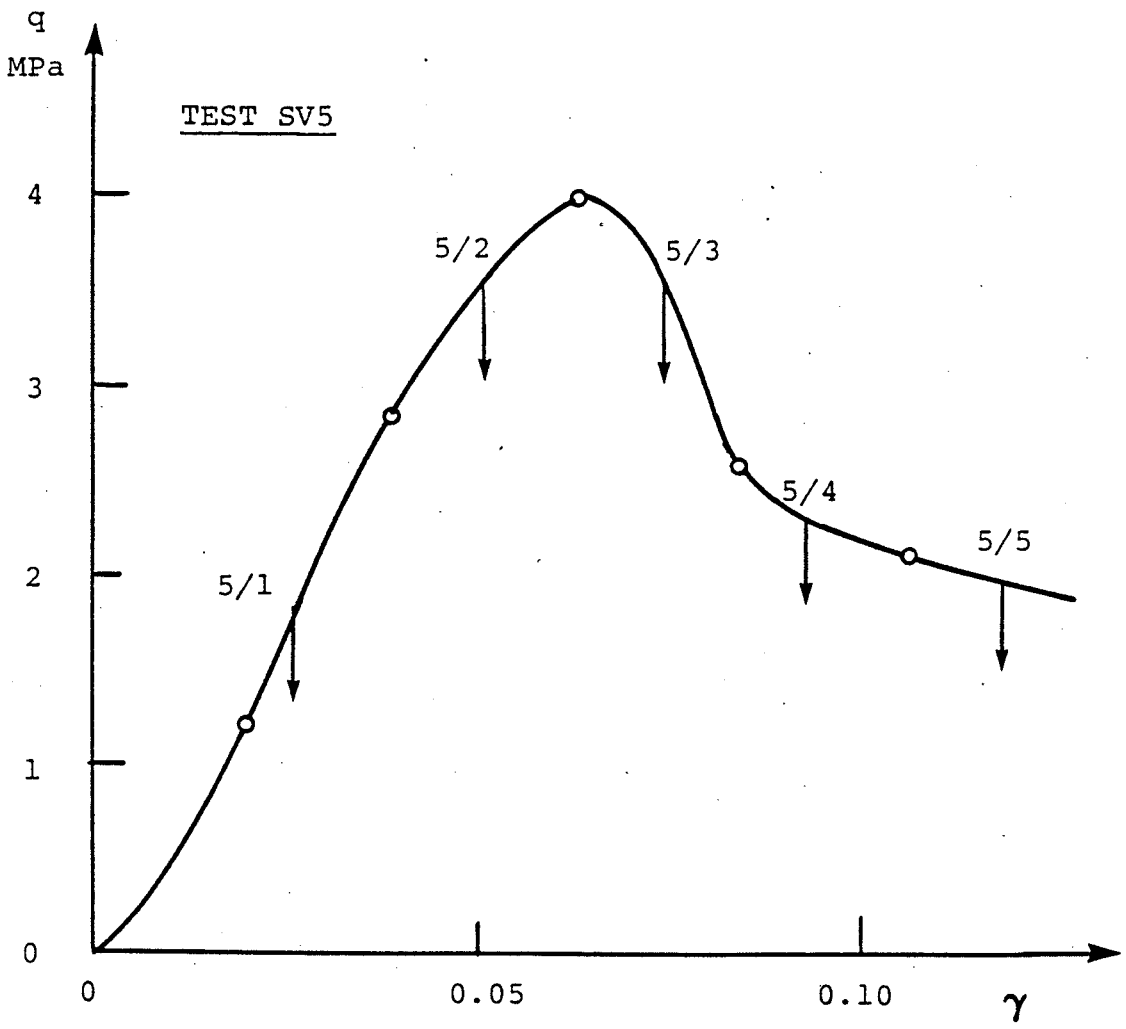

Fig.5.2.3. Stage-loaded relaxation test: 2-min stress-strain curve with relaxation-stage locations indicated. (Test SV5, Ladanyi et al., 1990)

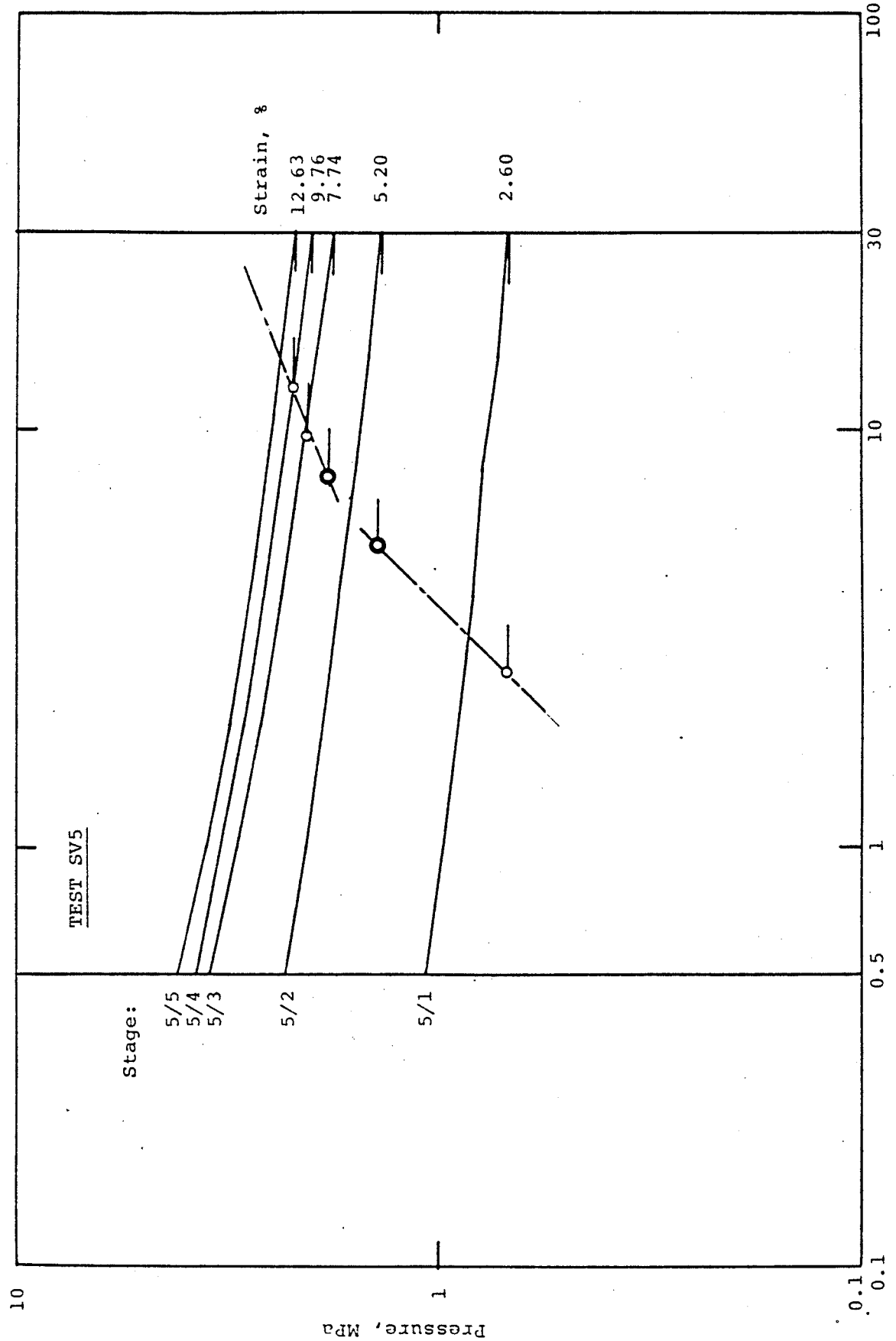

Fig.5.2.4. Relaxation curves in a log-log plot (Test SV5, Ladanyi et al.,1990)

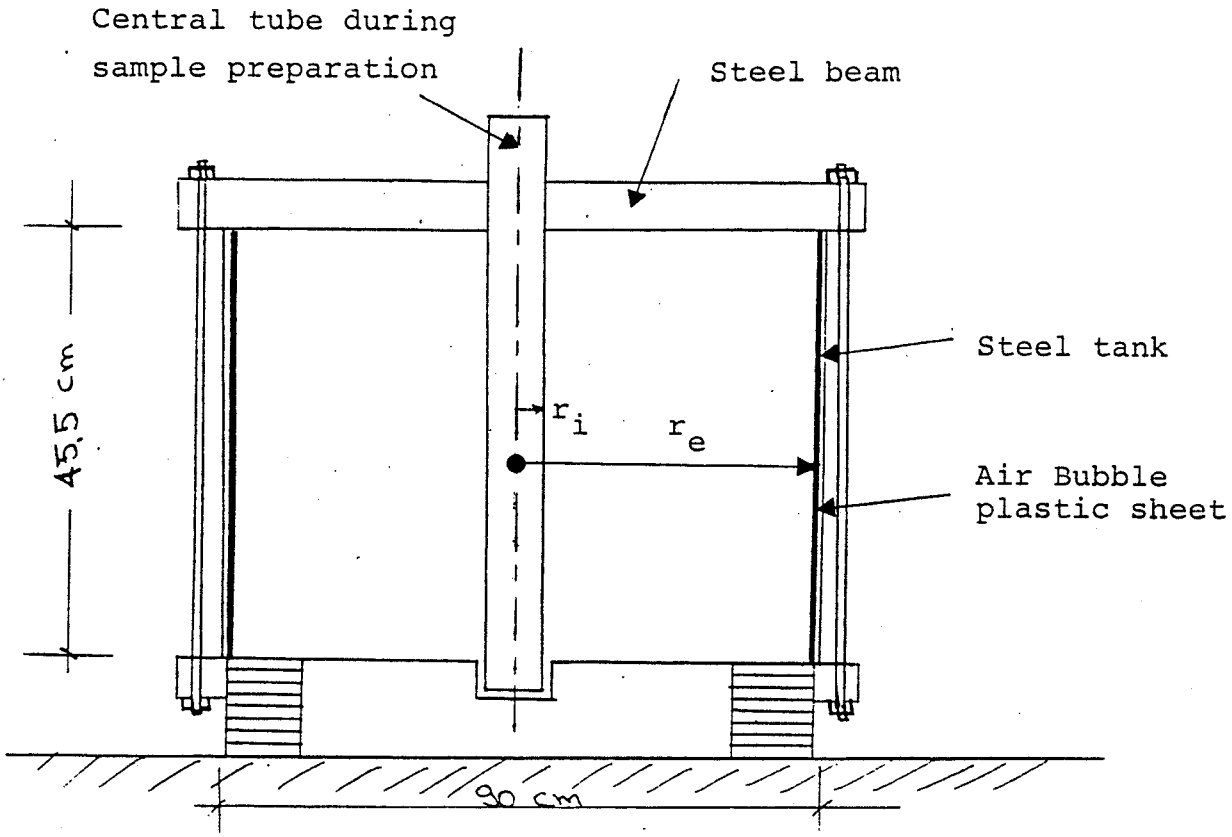

Fig.5.3.1. Test set-up used for borehole relaxation tests.

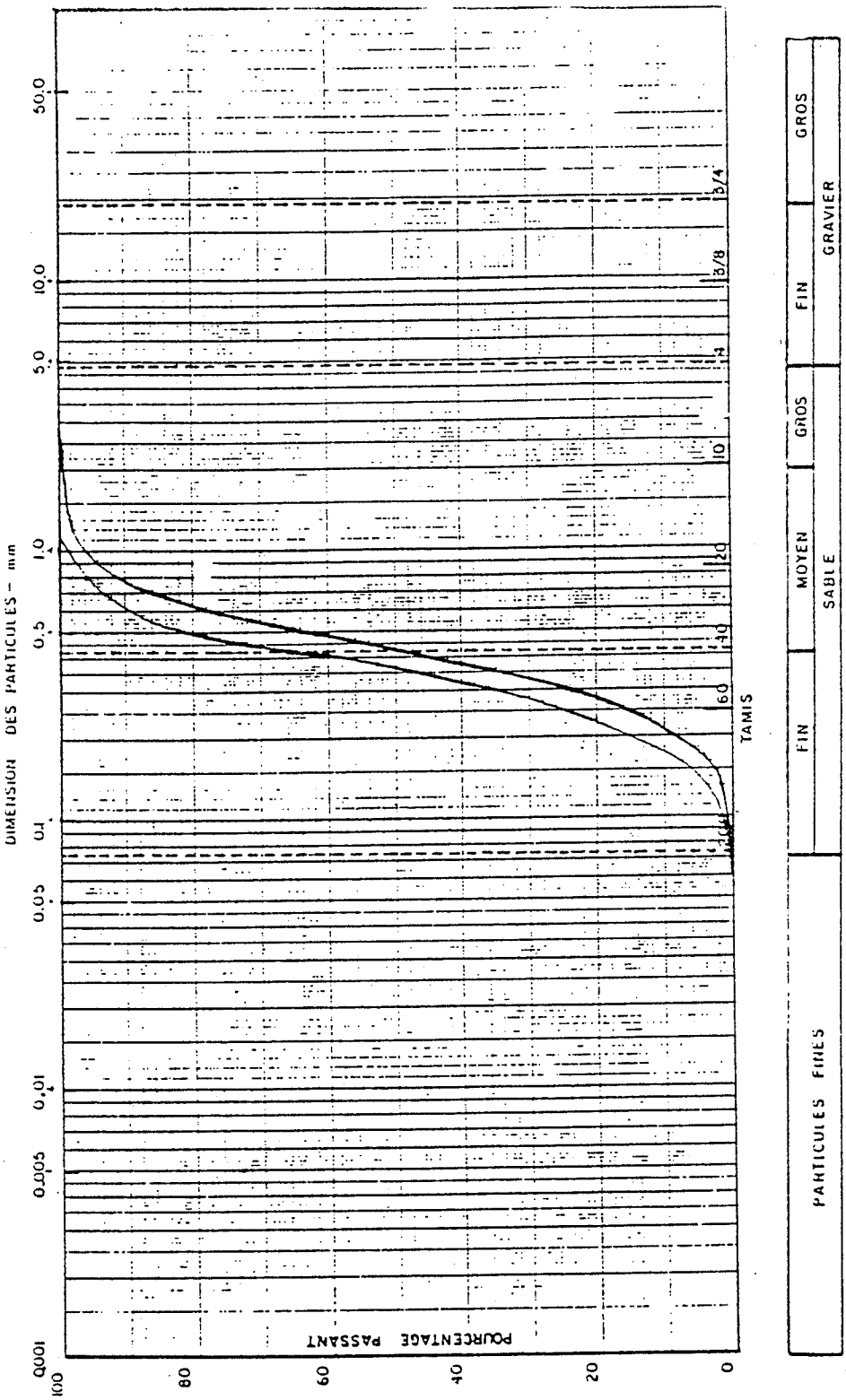

Fig.5.3.2. Grain-size distribution of the Joliette Sand.

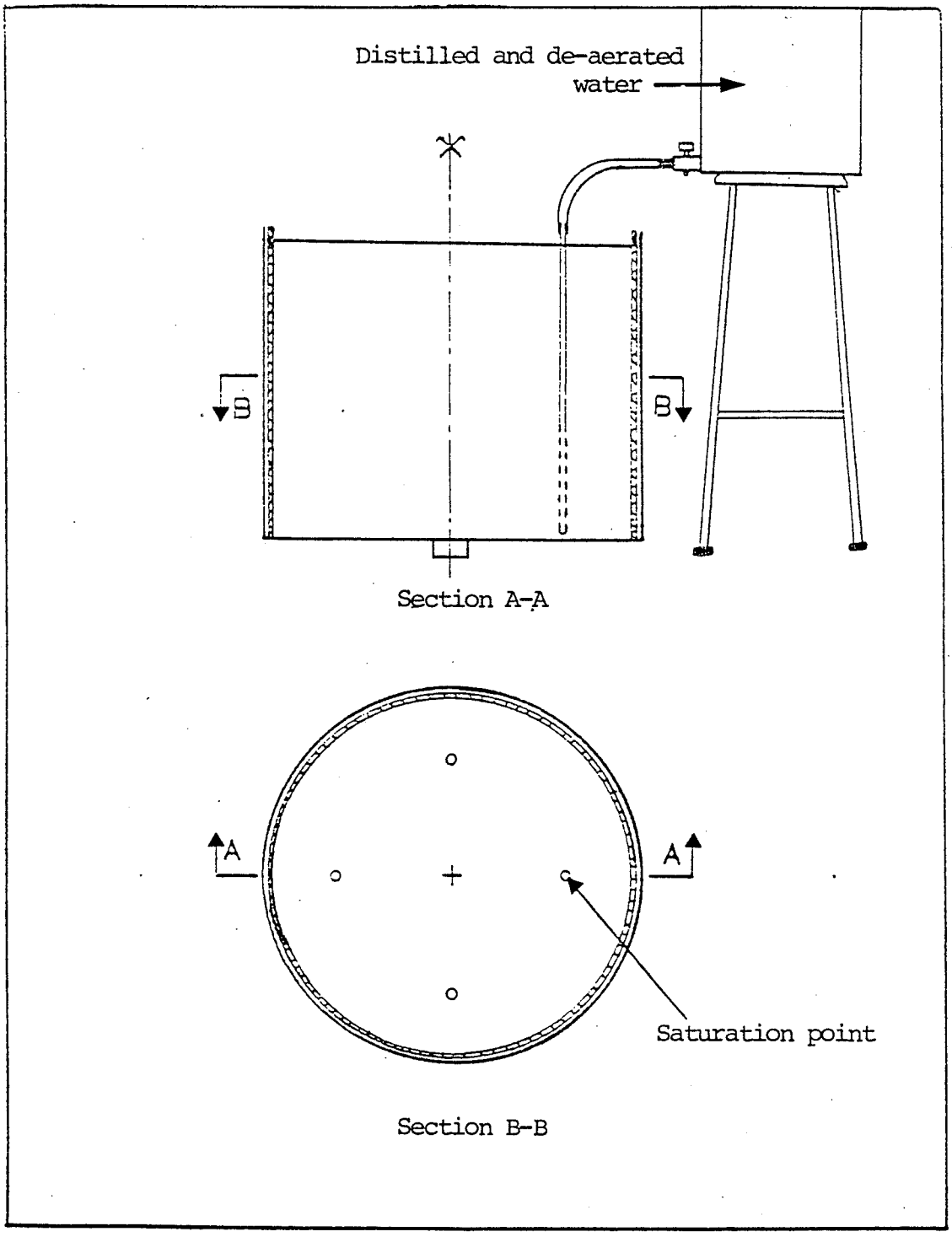

Fig.5.3.3. Saturation of sand in the container.

JOLIETTE FROZEN SAND

Fig.5.4.1. TO Fig.5.4.6.

RELAXATION CURVES

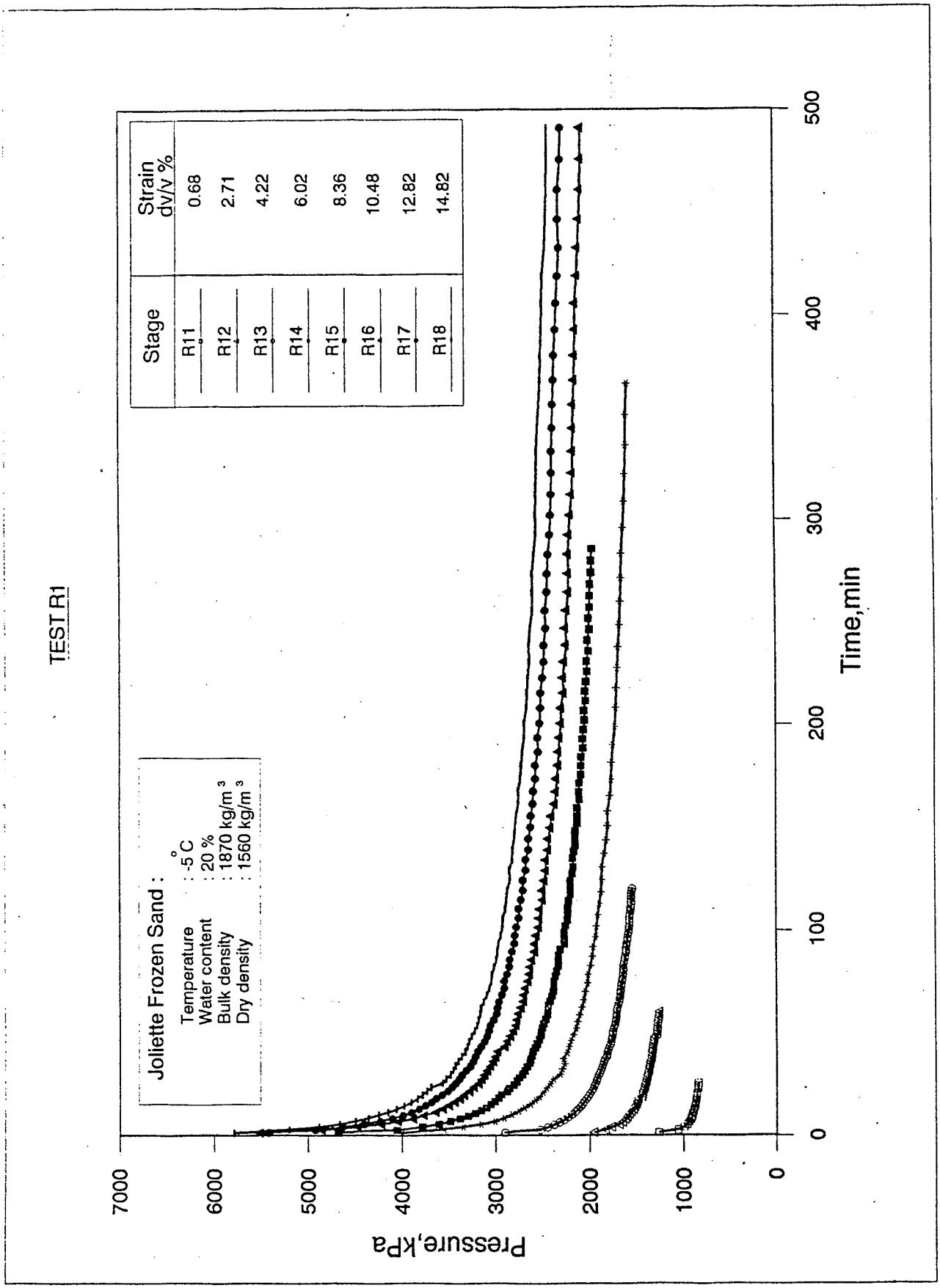

Fig.5.4.1. Test R1. Relaxation curves.

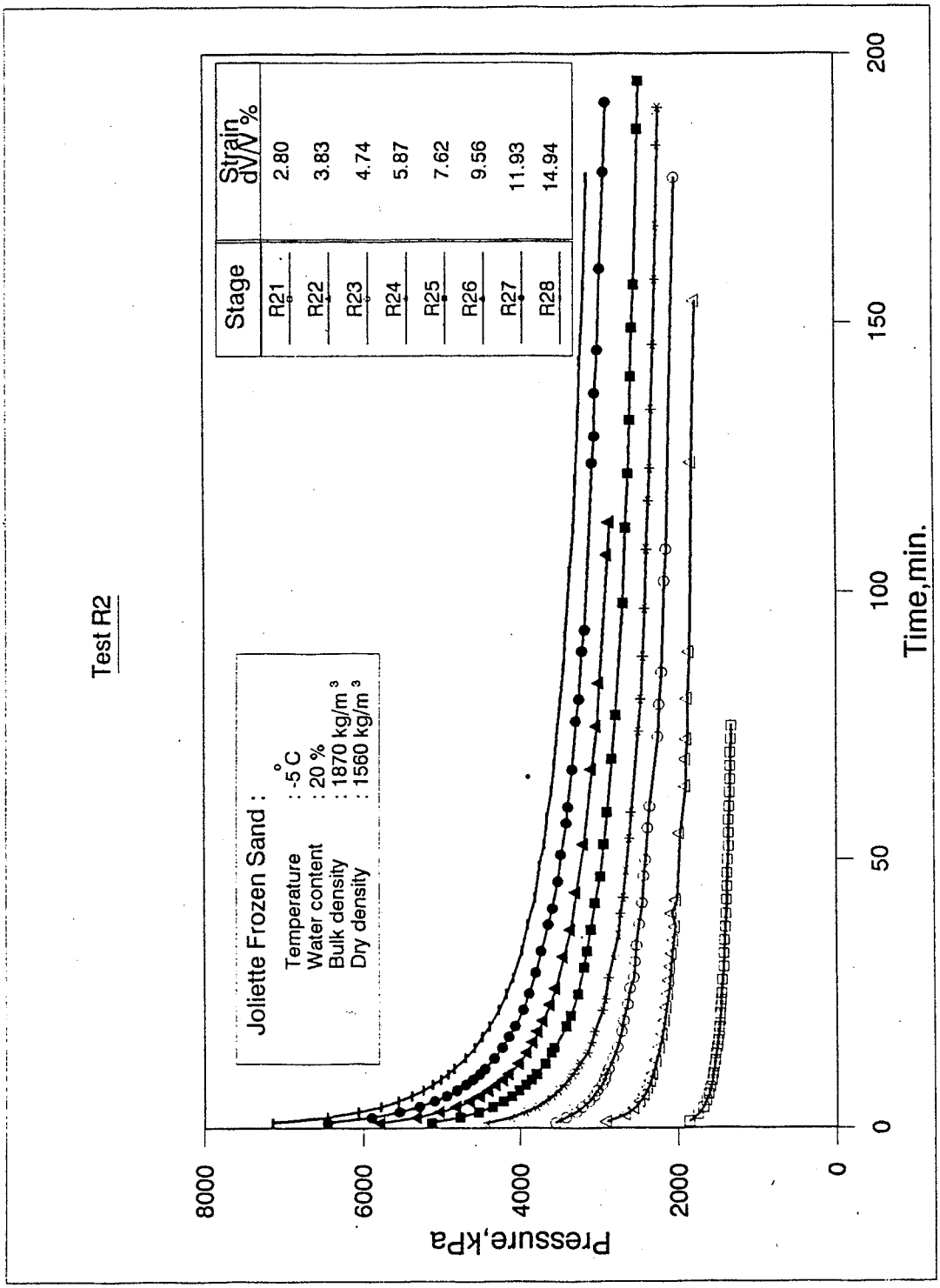

Fig.5.4.2. Test R2. Relaxation curves.

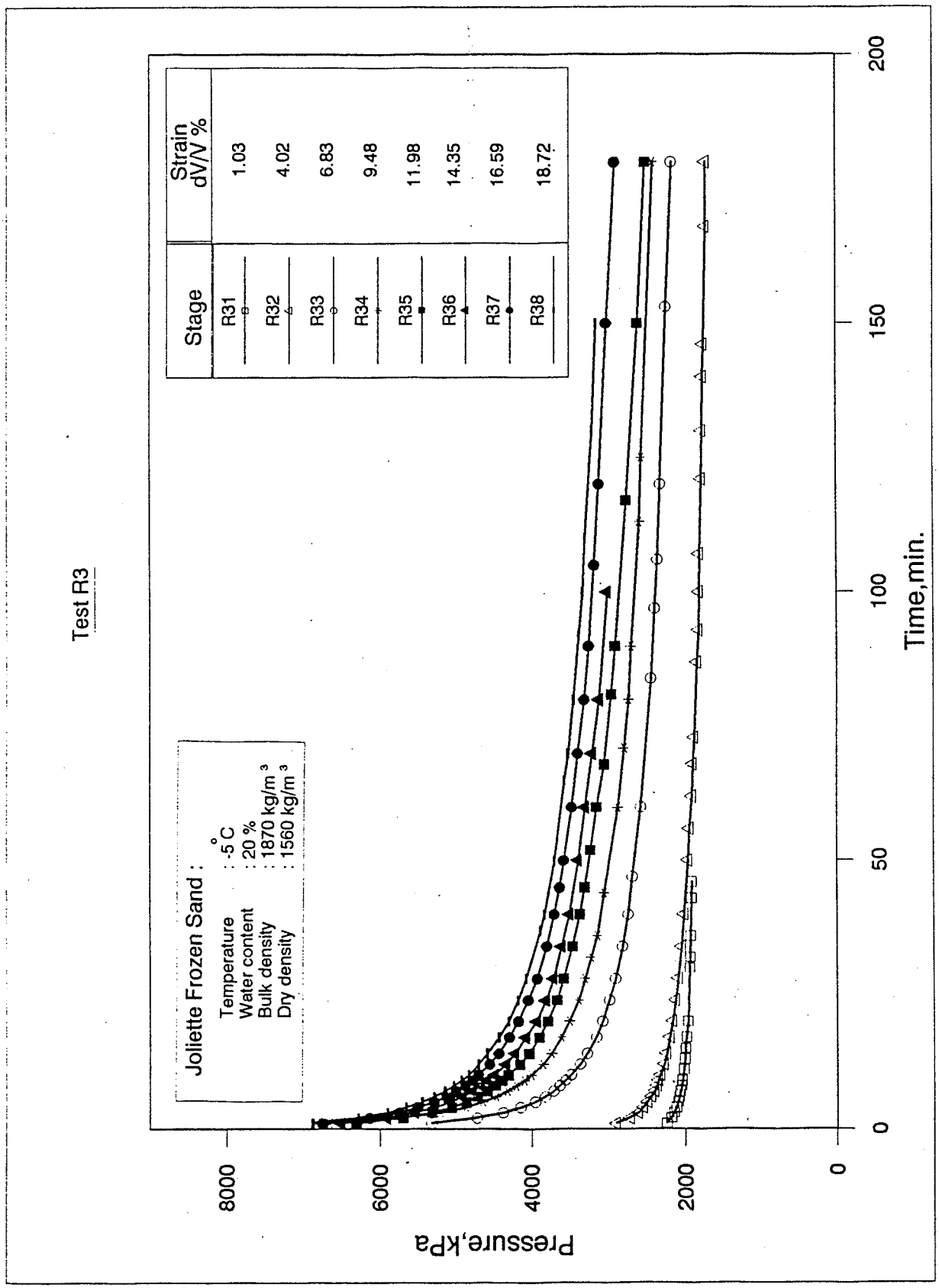

Fig.5.4.3. Test R3. Relaxation curves.

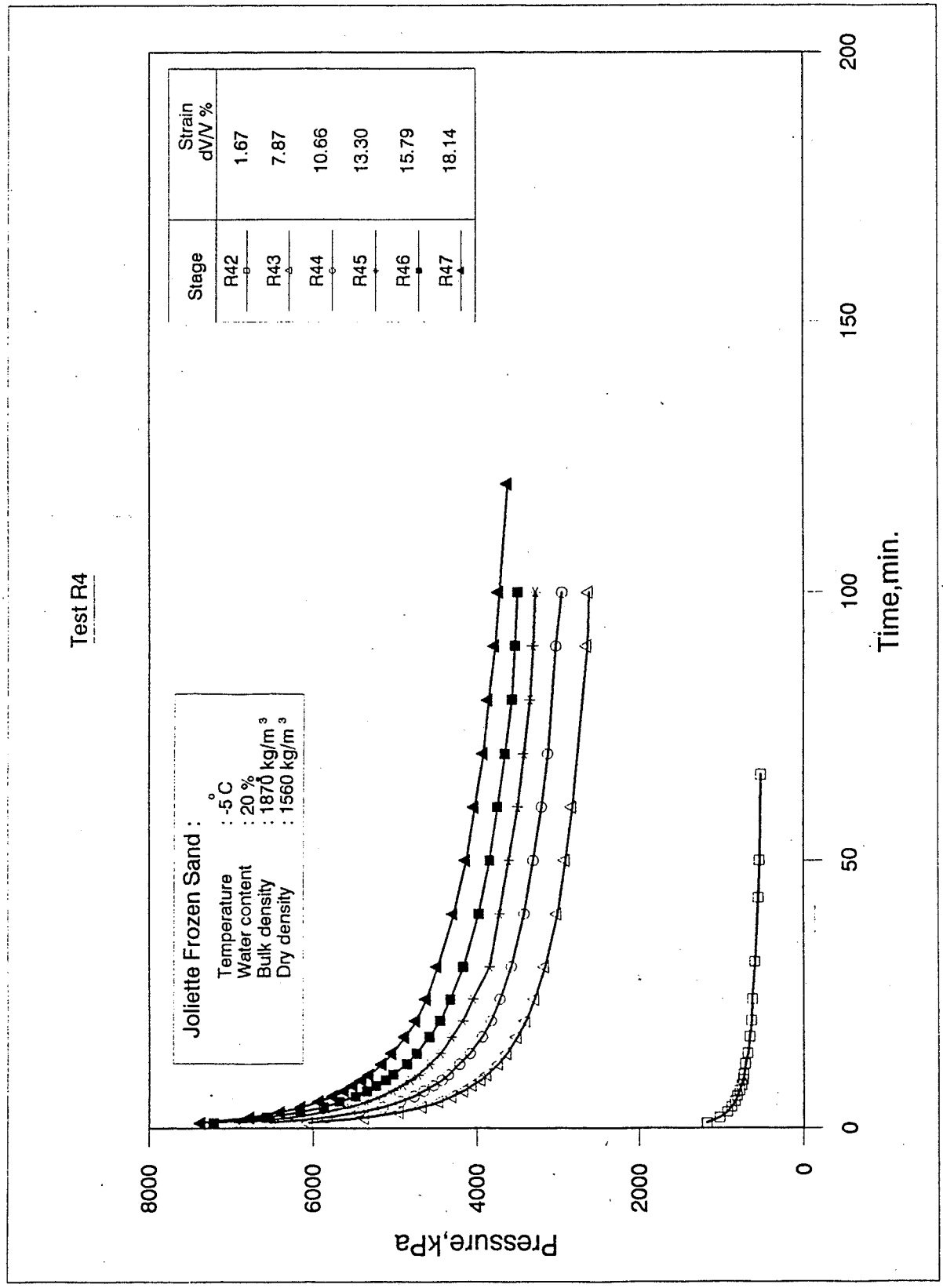

Fig.5.4.4. Test R4. Relaxation curves.

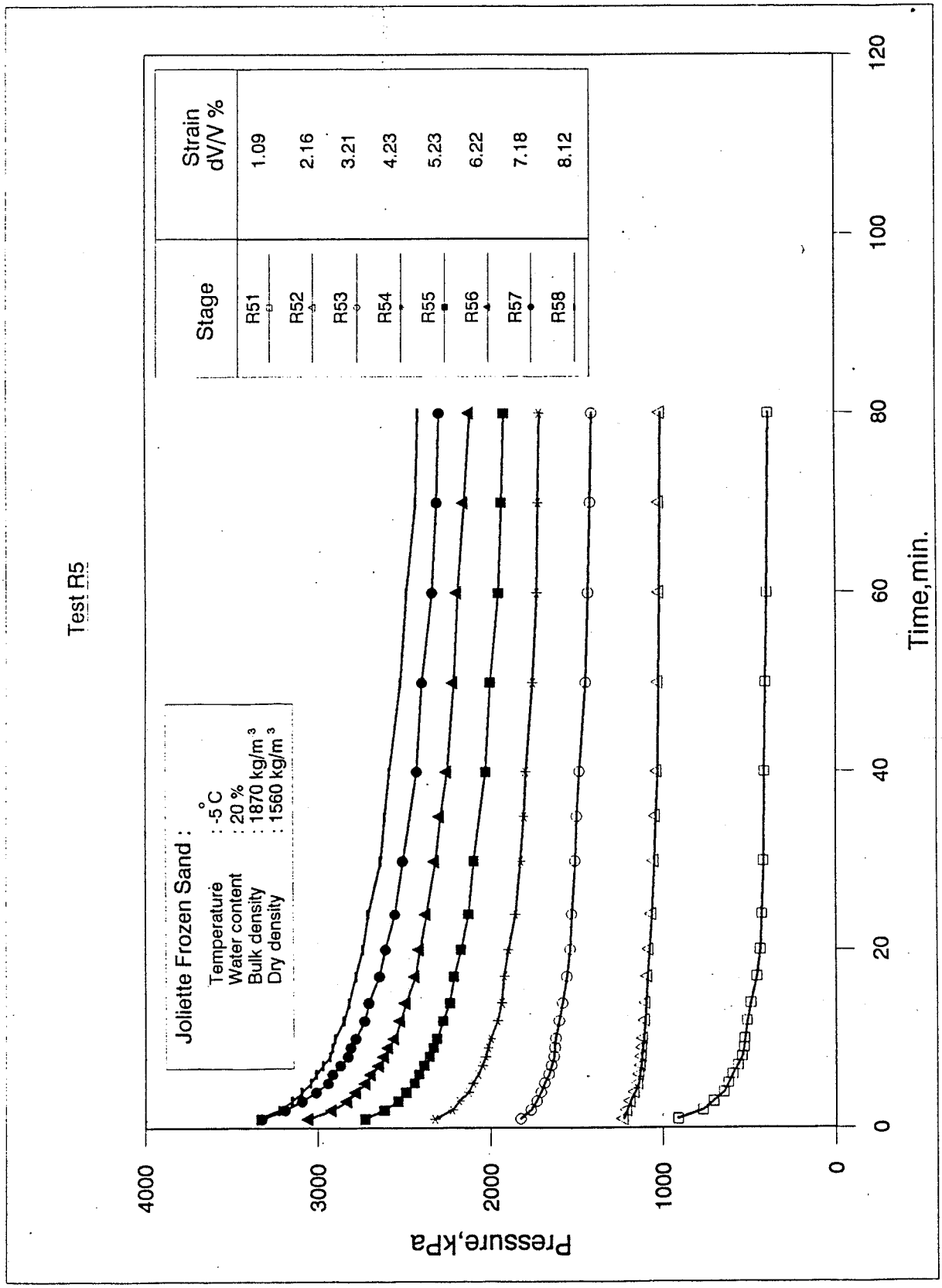

Fig.5.4.5. Test R5. Relaxation curves.

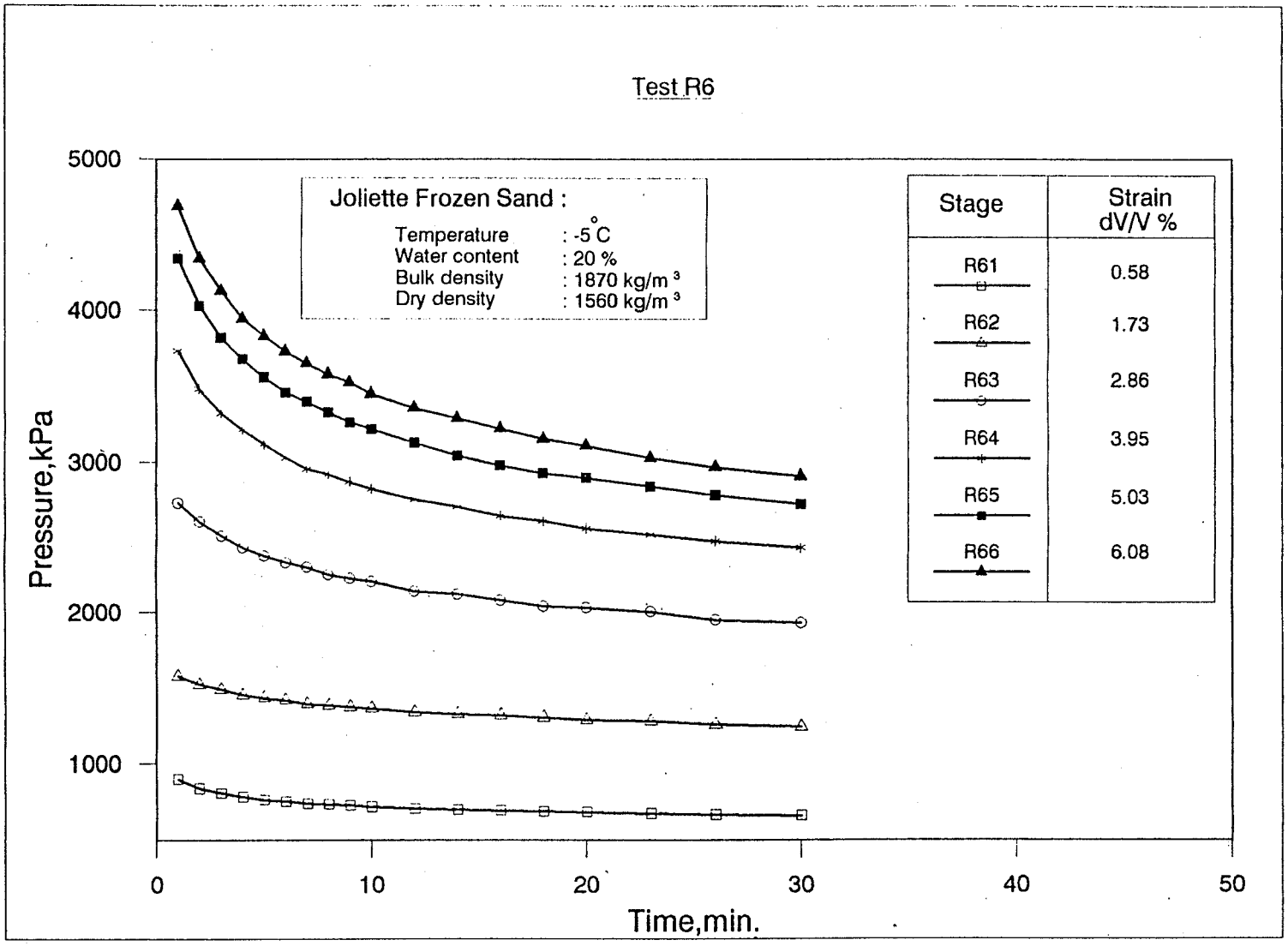

Fig.5.4.6. Test R6. Relaxation curves.

JOLIETTE FROZEN SAND

Fig.5.5.1. TO Fig.5.5.6

INTERPRETATION BY THE AGING CREEP THEORY

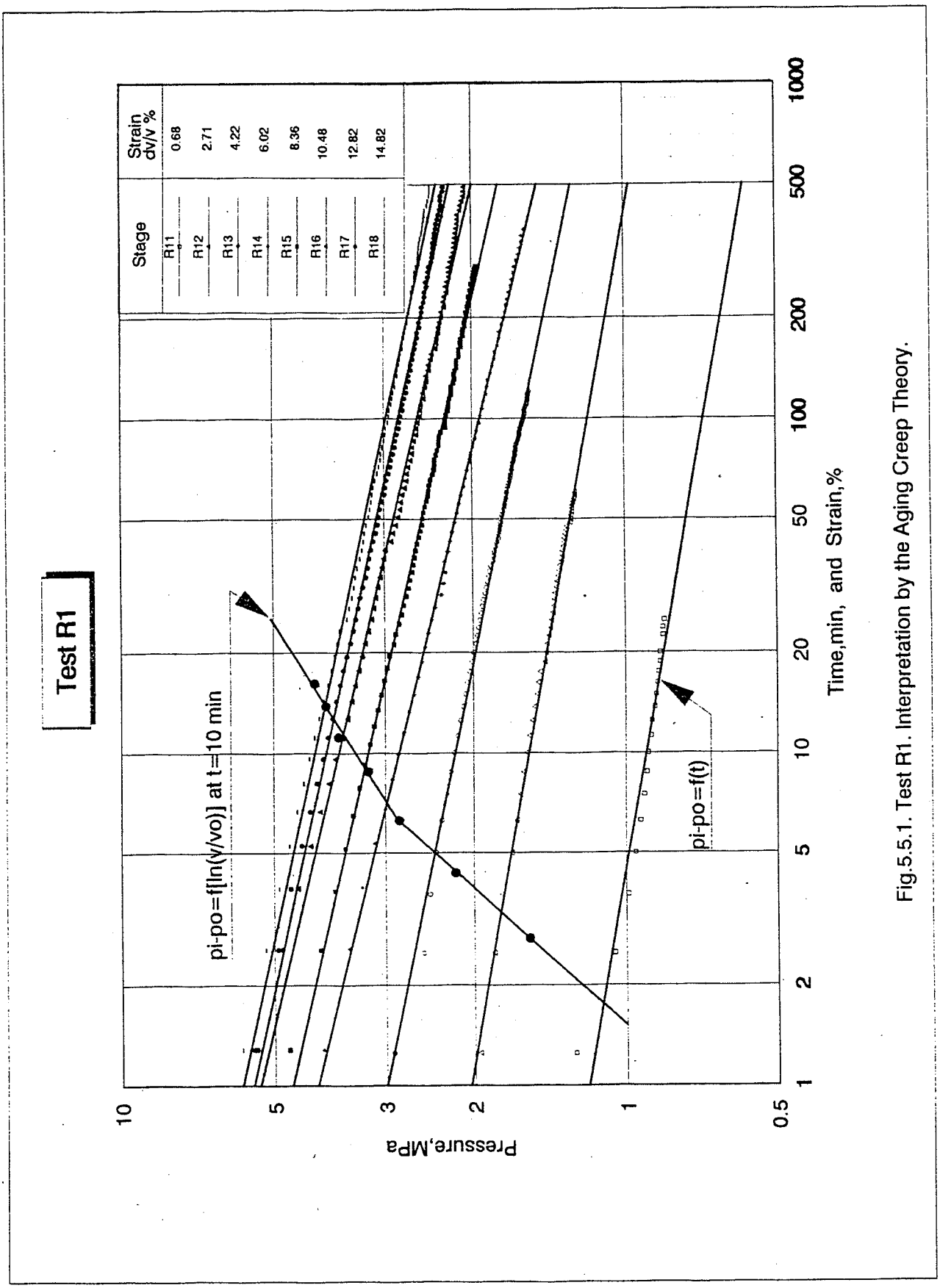

Fig.5.5.1. Test R1. Interpretation by the Aging Creep Theory.

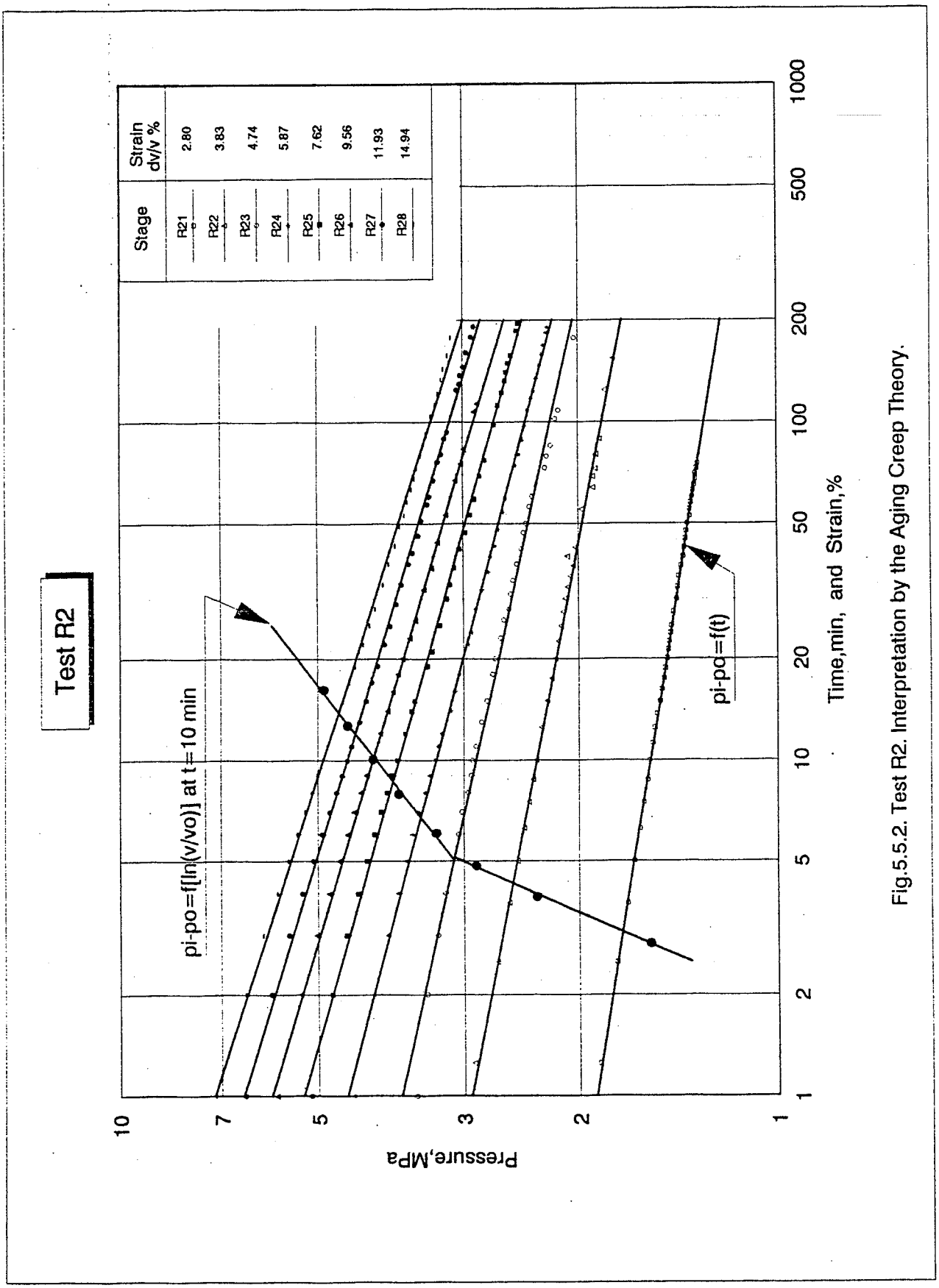

Fig.5.5.2. Test R2. Interpretation by the Aging Creep Theory.

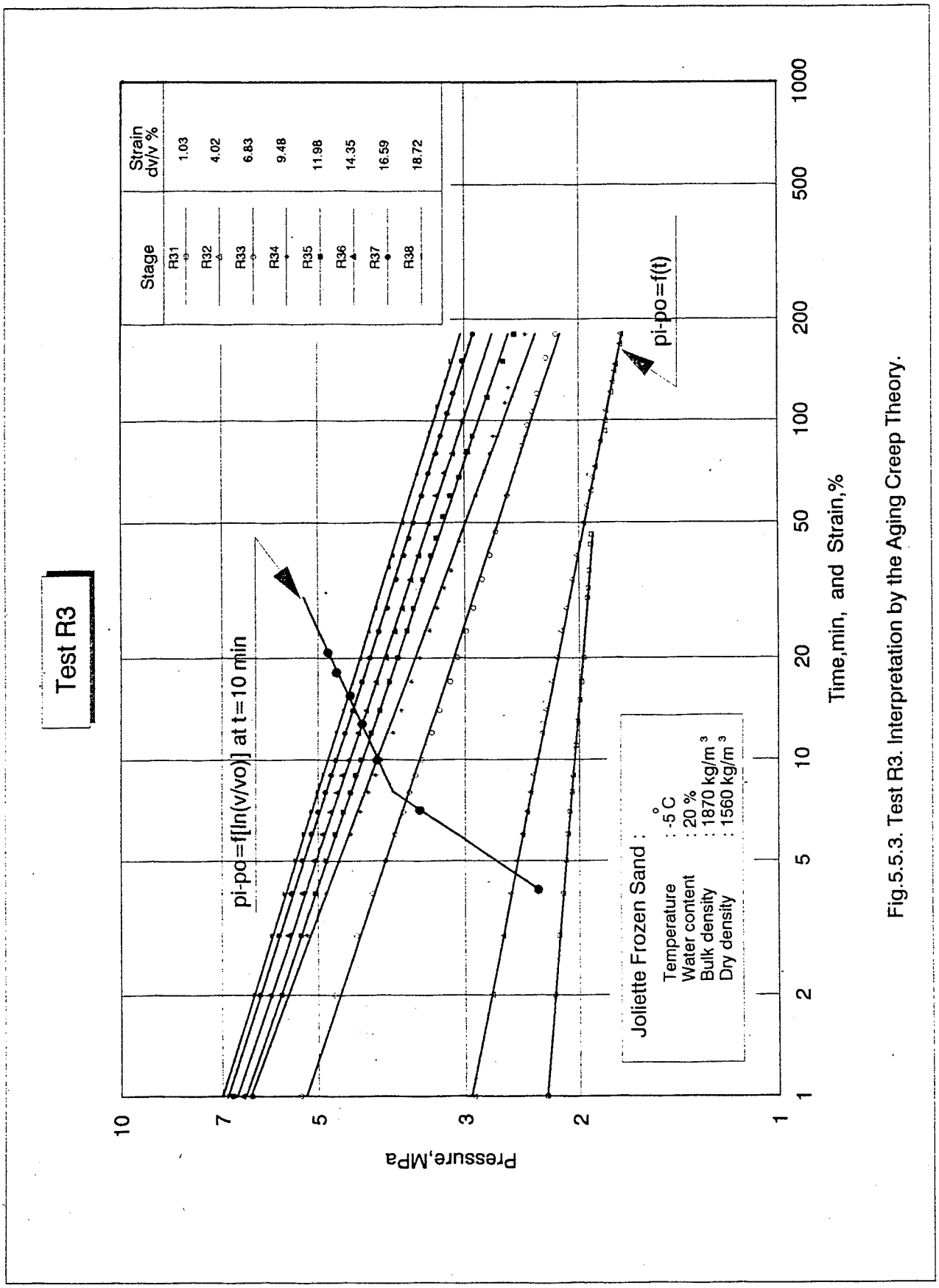

Fig.5.5.3. Test R3. Interpretation by the Aging Creep Theory.

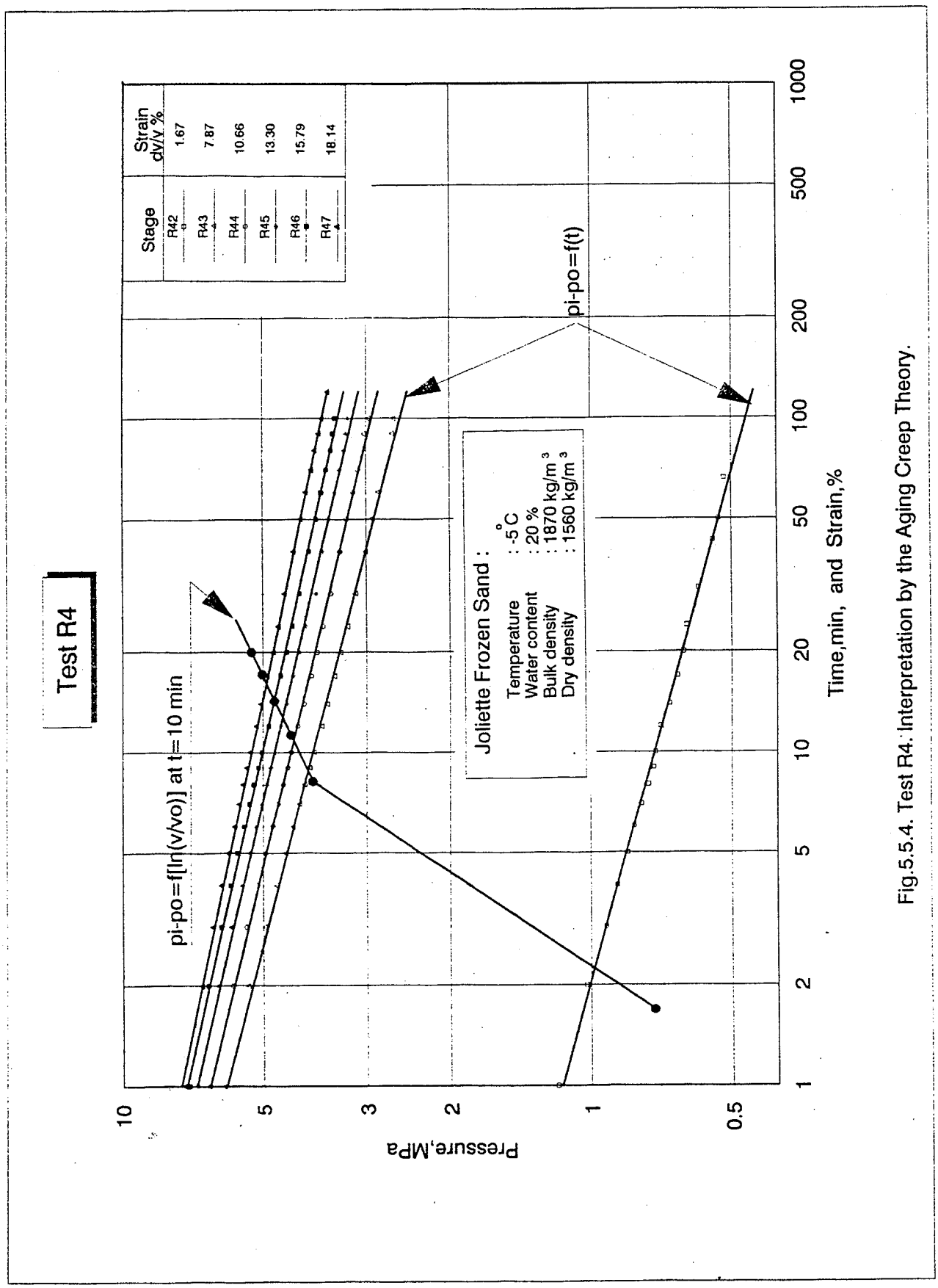

Fig.5.5.4. Test R4: Interpretation by the Aging Creep Theory.

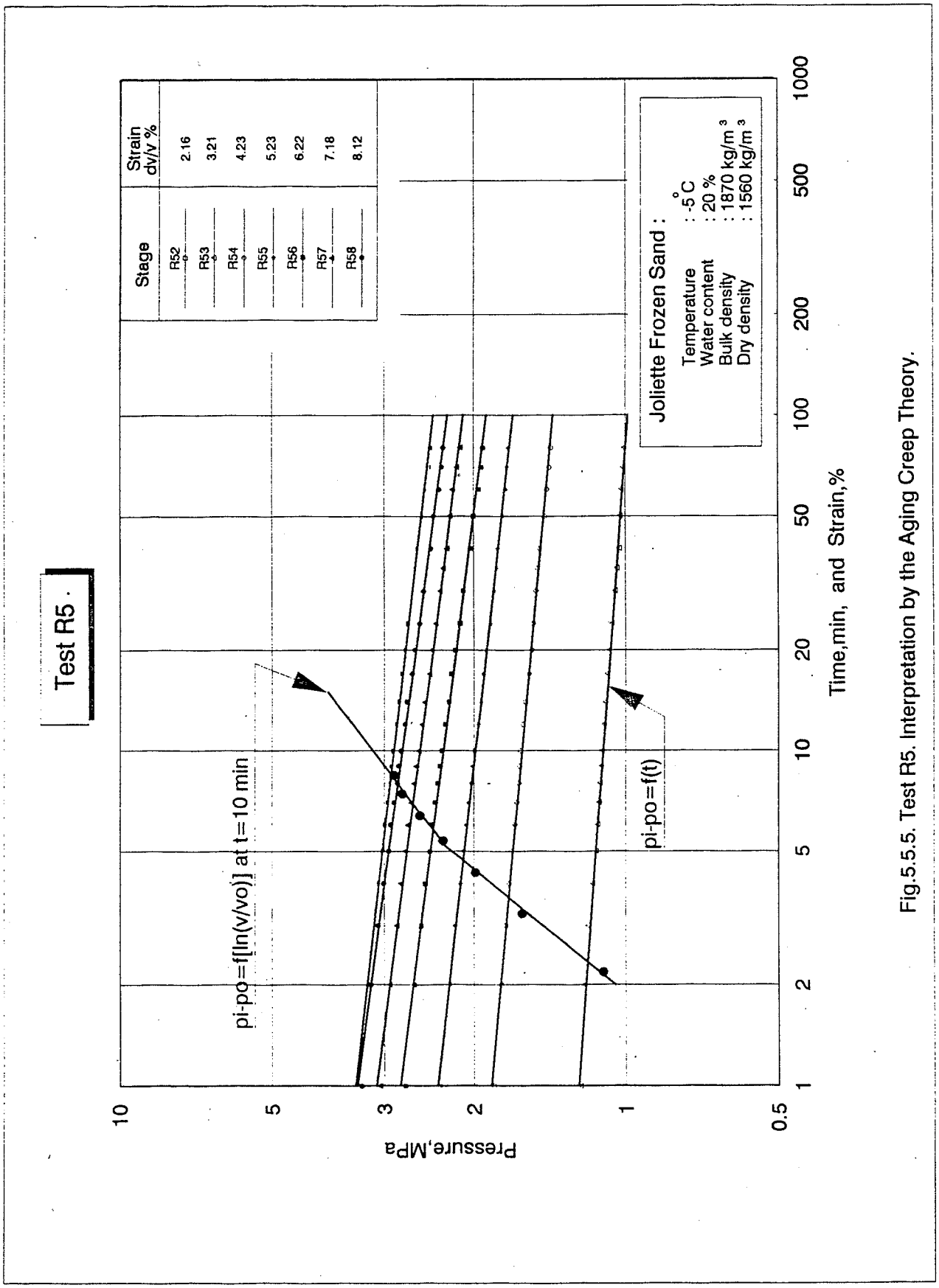

Fig.5.5.5. Test R5. Interpretation by the Aging Creep Theory.

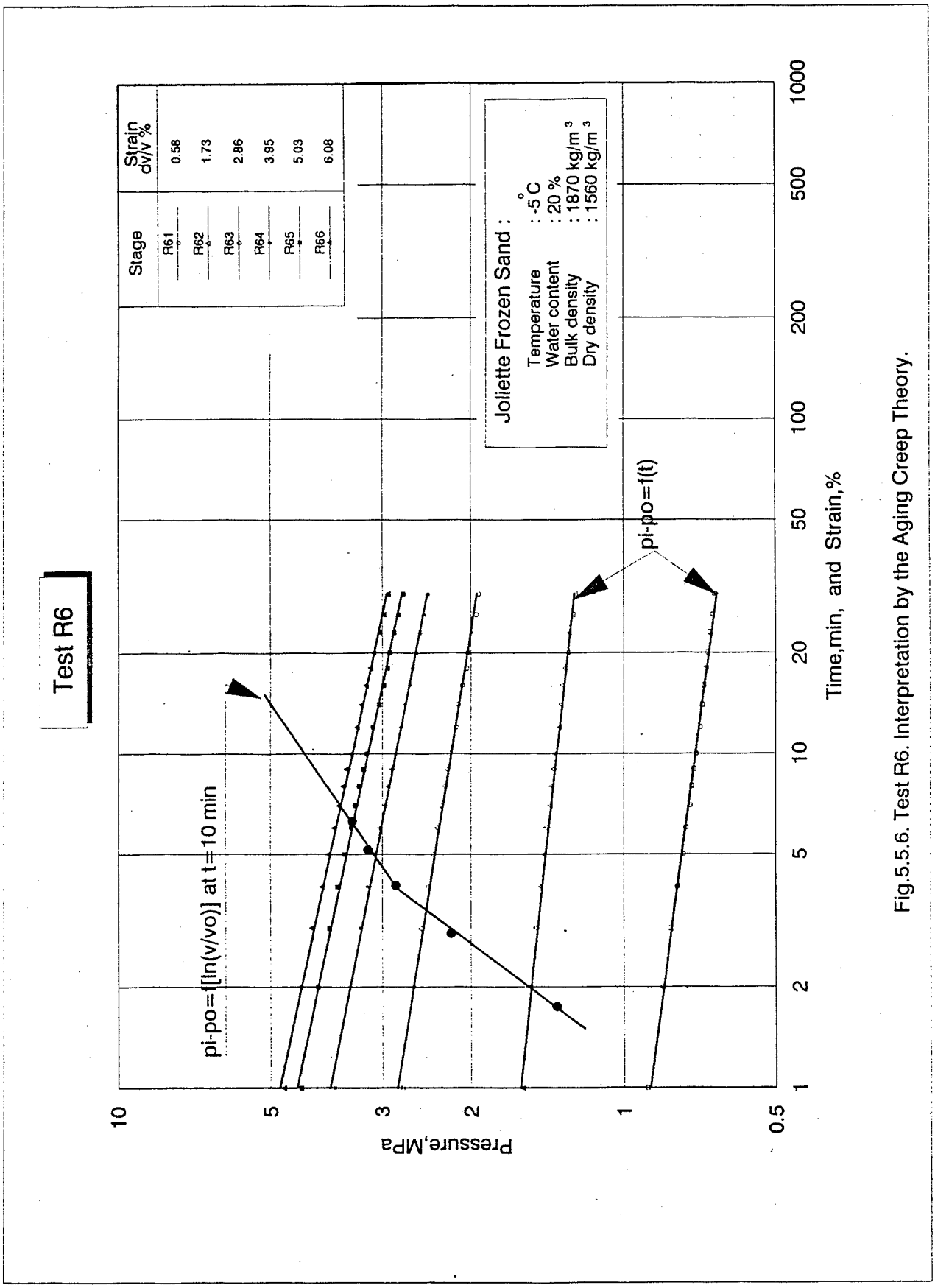

Fig.5.5.6. Test R6. Interpretation by the Aging Creep Theory.

JOLIETTE FROZEN SAND

Fig.5.6.1. TO Fig.5.6.9.

INTERPRETATION BY THE REFERENCE STRESS METHOD

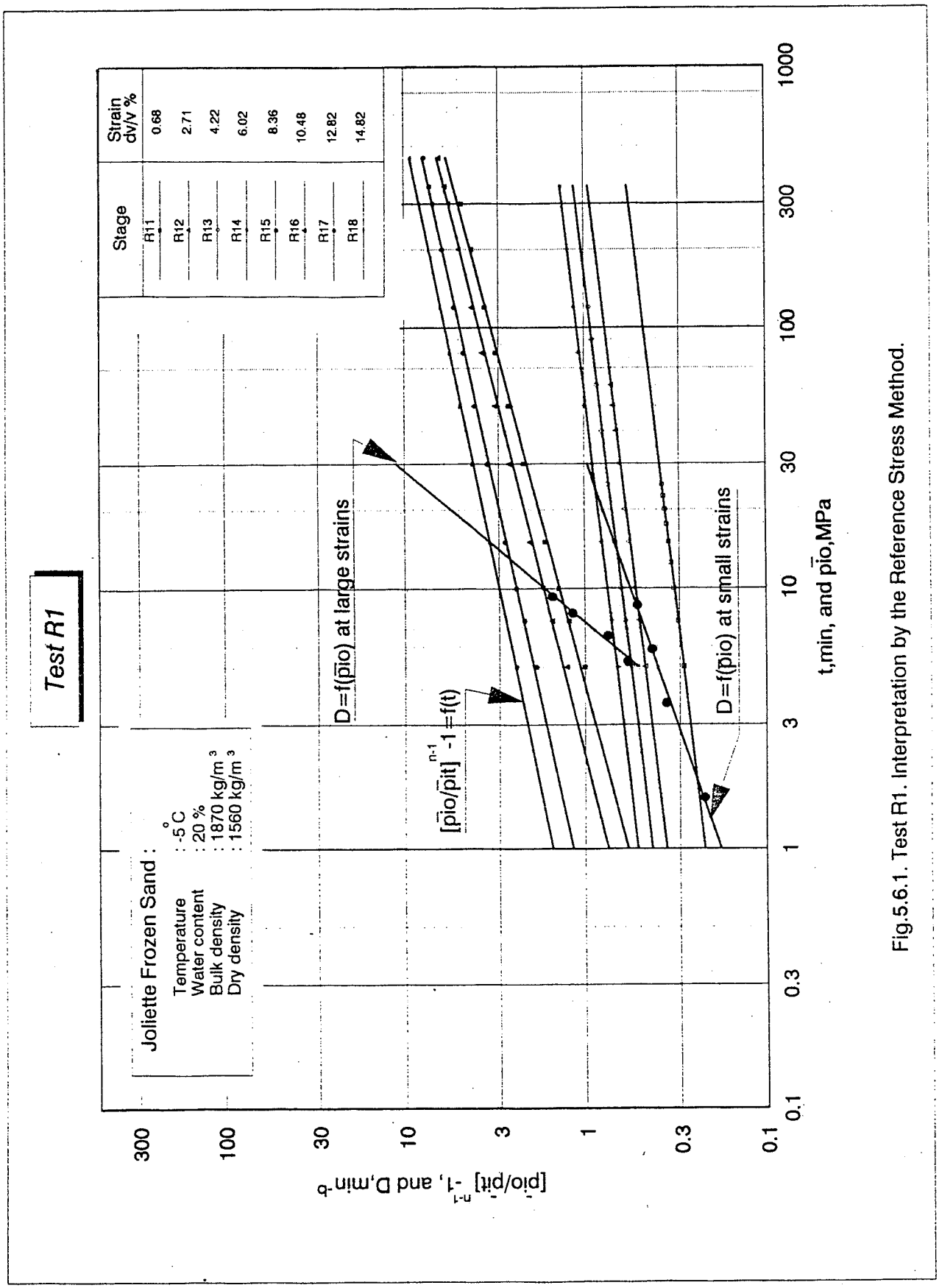

Fig.5.6.1. Test R1. Interpretation by the Reference Stress Method.

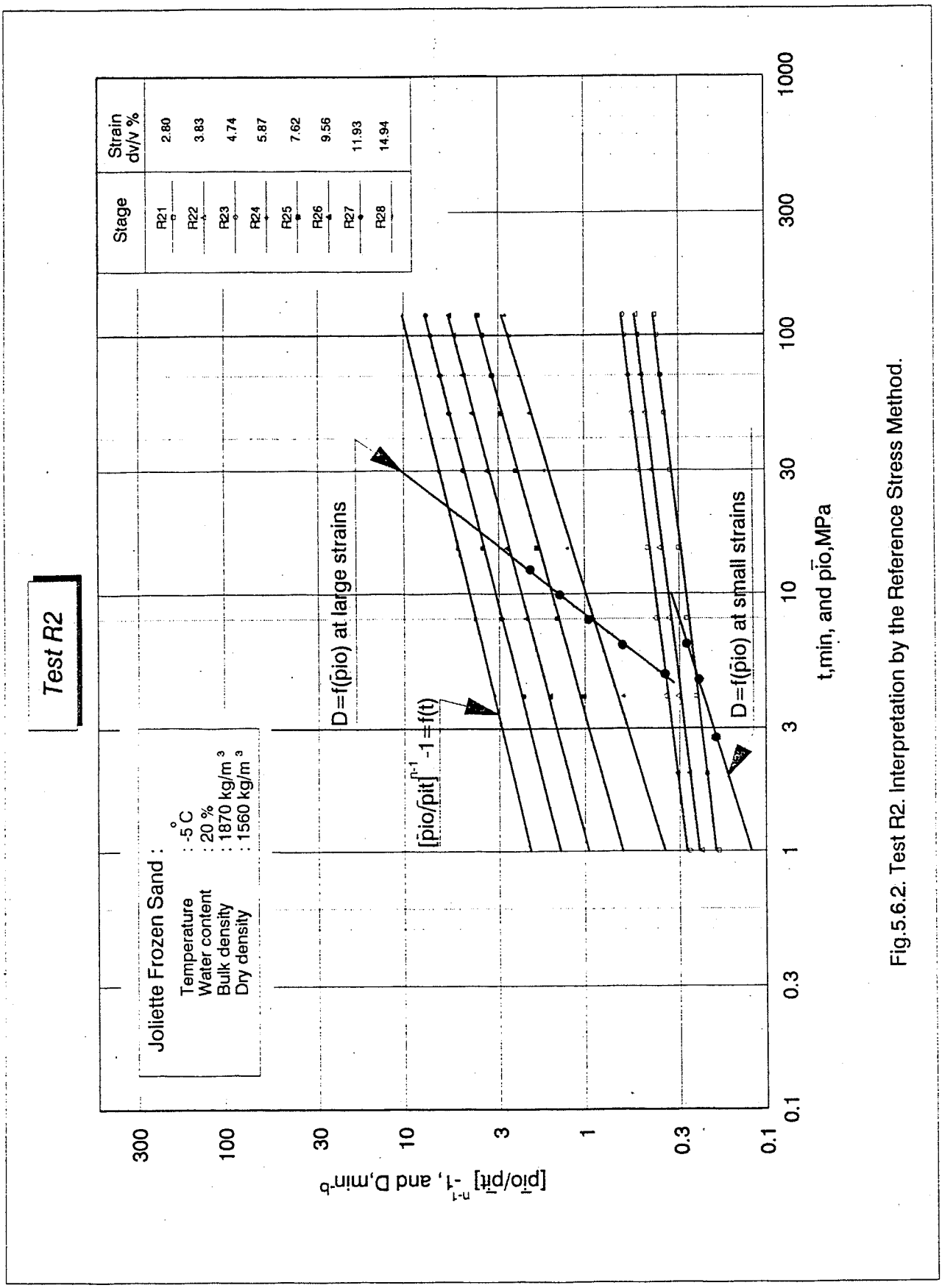

Fig.5.6.2. Test R2. Interpretation by the Reference Stress Method.

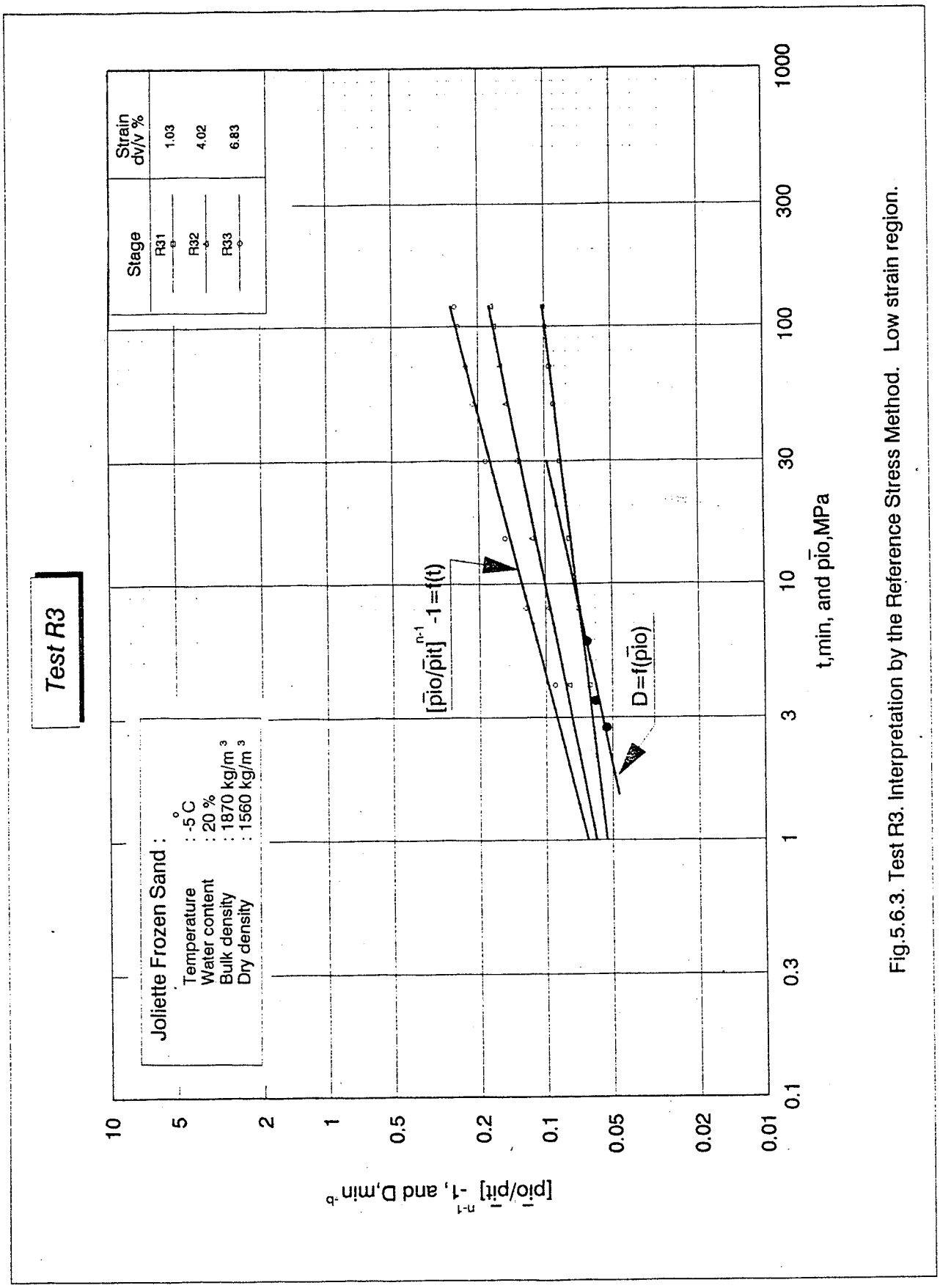

Fig.5.6.3. Test R3. Interpretation by the Reference Stress Method. Low strain region.

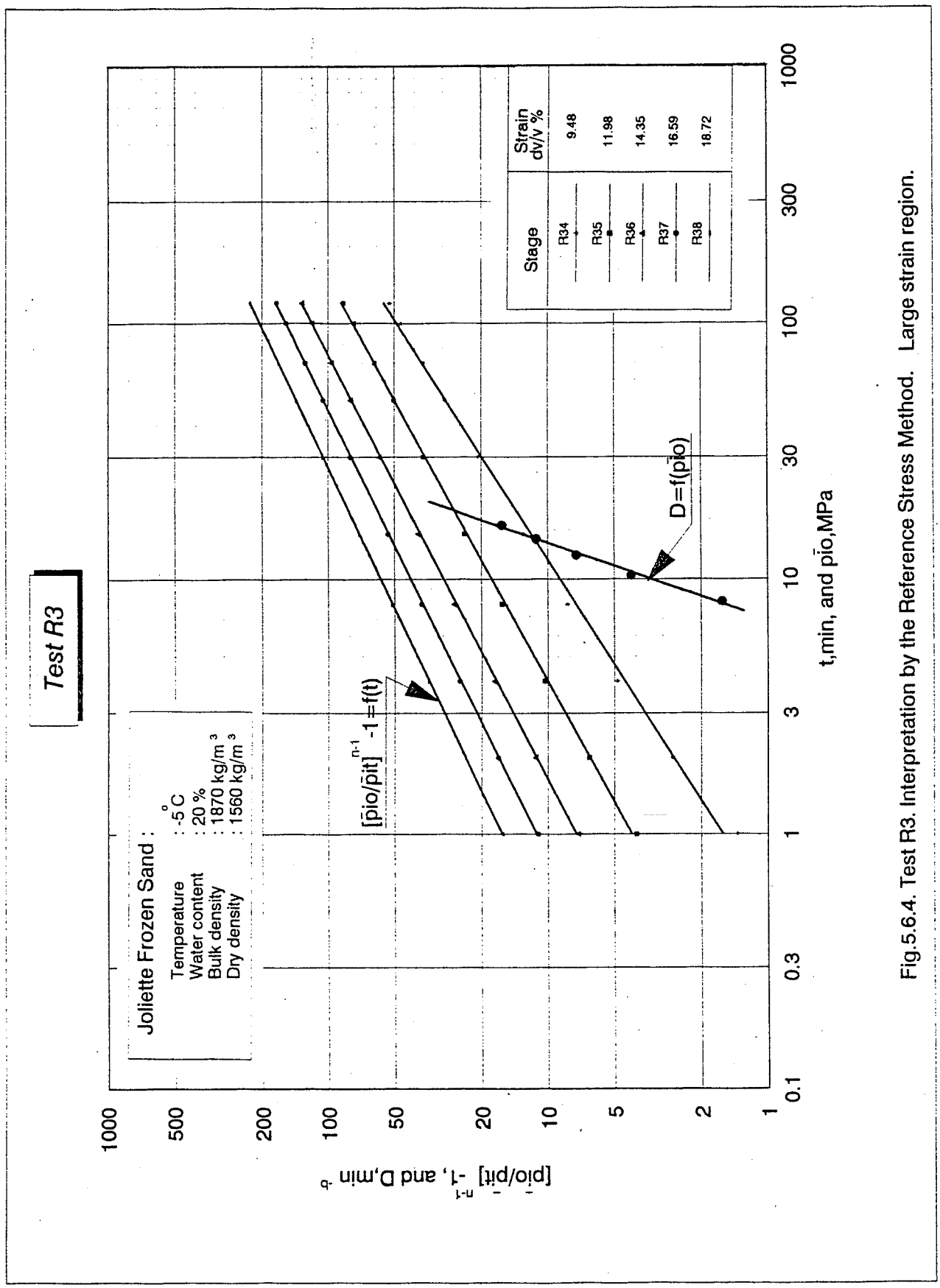

Fig.5.6.4. Test R3. Interpretation by the Reference Stress Method. Large strain region.

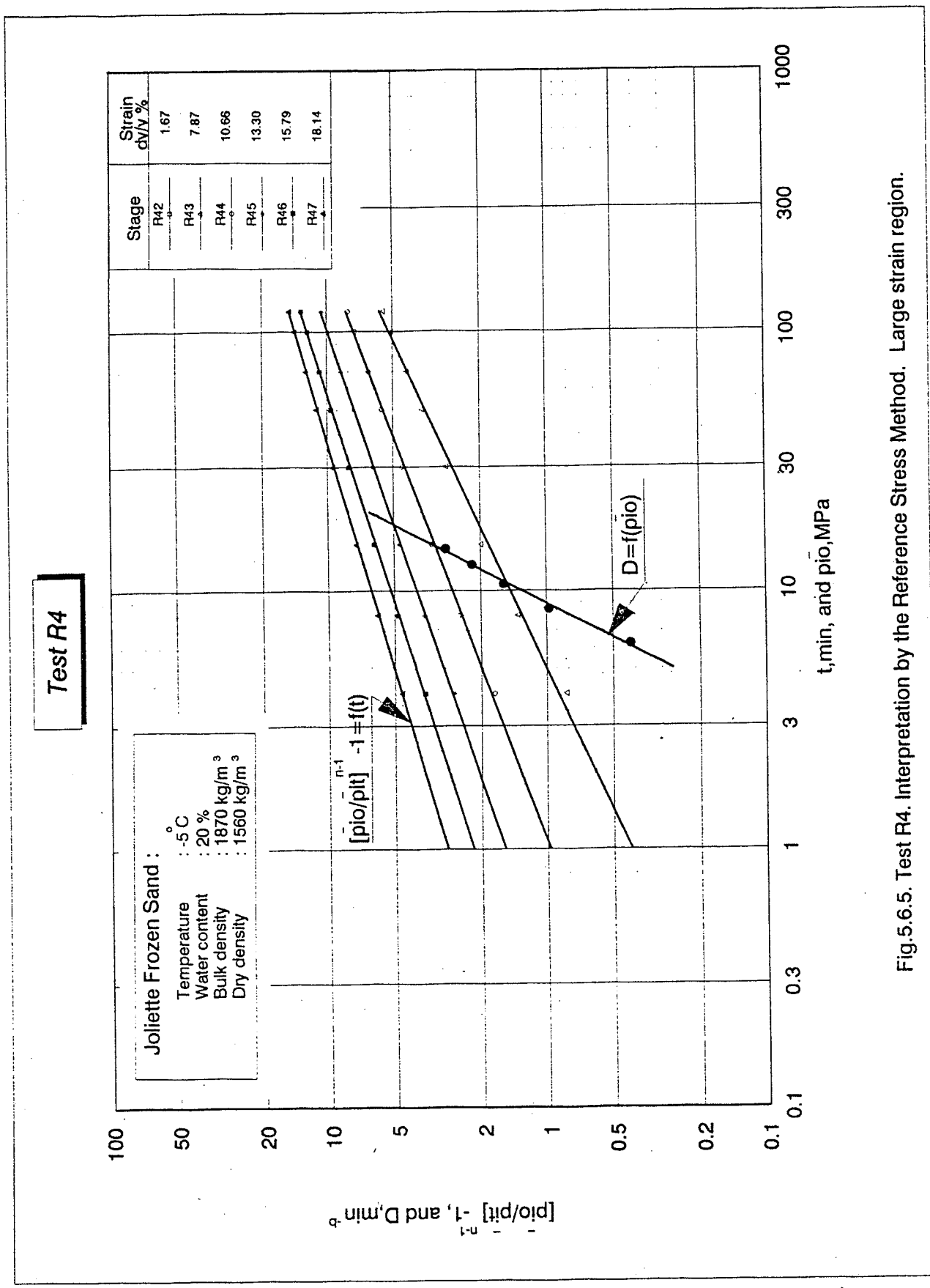

Fig.5.6.5. Test R4. Interpretation by the Reference Stress Method. Large strain region.

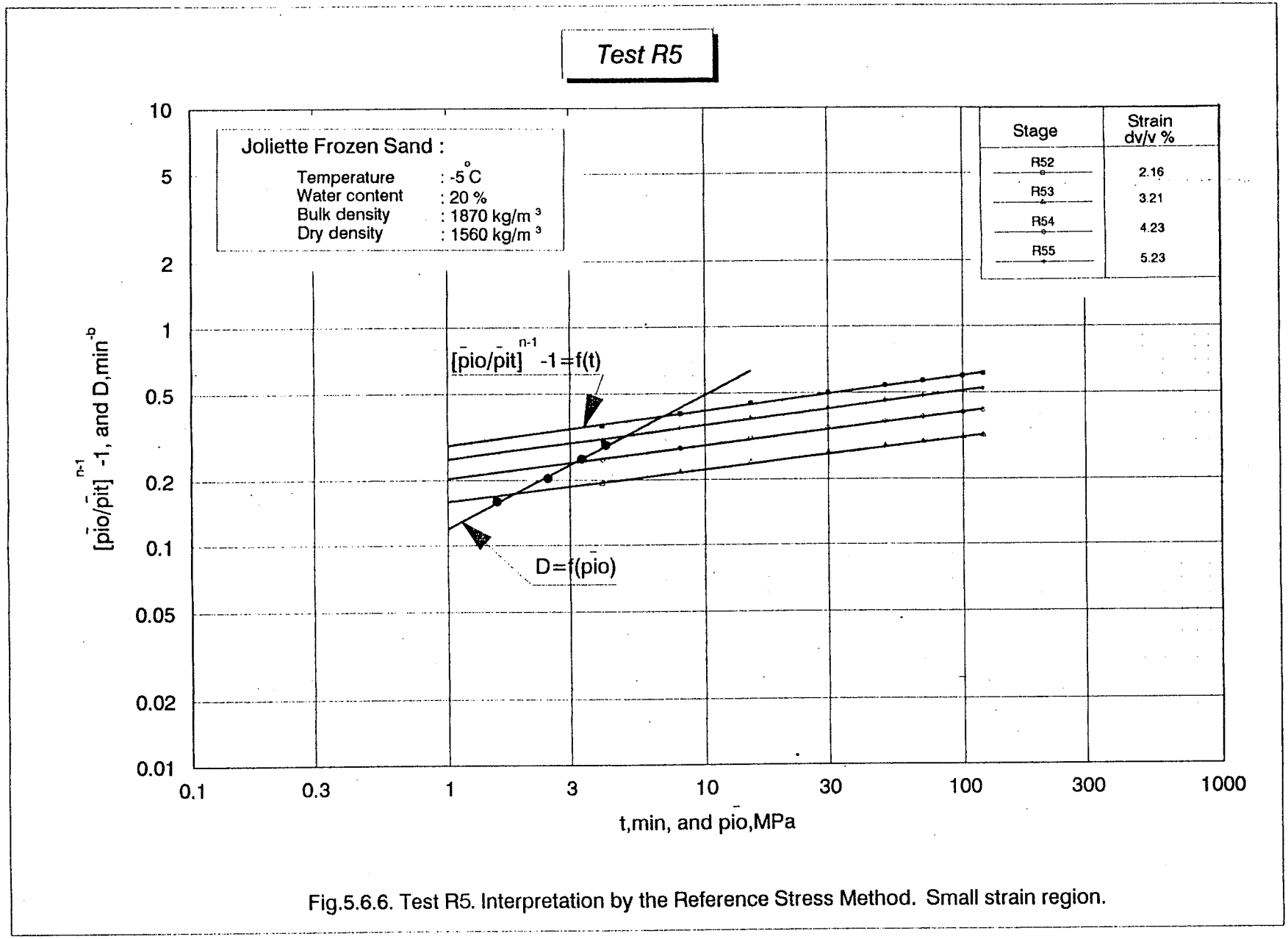

Fig.5.6.6. Test R5. Interpretation by the Reference Stress Method. Small strain region.

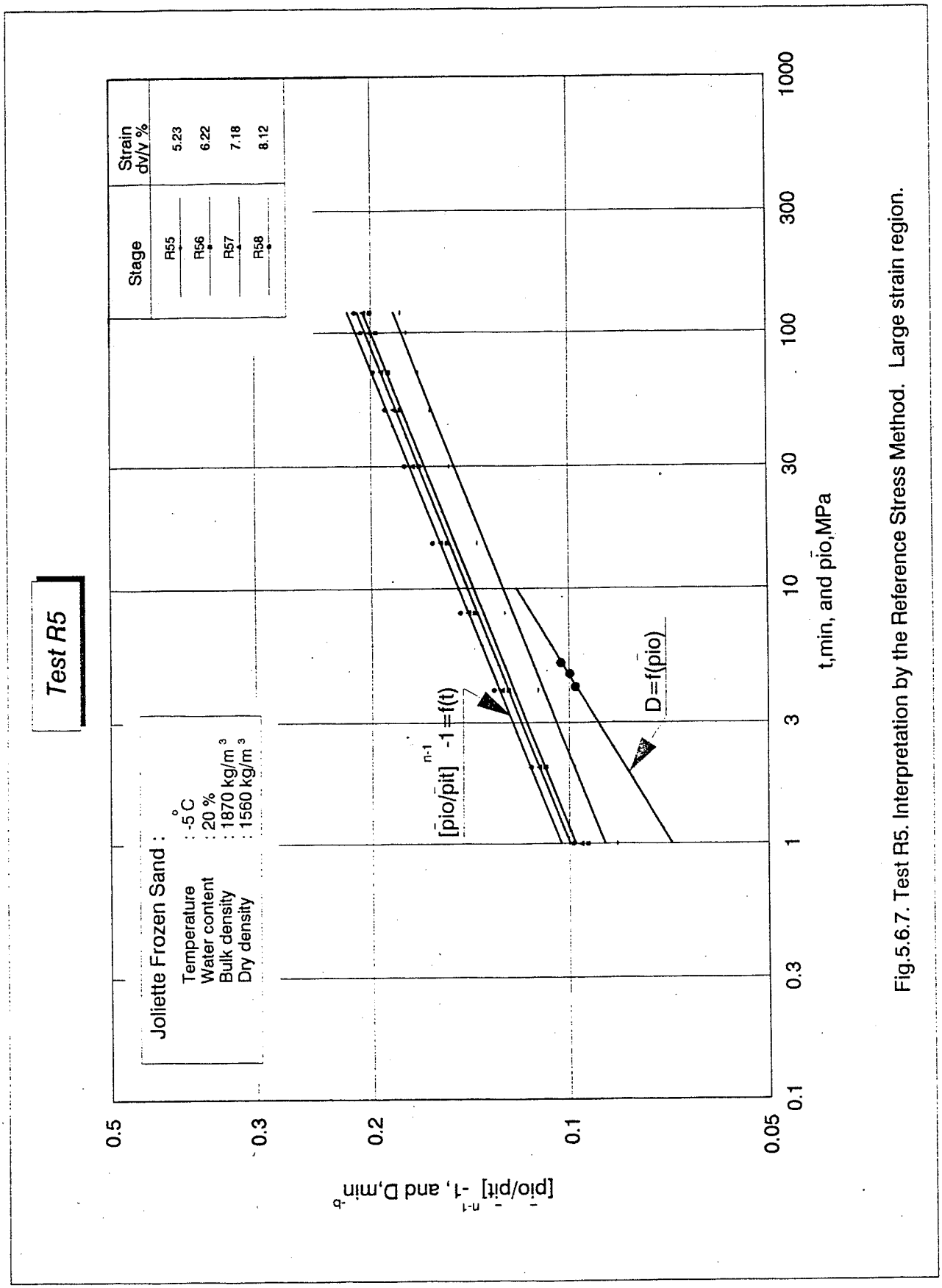

Fig.5.6.7. Test R5. Interpretation by the Reference Stress Method. Large strain region.

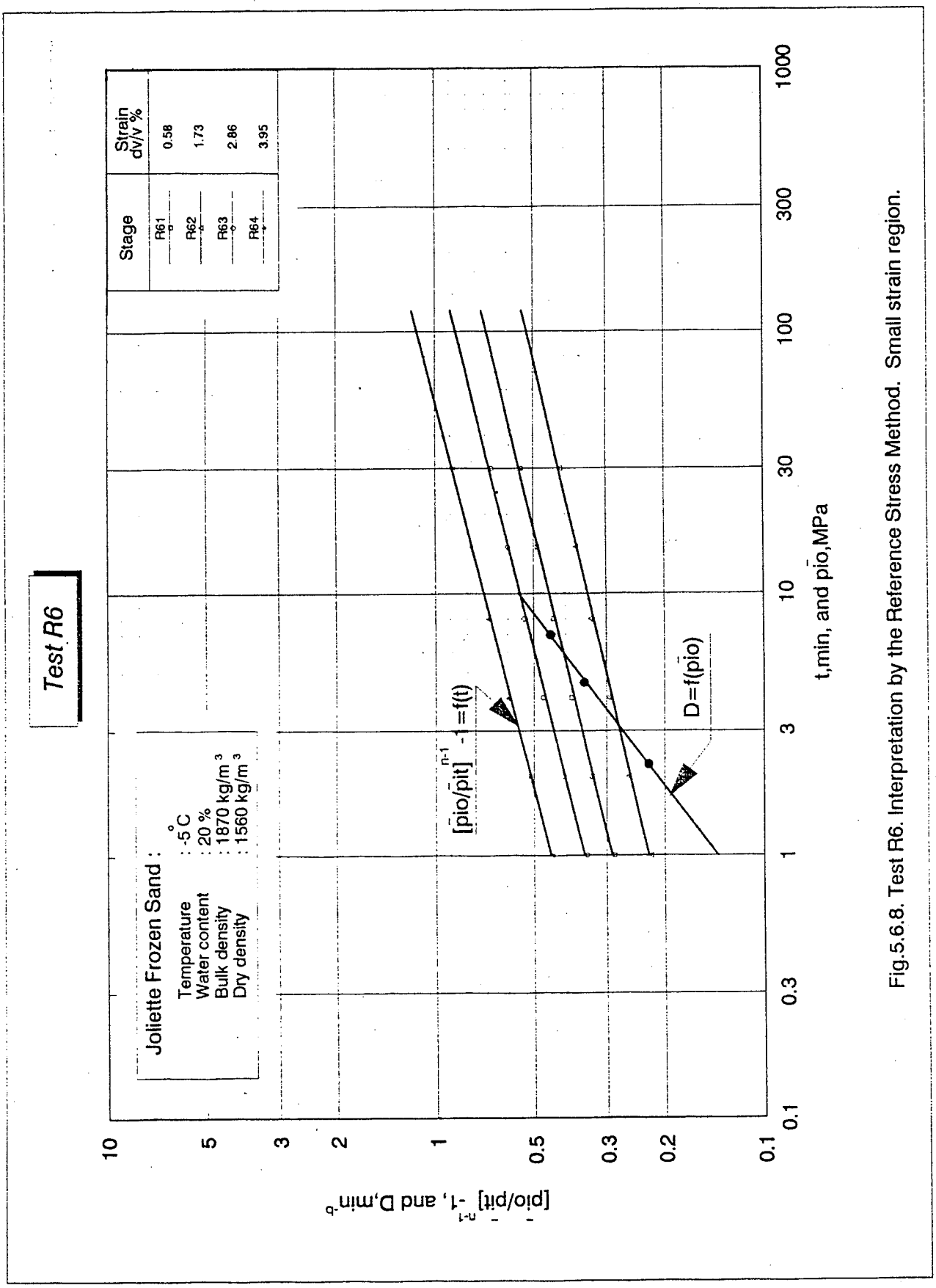

Fig.5.6.8. Test R6. Interpretation by the Reference Stress Method. Small strain region.

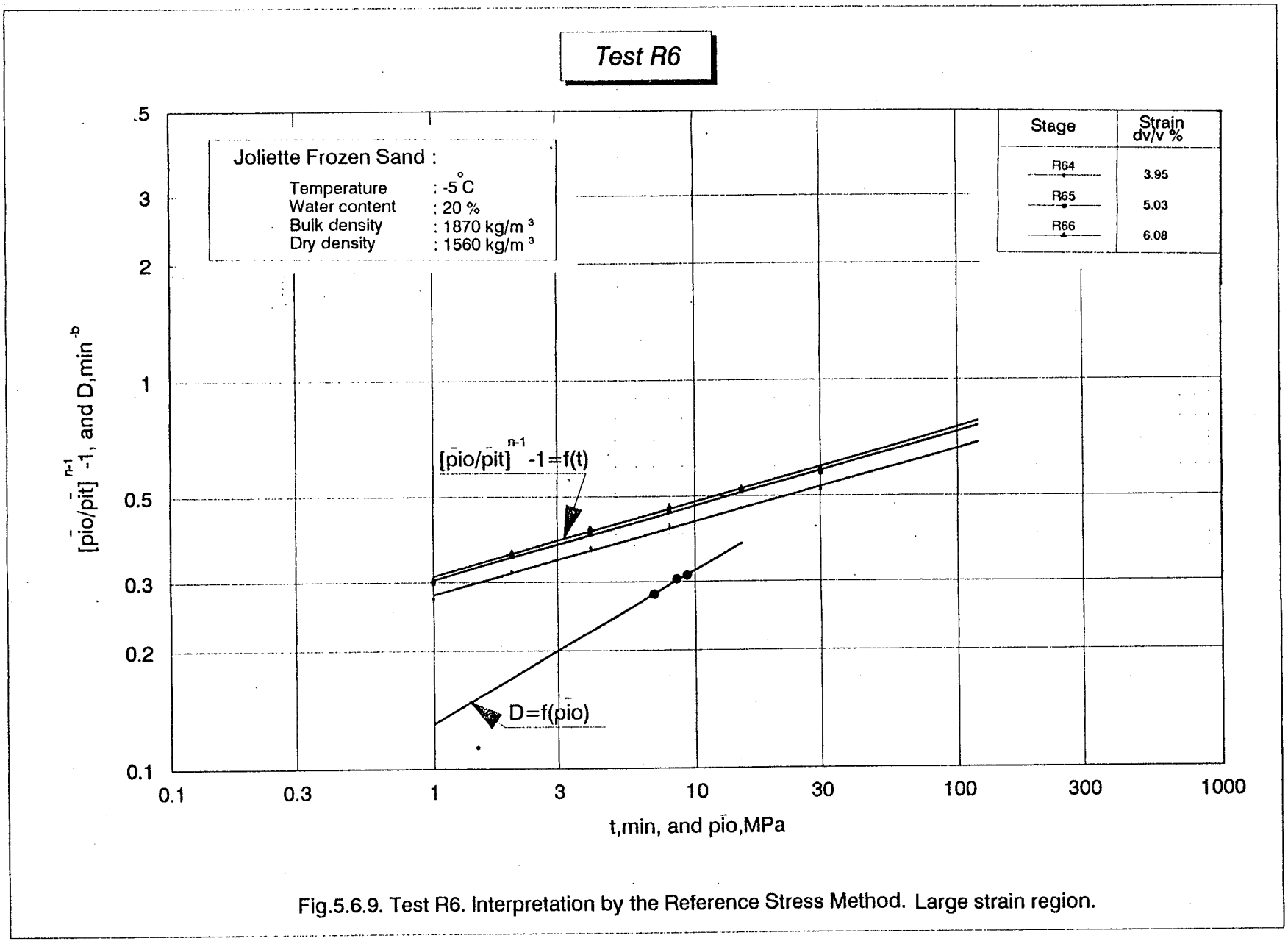

Fig.5.6.9. Test R6. Interpretation by the Reference Stress Method. Large strain region.

APPENDIX A

From a paper presented at OMAE 1987, Houston, Vol.IV, pp. 253-259.

USE OF THE BOREHOLE DILATOMETER STRESS-RELAXATION TEST FOR DETERMINING THE CREEP PROPERTIES OF ICE

B. Ladanyi and P.Huneault

1987

APPENDIX A

From OMAE 1987, Houston, Vol.IV, pp. 253-259.

USE OF THE BOREHOLE DILATOMETER STRESS-RELAXATION TEST FOR DETERMINING THE CREEP PROPERTIES OF ICE

B. Ladanyi and P. Huneault
Department of Civil Engineering
Ecole Polytechnique de Montreal
Montreal, Quebec, Canada

ABSTRACT

Field and laboratory tests carried out in the last 15 years have shown that the borehole dilatometer (pressuremeter) test offers a good possibility for determining the creep parameters of materials whose behavior can be described by a generalized power law, such as ice, frozen soils, rock salt and potash [7 - 15]. While, initially, mostly stage-loaded creep tests were performed, it was soon recognized that, because of the time limitation and stress redistribution problems in the former, borehole relaxation tests may offer certain practical advantages. For the latter type of tests, three different interpretation methods were proposed in previous papers by the senior author. Of these, two earlier ones were based on the aging creep theory[9, 10], while the last one [7], theoretically more advanced, was based on the flow creep theory. This paper presents a more general version of the latter solution, able to take into account the fact that the response of the host material may be different in loading and in unloading, as it is usually the case. It is considered that this new theory and interpretation method will lead to an improvement in the determination of creep parameters of ice from borehole relaxation tests.

NOMENCLATURE

a = radius of borehole
A = symbol defined by Eq A(11)
B = time exponent in Eq A(3)
D = symbol defined by Eq A(38)

e = basis of natural logarithms (2.71828...)
E = modulus of elasticity of ice in unloading
E_{sec} = secant deformation modulus of ice in loading
I = integral defined by EqA(23)
I^* = mI
k = stress exponent in EqA(2)
m = exponent in EqA(25)
n = stress exponent in EqA(3)
p_i = pressure applied on the borehole wall
p_{io} = initial pressure mobilized by rapidly expanding the borehole by Δa (Eq.A20)
p_{it} = value of p_i after relaxation time t
$\bar{p}_{io}$, $\bar{p}_{it}$ = net pressures defined by EqA(22)
p_o = total lateral far-field stress in ice
r = radius
s = exponent in EqsA(25)andA(26)
t = time
t^* = dimensionless time parameter defined by EqA(24)
V = current volume of the loaded portion of the borehole
α = parameter in EqsA(25) andA(26)
Δ = increment
ε = normal strain
$\dot{\varepsilon}_c$ = reference strain rate, related to σ_c
ε_e = Von Mises equivalent strain
ε_k = reference strain in EqA(13), related to σ_k
ρ = r/a
σ_c = stress at the rate $\dot{\varepsilon}_c$
σ_e = Von Mises equivalent stress
σ_{eo} = initial value of σ_e defined by EqA(13)
σ_{et} = relaxed value of σ_e after time t
σ_k = instantaneous stress at $\varepsilon = \varepsilon_k$
σ_r, σ_θ = principal stresses in radial and circumferential direction
σ_R = Reference Stress defined by EqA(33).

Subscripts:

i = instantaneous

c = creep

Dot above symbols denotes the time rate.

THEORY OF THE BOREHOLE RELAXATION TEST

As shown by Spence and Hult [20], in a kinematically determinate case, i.e., in which the strains and displacements are uniquely related, such as in a simple compression test, or in the expansion of hollow cylinders and spheres in incompressible materials, the solution of stress relaxation problems can be obtained by stating that at any point of the structure, the total displacement, equal to the sum of elastic and creep displacements at that point, should remain constant with time, or, alternatively, that the sum of elastic and creep displacement rates should be zero. Using this method, and assuming a power-law creep equation of Andrade type, these authors [20] have obtained both exact and approximate solutions for stress relaxation in a hollow sphere. Following the same procedure, the senior author [7] has extended their solutions to the problem of stress relaxation around a cylindrical cavity in an infinite medium under plane strain conditions.

In the two above mentioned papers [7, 20], it was assumed that the instantaneous response of the material is ideally elastic, with the same values of the modulus of elasticity in loading and unloading. The experience with performing borehole creep and relaxation tests in frozen soils and ice [1, 8], shows, however, that, invariably, the behavior in loading is different from that in unloading, the former being quite often non-linear and the latter linear. The reason is clearly that, under normal field conditions, the loading is in fact not quite "instantaneous", but takes several minutes, which is sufficient to include some transient creep effects.

In other words, as shown in [2, 18, 19 and 21], the response of ice in loading is a function of the loading rate, and so is also its apparent modulus of deformation.

For that reason, it was felt that for a more correct interpretation of borehole relaxation tests, a solution able to take into account this fact will be necessary. One such solution, assuming a non-linear pseudo-instantaneous response in loading, and a linear response in unloading during relaxation, is shown in the following.

In the following, two different kinds of solutions will be shown successively: First an "exact" solution, and then an approximate one, based on the Reference Stress Method. As the latter is necessary for field data processing, its degree of approximation will be checked against the results obtained by the exact solution for some typical values of creep parameters.

EXACT SOLUTION

For a non-linear visco-plastic material, such as frozen soil or polycrystalline ice, (or some other rheologically similar materials, e.g., rock salt and potash), the total strain attained after a given time under constant stress, can be expressed by

$$\varepsilon_e = \varepsilon_{e,pi} + \varepsilon_{e,c} \qquad A(1)$$

where $\varepsilon_{e,pi}$ is the pseudo-instantaneous (not necessarili linear-elastic) portion of the total strain, and $\varepsilon_{e,c}$ is the creep strain. The subscript "e" denotes here and hereafter the Von Mises equivalent stress or strain.

A non-linear pseudo-instantaneous response can be expressed by a power law of the form

$$\varepsilon_{e,pi} = \varepsilon_k(\sigma_e/\sigma_k)^k \qquad A(2)$$

and a similar power law form can be used also for expressing the creep strain accumulated during the time t, at a constant stress σ_e [4, 6]:

$$\varepsilon_{e,c} = (\dot{\varepsilon}_c/B)^B(\sigma_e/\sigma_c)^n\ t^B \qquad A(3)$$

In Eq.(2), σ_k is the value of σ_e at $\varepsilon_{e,pi} = \varepsilon_k$, and k is the exponent expressing the non-linearity of the response. (Note that for k = 1, $\sigma_k/\varepsilon_k = E$, and EqA(2) reverses to the Hooke's law).

EquationA(3) can also be written in a rate form, based on the time-hardening assumption:

$$\dot{\varepsilon}_{e,c} = d\varepsilon_{e,c}/d\tau = \bar{\dot{\varepsilon}}_c(\sigma_e/\sigma_c)^n \qquad A(4)$$

where τ denotes the time function

$$\tau = t^B \text{ , and} \qquad A(5)$$

$$\bar{\dot{\varepsilon}}_c = (\dot{\varepsilon}_c/B)^B \text{ .} \qquad A(6)$$

In these equations, B and n are the creep exponents, while σ_c denotes the value of σ_e at $\dot{\varepsilon}_{e,c} = \bar{\dot{\varepsilon}}_c$.

In unloading it is simply assumed that only the elastic portion of the total strain can be recovered, so that:

$$\Delta\varepsilon_e = \Delta\sigma_e/E \qquad A(7)$$

where E is the Young's modulus.

In a kinematically determinate case, such as the expansion of a cylindrical cavity in an incompressible medium, the relaxation formulation requires that the total strain rate is everywhere zero:

$$\dot{\varepsilon}_{e,i} + \dot{\varepsilon}_{e,c} = \dot{\varepsilon}_e = 0 \qquad A(8)$$

or, explicitly, using Eqs.(3) and (7),

$$\dot{\sigma}_e/E + F(t)\ \sigma_e^n = 0 \qquad A(9)$$

where

$$F(t) = A\ B\ t^{B-1}\ , \text{ and} \qquad A(10)$$

$$A = (\dot{\varepsilon}_c/B)^B\ \sigma_c^{-n}\ . \qquad A(11)$$

When EqA(9) is integrated between t = 0 and t, it gives [7]:

$$\sigma_{et}/\sigma_{eo} = [1 + (n-1)E\ \sigma_{eo}^{n-1}\ A\ t^B]^{-1/(n-1)} \qquad A(12)$$

where, according to EqA(2), for an applied constant strain ε_{eo}:

$$\sigma_{eo} = \sigma_k(\varepsilon_{eo}/\ \varepsilon_k)^{1/k} \qquad A(13)$$

and E is the modulus of elasticity in unloading.

EquationA(12) is a general relaxation equation for non-linear loading and linear unloading case. The corresponding relaxation equation for a cylindrical cavity in an infinite medium under plane strain conditions, is obtained by satisfying the radial equilibrium equation:

$$\frac{\partial\sigma_r}{\partial r} + \frac{\sigma_r - \sigma_\theta}{r} = 0 \qquad A(14)$$

where σ_r and σ_θ denote the radial and circumferential stress, respectively, at the radial distance r from the cavity axis.

Since, for plane strain,

$$\sigma_e = (\sqrt{3}/2)(\sigma_r - \sigma_\theta)\ , \qquad A(15)$$

EqA(14) can be integrated to give:

$$\sigma_r(r,t) = -(2/\sqrt{3})\int_a^r \sigma_e(r,t)(dr/r) + C(t) \qquad A(16)$$

where a denotes the cavity radius. With the boundary conditions: for r = a, $C(t) = \sigma_r(a,t) = p_{it}$, and for $r = \infty$, $\sigma_r(\infty,t) = p_o$, Eq.(16) becomes:

$$p_{it} = p_o + (2/\sqrt{3}) \int_{r=a}^{\infty} \sigma_e(r,t)(dr/r) \qquad A(17)$$

Substituting in EqA(17) for $\sigma_e(r,t)$ the value given by EqA(12), and considering that, for a non-linear Lamé's theory, with the Poisson's ratio equal to 0,5 [12]:

$$\sigma_e(r,0) = \sigma_e(a,0)(a/r)^{2/k} = (\sqrt{3}/k)(p_{io} - p_o)(a/r)^{2/k} \qquad (18)A$$

giving for t = 0, at the cavity wall (r = a):

$$\sigma_e = (\sqrt{3}/k)(p_{io} - p_o) \qquad A(19)$$

where, $p_{io} = p_i(a,0)$ is the value of the initial stress produced by expanding the hole by Δa , given by

$$p_{io} = \sigma_k(k/\sqrt{3})[(2/\varepsilon_k\sqrt{3})(\Delta a/a)_{t=0}]^{1/k} , \qquad A(20)$$

one gets finally,

$$\bar{p}_{it}/\bar{p}_{io} = (2/k)I \quad , \text{ where} \qquad A(21)$$

$$\bar{p}_{it} = p_{it} - p_o \ , \qquad A(22)$$

$$\bar{p}_{io} = p_{io} - p_o \ ,$$

and I denotes:

$$I = \int_{\rho=1}^{\infty} \frac{d\rho}{\rho\left[\rho^{2(n-1)/k} + (n-1)t^*/k^{n-1}\right]^{1/(n-1)}} \qquad (23)A$$

In EqA(23), $\rho = r/a$, and

$$t^* = E[\bar{p}_{io}\sqrt{3}]^{n-1} \, A \, t^B \qquad A(24)$$

where A is given by EqA(11).

It will be seen that the integral I has a general form:

$$I = \int_{1}^{\infty} \frac{dy}{y(y^m + \alpha)^s} \qquad A(25)$$

which, after substituting $y^m = w$, reduces to

$$I = \frac{1}{m}\int_1^\infty \frac{dw}{w(w+\alpha)^s} = \frac{1}{m} I^* \qquad A(26)$$

where, $m = 2(n-1)/k$, $\alpha = t^*(n-1)/k^{n-1}$, and $s = 1/(n-1)$.

Solutions of integrals of the type I^* can be found, e.g., in Gradshteyn and Ryzhik [3]. When I^* is known, the relaxation equation (21) becomes:

$$\bar{p}_{it}/\bar{p}_{io} = (2/k)I = I^*/(n-1) \qquad A(27)$$

This integration gives the following expressions for $\bar{p}_{it}/\bar{p}_{io}$, for different values of the exponent n:

For n = 1.5:

$$\bar{p}_{it}/\bar{p}_{io} = (8k/t^{*2})[\ln(1 + t^*/2\sqrt{k}) - (1 + 2\sqrt{k}/t^*)^{-1}] \qquad A(28)$$

For n = 2:

$$\bar{p}_{it}/\bar{p}_{io} = \frac{k}{t^*}\ln(1 + \frac{t^*}{k}) \qquad A(29)$$

For n = 3:

$$\bar{p}_{it}/\bar{p}_{io} = \frac{k}{2\sqrt{2t^*}}\ln\left(\frac{\sqrt{k^2 + 2t^*} + \sqrt{2t^*}}{\sqrt{k^2 + 2t^*} - \sqrt{2t^*}}\right) \qquad A(30)$$

For n = 4:

$$\frac{\bar{p}_{it}}{\bar{p}_{io}} = \frac{k}{3\sqrt[3]{3t^*}}\left\{\sqrt{3}\left[\frac{\pi}{3} - \arctan\left(\frac{\sqrt{3}\,\sqrt[3]{k^3 + 3t^*}}{\sqrt[3]{k^3 + 3t^*} + 2\sqrt[3]{3t^*}}\right)\right] - \frac{3}{2}\ln\left(\frac{\sqrt[3]{k^3 + 3t^*} - \sqrt[3]{3t^*}}{k}\right)\right\} \qquad A(31)$$

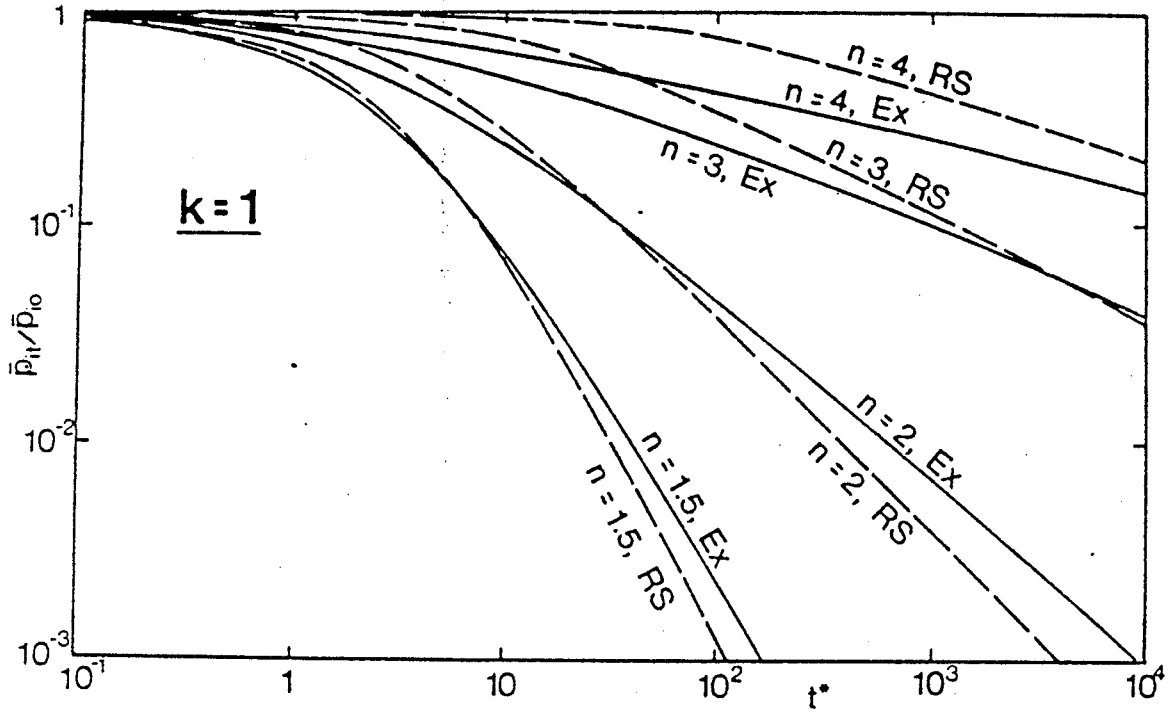

Fig. 1. Calculated Stress-Relaxation Curves:
EX = Exact Solution;
RS = Reference Stress Approximation.
k = 1, n = 1.5, 2, 3, 4.

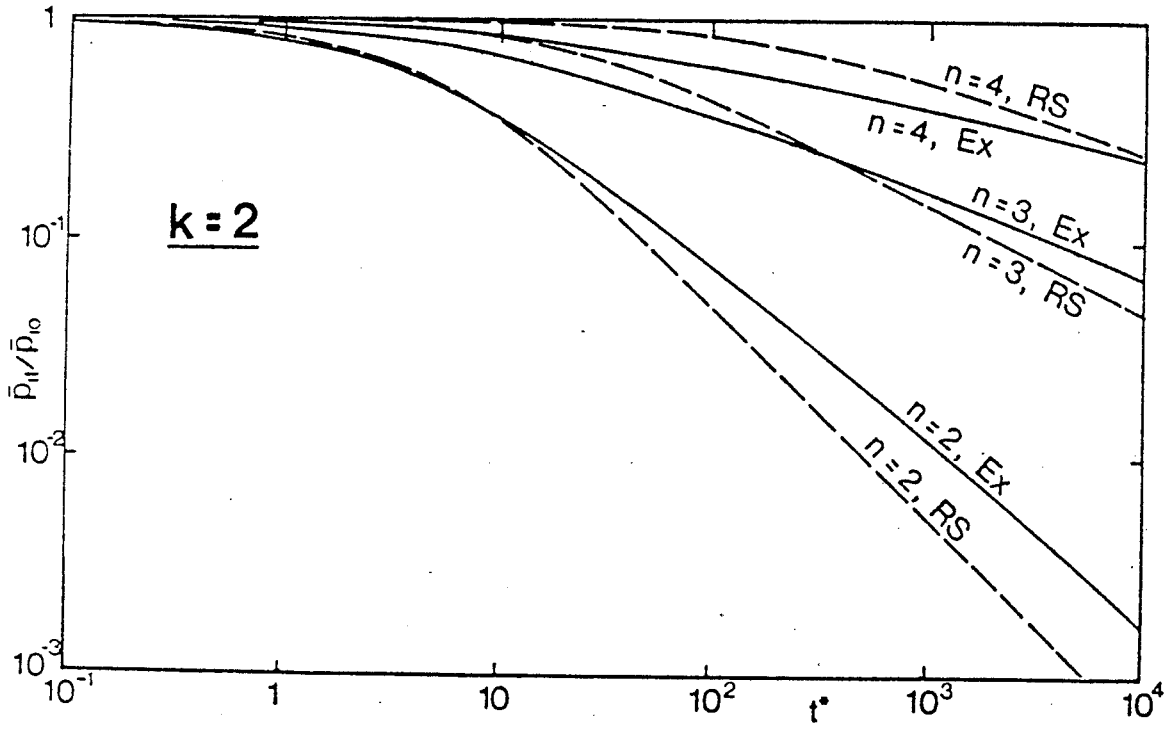

Fig. 2. Calculated Stress-Relaxation Curves:
EX = Exact Solution;
RS = Reference Stress Approximation.
k = 2, n = 2, 3, 4.

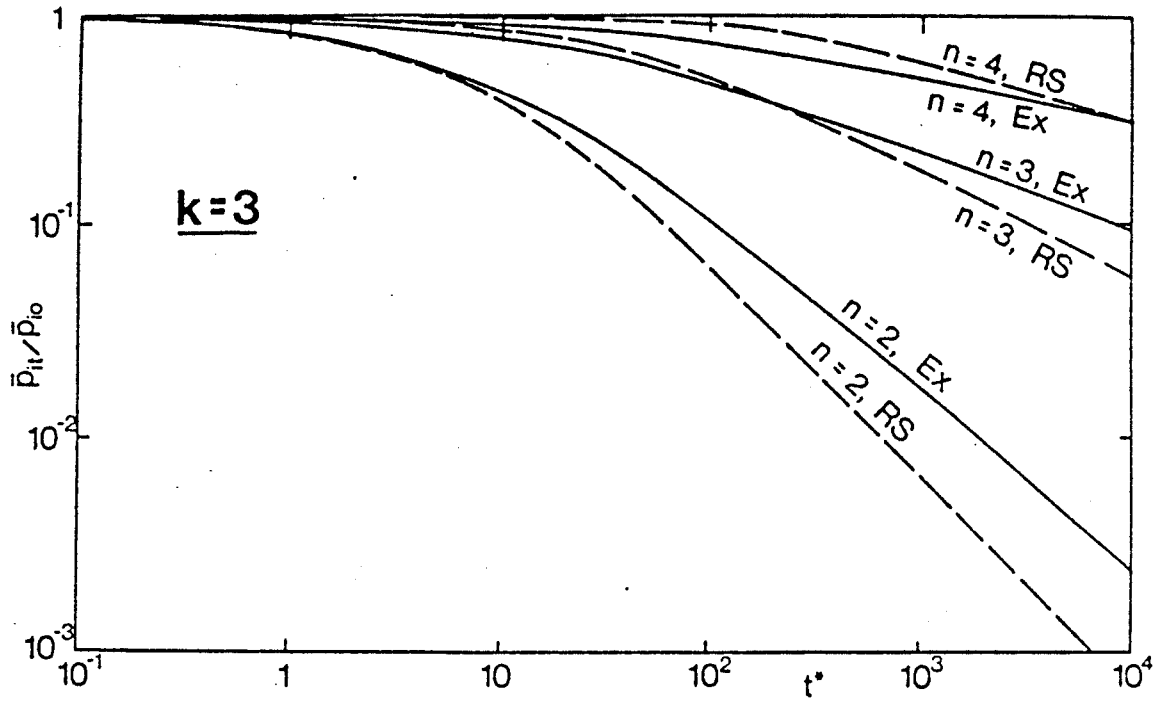

Fig. 3. Calculated Stress-Relaxation Curves:
EX = Exact Solution;
RS = Reference Stress Approximation.
k = 3, n = 2, 3, 4.

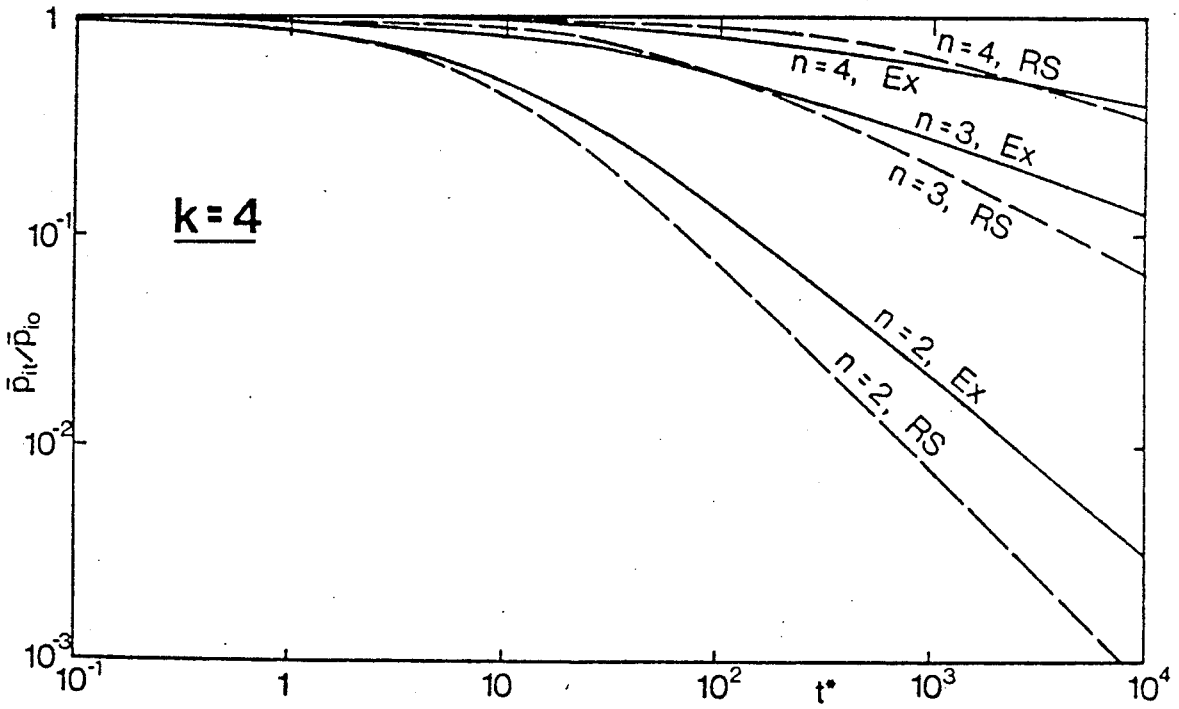

Fig. 4. Calculated Stress-Relaxation Curves:
EX = Exact Solution;
RS = Reference Stress Approximation.
k = 4, n = 2, 3, 4.

The above exact solutions, valid for the region of n-values which are of most interest for frozen soils and ice (n = 1.5, 2, 3, 4), enable to predict the relaxation behavior around a cylindrical cavity in a material whose general behavior under instantaneous loading, elastic unloading and creep has been previously experimentally determined. For the values of n other than 1.5, 2, 3, and 4, an interpolation is necessary.

Figures 1 to 4 show a set of dimensionless relaxation curves calculated from Eqs A(28) to A(31), for k = 1, 2, 3, and 4. The curves relate the relaxation ratio p_{it}/p_{io} with the dimensionless time t*, defined by A(24).

REFERENCE STRESS METHOD SOLUTION

Since the foregoing exact solution yields a different analytical expression for each different value of n, it does not lend itself well for solving the inverse problem, i.e., that of finding the values of creep parameters from the borehole relaxation data. For the latter purpose, it is proposed to use an approximate solution, based on the well-known Reference Stress Method. (E.g., Mackenzie [16], Spence and Hult [20]).

The Reference Stress, σ_R, is the stress at a characteristic locus in certain structures undergoing creep, where the stress remains constant (or nearly so) during the stress redistribution after loading. The existence of such a locus, whose position is independent of n - value, has been observed in rectangular beams under uniform bending, and in expansion of thick-walled cylinders and spheres. According to Mackenzie [16], a reference stress for a hollow pressurized cylinder in forward creep can be found by equating the stationary interior displacement rate, da/dt, for the actual n to the same quantity for n = 1. For a cylindrical cavity, expanding under plane strain conditions, in a material characterized by a power-law creep, Eq A(3), with $n \neq k \geq 1$, this gives:

$$\frac{da/a}{dt} = \left(\frac{\sqrt{3}}{2}\right)^{n+1} \bar{A} \left(\frac{2}{n}\right)^{n} \left(\frac{p_i - p_o}{\sigma_R}\right)^{n} = \left(\frac{\sqrt{3}}{2}\right)^{k+1} \bar{A} \left(\frac{2}{k}\right)^{k} \left(\frac{p_i - p_o}{\sigma_R}\right)^{k} \qquad A(32)$$

where $\bar{A} = (\dot{\varepsilon}_c/B)^B \; B \; t^{B-1}$. From Eq A(32) the Reference Stress is:

$$\sigma_R = \sqrt{3}(k^k/n^n)^{1/(n-k)} (p_i - p_o) \qquad A(33)$$

Substituting in Eq A(12) for σ_{eo} the value or σ_R given by Eq A(33), yields:

$$\bar{p}_{it}/\bar{p}_{io} = \left[1 + (n-1)t^*(k^k/n^n)^{(n-1)/(n-k)}\right]^{-1/(n-1)} \qquad A(34)$$

valid for any value of $k \neq n$. For $k = n$, the last term in the brackets in Eq A(34) becomes indeterminate, but it can be shown that it tends to the value:

$$(k^k/n^n)^{(n-1)/(n-k)} \underset{(k \to n)}{\to} (ne)^{-(n-1)} \qquad A(35)$$

where $e = 2.71828...$ is the basis of natural logarithms.

Dashed lines in Figs. 1 to 4 show the approximate relaxation curves calculated from Eqs A(34) and A(35). Comparison with the exact solution leads to the conclusion, expressed also in the previous paper [7], that the agreement is good for low values of n, but the discrepancy increases steadily with increasing n - values. Also, for large t* values, the Reference Stress Solution shows systematically a faster relaxation than the exact solution. Finally, it is also found that an increasing non-linearity of instantaneous response (a larger k - value) leads to an increased relaxation time, which, at first sight, seems to be contrary to the expectations. This result, however, is the consequence of assuming a power law (Eq.A13) for the instantaneous response. This law, for constant values of parameters $(\sigma_k, \varepsilon_k)$ and an increasing k, defines in fact a material of increasing rigidity.

REFERENCES

[1] Eckardt, H., and Ladanyi, B., "Dilatometer Laborversuche mit gefrorenem Sand," Die Bautechnik, Vol.60, No.2, 1982, pp. 56-65.

[2] Gold, L.W., and Sinha, N.K., "The Rheological Behavior of Ice at Small Strains," in Physics and Mechanics of Ice, Proceedings of the IUTAM Symposium (P. Tryde, ed.), Copenhagen,1979, pp. 117-128.

[3] Gradshteyn, I.S., and Ryzhik, I.M., "Table of Integrals, Series and Products," Academic Press, New York, 1965, 1086 p.

[4] Hult, J.A.H., "Creep in Engineering Structures," Blaisdel Publishing Company, Waltham, MA, 1966, 115 p.

[5] ISRM, "Suggested Methods for Deformability Determination using a Flexible Dilatometer," International Society for Rock Mechanics, Commission on Testing Methods, 1986, In Print.

[6] Ladanyi, B., "An Engineering Theory of Creep of Frozen Soils," Canadian Geotechnical Journal, Vol.19, 1972,pp.63-80.

[7] Ladanyi, B., "Borehole Relaxation Test as a Means for Determining the Bearing Capacity of Ice Covers," Proceedings 5th International Conference on Port and Ocean Engineering under Arctic Conditions, Trondheim, Norway, 1979, Vol.1, pp. 757-770.

[8] Ladanyi, B., "Stress- and Strain-Rate-Controlled Borehole Dilatometer Tests in Ice," Proceedings Permafrost Engineering Workshop, Quebec City, 1979, NRCC-ACGR Technical Memo No.130, 1980, pp. 57-69.

[9] Ladanyi, B., "Borehole Creep and Relaxation Tests in Ice-Rich Permafrost," R.J.E. Brown Memorial Volume, NRCC-ACGR, Ottawa, 1982, pp. 406-415.

[10] Ladanyi, B., Barthelemy, E., and Saint-Pierre, R., "In-Situ Determinetion of Creep Properties of Ice Covers by Means of Borehole Creep and Relaxation Tests," Proceedings, Workshop on the Bearing Capacity of Ice Covers, Winnipeg, NRCC-ACGR, Technical Memo No.123, 1978, pp. 44-64.

[11] Ladanyi, B., and Eckardt, H., "Dilatometer Testing in Thick Cylinders of Frozen Sand," Proceedings, 4th International Conference on Permafrost, Fairbanks, Alaska, National Academy Press, Washington, 1983, Vol.1, pp. 677-682.

[12] Ladanyi, B., and Gill, D.E., "In-Situ Determination of Creep Properties of Rock Salt," Proceedings, 5th Congress of the International Society for Rock Mechanics, Melbourne, Australia, 1983, Vol.1A, pp. A219-A225.

[13] Ladanyi, B., and Gill, D.E., "Determination of Creep Parameters of Rock Salt by Means of a Borehole Dilatometer," Proceedings, First Conference on the Mechanical Behavior of Salt, Penn State University, 1981, TransTech Publications, 1984, pp. 473-491.

[14] Ladanyi, B., and Johnston, G.H., "Evaluation of In-Situ Properties of Frozen Soils with the Pressuremeter," Proceedings, Second International Conference on Permafrost, Yakutsk, USSR, North American Volume, NAS, Washington, 1973, pp. 310-318.

[15] Ladanyi, B., and Saint-Pierre, R., "Evaluation of Creep Properties of Sea Ice by Means of a Borehole Dilatometer," Proceedings, IAHR Symposium on Ice Problems, Lulea, Sweden, 1978, Vol.I, pp. 97-115.

[16] Mackenzie, A.C., "On the Use of Simple Uniaxial Test to Estimate Deformation Rates in Some Structures Undergoing Creep," International Journal of Mechanical Sciences, Vol. 10, 1968, pp. 441-453.

[17] Rabotnov, Y.N., "Creep Problems in Structural Members," Translated from Russian, North Holland Publishing Company, 1969.

[18] Sinha, N.K., "Short-Term Rheology of Polycrystalline Ice," Journal of Glaciology, Vol. 21, No.85, 1978, pp.457-473.

[19] Sinha, N.K., "Constant Stress Rate Deformation Modulus of Ice," Proceedings, 6th Internat. Conf.on Port and Ocean Engrg. under Arctic Conditions, Quebec City, 1981, Vol. 1, pp. 216-224.

[20] Spence, J., and Hult, J.A.H., "Simple Approximations for Creep Relaxation," Int. Journal of Mechanical Sciences, Pergamon Press, Vol. 15, 1973, pp. 741-755.

[21] Traetteberg, A., Gold, L.W., and Frederking, R., "The Strain Rate and Temperature Dependence of Young's Modulus of Ice," Proc. 3rd IAHR Symp. on Ice Problems, Hanover, NH, 1975, pp. 479-486.

APPENDIX B

RELAXATION SOLUTIONS FOR CREEP

Paul A. Huneault
R.S.W. Consultants, Montréal
1990

RELAXATION SOLUTIONS FOR CREEP

Paul A. Huneault
Researcher
Institute for Research in Construction
National Research Council Canada
Ottawa, Ontario, Canada
K1A 0R6

Abstract

Relaxation testing is an important alternative for investigating the creep properties of a material. The solution for the strain-hardening form of the power law is derived and compared to the solution for the time-hardening form of the same power law. Relaxation solutions for the exponential and hyperbolic creep are also presented, confirming the affinities between the power, exponential and hyperbolic sine creep laws for the proper stress levels.

Introduction

Stress relaxation is a fundamental process by which an effective measure of the stress state within a solid can be seen to decrease in time due to the conversion of elastic strain into inelastic strain. Events unseemingly related as the tuning of a guitar, a loose bolt or a faulty gasket may have in common the stress relaxation. Designers in the fields of nuclear power, prestressed concrete and even foundations in permafrost, but to name a few, eventually have to take into consideration stress relaxation effects albeit to varying degrees.

In relation with creep, integral forms for relaxation are given in Findley et al. (1976) whereas related phenomenological theories are discussed in Rabotnov (1969) and Boyle and Spence (1983). Various experimental aspects of stress relaxation testing are to be found in ASTM (1979).

A relaxation test can generally be viewed as the inverse of a creep test: instead of maintaining a constant load and recording strain levels in time, an initial strain level is maintained and the decaying stress monitored over time. The importance of relaxation testing lies essentially in the potential it offers for verifying experimentally and independently a material flow rule based solely on creep testing. Intuitively, if a mathematical formulation models adequately

both creep and relaxation, it is well on its way to reliably modelling intermediate states for the material. The following attempts to provide additional tools for probing non-linear and time-dependent material behaviour by means of the relaxation test. Specifically, we concentrate on the popular time- and strain-hardening formulations as well as the exponential and hyperbolic creep laws.

Time-Hardening Versus Strain-Hardening

Creep testing consists of recording the strain over time of uniaxial specimens submitted to constant stress. A form of creep law that has widely been fitted to such experimental data, for various materials, is a power law in both stress σ and time t

$$\varepsilon^c = K\sigma^n t^b \tag{1}$$

where ε^c is the creep strain and

$$\begin{aligned} &K > o, \\ &n \geq 1, \\ &o < b \leq 1, \end{aligned} \tag{2}$$

are the creep parameters. Deriving the latter with respect to time t for a constant stress state yields the so-called "time-hardening" creep equation

$$\dot{\varepsilon}^c = K\sigma^n\, bt^{b-1}. \tag{3}$$

The "strain-hardening" form for (1) is then obtained by substituting t from Eq. (1) into eq. (3), i.e.,

$$\dot{\varepsilon}^c = Q\sigma^m(\varepsilon^c)^p \tag{4}$$

where, in terms of the parameters given in eq. (2),

$$\begin{aligned} Q &= b\,K^{1/b} && > 0, \\ m &= n/b && \geq 1, \\ p &= (b-1)/b && \leq 0. \end{aligned} \tag{5}$$

Under constant stress, eqs. (3) and (4) are equivalent. If the effects of the stress variation rates on creep are negligible, applying eqs. (3) and (4) to a variable stress condition generally leads upon integration to different cumulative values ε^c. Exceptionally, for (b = 1) or (p = 0), eqs. (3) and (4) are equivalent regardless of the stress history over time.

To complement the creep testing, we may wish to apply eqs. (3) and (4) to a relaxation test characterized by maintaining a zero total strain-rate over time. Upon submitting, for example, a uniaxial specimen to an initial stress level σ_o, the test plattens may be fixed in a stationary position and stress levels recorded in time. Under these conditions, total strain-rate $\dot{\varepsilon}^{tot}$ approaches zero(1)

$$\dot{\varepsilon}^{tot} = \dot{\varepsilon}^c + \dot{\varepsilon}^e = 0 \tag{6}$$

where $\dot{\varepsilon}^c$ and $\dot{\varepsilon}^e$ are the components of $\dot{\varepsilon}^{tot}$ and $\dot{\varepsilon}^e$ refers to the elastic strain-rate portion

$$\dot{\varepsilon}^e = \dot{\sigma}/E \tag{7}$$

with E denoting the Young's modulus. Hence, from eqs. (3), (6) and (7), the relaxation of a time-hardening specimen follows

$$K\sigma^n b t^{b-1} + (\dot{\sigma}/E) = 0 \tag{8}$$

whereas, from eqs. (4), (6) and (7), the relaxation of a strain-hardening material must satisfy

$$Q\sigma^m(\varepsilon^c)^p + (\dot{\sigma}/E) = 0. \tag{9}$$

Spence and Hult (1973) relate the time-hardening solution to eq. (8) in the form

$$\chi(t) = \left[1 + (n-1)\,\sigma_o^{n-1}\,t^*\right]^{-1/(n-1)} \tag{10}$$

---

(1) for a relative (test machine/specimen) stiffness ratio >> 1

with

$$\chi(t) = \sigma(t)/\sigma_o \tag{11}$$

and t* denoting the transformed "time"

$$t^* = EKt^b \tag{12}$$

under the boundary condition

$$(\sigma = \sigma_o) @ (t = 0). \tag{13}$$

The purpose of the following is to define strain-hardening relaxation for a material that creeps according to eq. (4) and compare it to its time-hardening counterpart eq. (10). Rabotnov (1969) discusses the relaxation of a strain-hardening law associated with an exponential function of the stress.

Strain-Hardening Relaxation

Whereas expression (8) is explicit in the stress σ, expression (9) is implicit in the same. Thus, noting the Bernouilli differential equation form of eq. (4), we first obtain for the strain-hardening creep strain ε^c

$$(\varepsilon^c)^{1-p} = (1-p)\int Q\sigma^m dt + C_1 \tag{14}$$

where C_1 is an integration constant. Imposing for virgin specimens the condition

$$(\varepsilon^c = 0) @ (t = 0) \tag{15}$$

then $(C_1 = 0)$ and

$$\varepsilon^c = \left[(1-p)\int Q\sigma^m\, dt\right]^{1/(1-p)} \tag{16}$$

which when combined with eq. (9) yields

$$\dot{\sigma} + A\,\sigma^m \left[\int \sigma^m\, dt\right]^B = 0 \tag{17}$$

with

$$A = EQ\,[(1 - p)Q]^B$$
$$B = p/(1 - p) \tag{18}$$

Expression (17) is the explicit fundamental law for relaxation of a strain-hardening material and may be solved as follows. Denoting

$$v \equiv \int \sigma^m\, dt \tag{19}$$

then

$$\dot{v} = \sigma^m \tag{20}$$

and eq. (17) transforms to

$$\dot{\sigma} = -A\dot{v}v^B \tag{21}$$

the solution of which is

$$\sigma = \frac{-A}{B+1} v^{B+1} + C_2 \tag{22}$$

where C_2 is a second integration constant. Expanding eq. (22) using eq. (19) now gives

$$\sigma = \frac{-A}{B+1}\left[\int \sigma^m dt\right]^{B+1} + C_2 \tag{23}$$

for which, from eq. (13), we get $(C_2 = \sigma_o)$. Thereafter

$$\left[\left(\frac{B+1}{A}\right)(\sigma_o-\sigma)\right]^{1/(B+1)} = \int \sigma^m dt \tag{24}$$

and retaking the derivatives on both sides of eq. (24), with respect to t, along with eq. (18), yields

$$\frac{\dot{\sigma}}{\sigma^m(\sigma_o-\sigma)^p} = -E^{1-p}Q \tag{25}$$

or

$$\int_{\sigma_o}^{\sigma} \frac{(\sigma_o-\sigma)^M}{\sigma^m} d\sigma = -E^{1+M} Q \int_0^t dt \tag{26}$$

with, from eq. (5),

$$M = -p \geq 0 \cdot \tag{27}$$

Denoting

$$\varnothing_m^M \equiv \int_{\sigma_o}^{\sigma} \frac{(\sigma_o - \sigma)^M}{\sigma^m} d\sigma, \tag{28}$$

eqs. (5), (12) and (27) now give

$$\varnothing_m^M + \frac{(t^*)^{M+1}}{M+1} = 0 \tag{29}$$

where, for example and in particular (Gradshteyn & Ryzhik (1965)),

$$\varnothing_m^o = \frac{\sigma^{1-m} - \sigma_o^{1-m}}{1-m}$$

$$\varnothing_m^1 = \frac{\sigma^{1-m}(\sigma_o-\sigma)}{2-m} + \frac{\sigma^{1-m}\sigma_o}{(2-m)(1-m)} - \frac{\sigma_o^{2-m}}{(2-m)(1-m)}$$

$$\varnothing_m^2 = \frac{\sigma^{1-m}(\sigma_o-\sigma)^2}{(3-m)} + \frac{2\sigma^{1-m}(\sigma_o-\sigma)\sigma_o}{(3-m)(2-m)} + \frac{2\sigma^{1-m}\sigma_o^2}{(3-m)(2-m)(1-m)} - \frac{2\sigma_o^{3-m}}{(3-m)(2-m)(1-m)} \tag{30}$$

$$\varnothing_m^3 = \frac{\sigma^{1-m}(\sigma_o-\sigma)^3}{(4-m)} + \frac{3\sigma^{1-m}(\sigma_o-\sigma)^2\sigma_o}{(4-m)(3-m)} + \frac{(3\cdot 2)\sigma^{1-m}(\sigma_o-\sigma)\sigma_o^2}{(4-m)(3-m)(2-m)} + \frac{(3\cdot 2)\sigma^{1-m}\sigma_o^3}{(4-m)(3-m)(2-m)(1-m)} - \frac{(3\cdot 2)\sigma_o^{4-m}}{(4-m)(3-m)(2-m)(1-m)}$$

Here, we may verify that

$$\varnothing_m^M = \frac{\sigma^{1-m}}{(M-m+1)}(\sigma_o-\sigma)^M + \frac{M\sigma_o}{(M-m+1)}\varnothing_m^{M-1} \tag{31}$$

with this recursion formula ultimately leading to

$$\varnothing_m^M = \left[\sigma^{1-m}\sum_{r=0}^{M}(\sigma_o-\sigma)^{M-r}\sigma_o^r\frac{M!}{(M-r)!}\frac{\prod_{k=0}^{M-r}(k-m)}{\prod_{k=0}^{M+1}(k-m)}\right] - \frac{M!\sigma_o^{M+1-m}}{\prod_{k=1}^{M+1}(k-m)} \tag{32}$$

under the usual notation

$$M! = M(M-1)(M-2)\ldots(1) \tag{33}$$

$$0! = 1$$

$$\prod_{y=0}^{s} f(y) = f(0)\cdot f(1)\cdot f(2)\cdots f(s-1)\cdot f(s)$$

Reintroducing the dimensionless form (11), eq. (32) transforms to

$$\varnothing_m^M = \frac{\sigma_o^{M+1-m}(M!)}{\prod_{k=1}^{M+1}(k-m)} \left\langle \chi^{1-m} \left[\sum_{r=0}^{M} (1-\chi)^{M-r} \frac{\prod_{k=0}^{M-r}(k-m)}{(M-r)!m} \right] + 1 \right\rangle \tag{34}$$

Turning now to the binomial series

$$(a+x)^n = \sum_{k=0}^{n} \binom{n}{k} x^k a^{n-k}$$

$$\binom{n}{k} \equiv \frac{n!}{(n-k)!k!} \tag{35}$$

we have for a component of eq. (34)

$$(1-\chi)^{M-r} = \sum_{z=0}^{M-r} \binom{M-r}{z} \chi^z (-1)^{2(M-r)-z} \tag{36}$$

such that expressions (29), (34) and (36) finally combine to give the relaxation equation for a strain-hardening material as

$$\left[\sum_{r=o}^{M} \frac{\prod_{k=o}^{M-r}(k-m)}{\prod_{k=0}^{M+1}(k-m)} \sum_{z=o}^{M-r} \frac{(-1)^{2(M-r)-z}}{(M-r-z)!Z!} \chi^{1-m+z} \right]$$

$$+ \frac{(t^*)^{M+1}}{(M+1)!\sigma_o{}^{M+1-m}} - \frac{1}{\prod_{k=1}^{M+1}(k-m)} = 0 \tag{37}$$

Expression (37) is a polynomial of degree (m-1) in $\chi(t) = \sigma(t)/\sigma_o$. The relaxation solution $[\chi(t)]$ is that root bracketed between the values 0 and 1 for particular values of σ_o, t*, M and m. The numerical solution of eq. (37) is straightforward. Newton-Raphson combined with bisection are the methods of choice (Press et al. (1986)). The singularity of the root between the values of 0 and 1 and hence of the solution, can easily be verified by further bracketing.

For comparison purposes, the time-hardening relaxation solution as given in eq. (10) can be transformed to the notation prevalent in eq. (37) as

$$\chi(t) = \left[1 + \frac{m - (M+1)}{M+1}\, \sigma_o^{(m-(M+1))/(M+1)}\, t^*\right]^{(M+1)/(M+1-m)} \qquad (38)$$

From a previous discussion of eqs. (3) and (4), eq. (37) should reduce to eq. (38) for ($M = -p = 0$). That such is the case can easily be verified.

The time- and strain-hardening relaxation solutions are compared for those ranges of parameters given in Table (1). The n values cited span a broad range of materials including but not limited to most structural metals, ice, permafrost, rock salt, etc.

TABLE 1: EQUIVALENCIES BETWEEN CREEP PARAMETERS, EQS. (5) AND (27)

	m VALUES					M VALUES
b \ n	2	3	4	5	6	
1/4	8	12	16	20	24	3
1/3	6	9	12	15	18	2
1/2	4	6	8	10	12	1
1	2	3	4	5	6	0

Although the relaxation is a function of the initial stress level σ_o as given in eqs. (37) and (38), this feature has effectively been subtracted from Figures (1) to (4) by first isolating from eq. (38) a value of t* for a given value of $\chi(t)$ and inserting the same into eq. (37). Thus Figures (1) to (4) are master curves, independent of σ_o.

As shown in Figure (1), time-hardening and strain-hardening relaxation are equivalent for ($b = 1$), regardless of the value of n. In Figures (2), (3) and (4), strain-hardening relaxation is shown to be an altogether slower process. Further, the lower the value of the parameter b, the greater the difference between strain- and time-hardening relaxation. The

influence of the parameter n in strain-hardening relaxation is more complex: for strain-hardening $\chi(t)$ values greater than about 0.5, the greater the value of n, the slower the process whereas for $\chi(t) < 0.5$, the higher n values lead to an accelerated relaxation.

Based on Figures (1) to (4), it can be said that:

i) the time-hardening formulation yields an upper-bound to the relaxation process occurring in a strain-hardening material,

ii) relaxation testing has the potential of differentiating between time- and strain-hardening creep.

Hyperbolic And Exponential Relaxation

For various materials, the hyperbolic sine creep law has been shown to depict more faithfully the dependence of creep strain-rate on stress:

$$\dot{\varepsilon}^c = K''(\text{sh}\,\sigma)^n f(t) \tag{39}$$

where K" is a constant and f(t), an appropriate time function. Then, from eqs. (6) and (7), hyperbolic relaxation is characterized by

$$K''(\text{sh}\,\sigma)^n f(t) + \dot{\sigma}/E = 0 \tag{40}$$

or

$$\int \frac{d\sigma}{(\text{sh}\,\sigma)^n} = -EK'' \int f(t)dt + C_3 \tag{41}$$

with C_3 as the integration constant. Denoting

$$t^* = EK'' \int f(t)\,dt \tag{42}$$

and considering eqs. (11) and (13), we find in particular, for hyperbolic relaxation, (Gradshteyn and Ryzhik (1965))

n = 1:

$$\chi(t) = \frac{2}{\sigma_o} \operatorname{argth}\left[\frac{\operatorname{th}\left(\frac{\sigma_o}{2}\right)}{\exp(t^*)}\right] \tag{43}$$

n = 2:

$$\chi(t) = \frac{1}{\sigma_o} \operatorname{argth}\left[\left(t^* + \operatorname{cth}(\sigma_o)^{-2}\right)\right] \tag{44}$$

n = 3:

$$\frac{\operatorname{ch}(\sigma)}{2\operatorname{sh}^2(\sigma)} + \frac{1}{2}\ln \operatorname{th}\left(\frac{\sigma}{2}\right) = t^* + \frac{\operatorname{ch}(\sigma_o)}{2\operatorname{sh}^2(\sigma_o)} + \frac{1}{2}\ln\left(\operatorname{th}\left(\frac{\sigma_o}{2}\right)\right) \tag{45}$$

n = 4:

$$\operatorname{cth}(\sigma) - \frac{1}{3}\operatorname{cth}^3(\sigma) = -t^* + \operatorname{cth}(\sigma_o) - \frac{1}{3}\operatorname{cth}^3(\sigma_o) \tag{46}$$

n = 5:

$$\frac{-\operatorname{ch}(\sigma)}{4\operatorname{sh}^4(\sigma)} + \frac{3}{8}\frac{\operatorname{ch}(\sigma)}{\operatorname{sh}^2(\sigma)} + \frac{3}{8}\ln\left(\operatorname{th}\left(\frac{\sigma}{2}\right)\right) = -t^* - \frac{\operatorname{ch}(\sigma_o)}{4\operatorname{sh}^4(\sigma_o)} + \frac{3}{8}\frac{\operatorname{ch}(\sigma_o)}{\operatorname{sh}^2(\sigma_o)} + \frac{3}{8}\ln\left(\operatorname{th}\left(\frac{\sigma_o}{2}\right)\right) \tag{47}$$

For $(n \geq 3)$ the complexity of the solutions increases and the quantity $\chi(t)$ must be extracted numerically. In lieu of this approach, alternate solutions can be found by taking eq. (39) to limiting levels of stress σ.

For higher stress levels $(\sigma > \sigma^H)$ where σ^H remains to be defined, eq. (39) reduces to the exponential form

$$\dot{\varepsilon}^c = K' \exp(n\sigma) f(t) \tag{48}$$

with

$$K' = K''/2^n. \tag{49}$$

From eqs. (6) and (7), exponential relaxation is then given as

$$K' \exp(n\sigma)\, f(t) + \dot{\sigma}/E = 0 \tag{50}$$

or, from eq. (42),

$$\int \frac{d\sigma}{\exp(n\sigma)} = -\frac{K'}{K''} t^* + C_4 \tag{51}$$

C_4 being an integration constant. Finally, combining eq. (51) with the eqs. (11) and (13) leads to the exponential relaxation solution

$$\chi(t) = \frac{-1}{n\sigma_o} \ln\left[\frac{1}{\exp(n\sigma_o)} + n\frac{K'}{K''} t^*\right] \tag{52}$$

Otherwise, for sufficiently low stress levels $(\sigma < \sigma^L)$ where σ^L is a reference value, only the linear terms of a Taylor series expansion of the hyperbolic law (39) may be required in order to arrive in effect at

$$\dot{\varepsilon}^c = K''\, \sigma^n\, f(t) \tag{53}$$

Expression (53) is essentially the power law form (3) discussed previously and hence all the elements of the time-hardening relaxation solution (eqs. (10) to (13)) apply here for $(K'' = K)$ and $(f(t) = bt^{b-1})$.

The accuracies related to approximating hyperbolic by exponential or power law relaxation are of course dependent on the limits σ^H and σ^L. In relation to the steady state creep of metals, Garofalo (1965) proposes $(\sigma^H = 1.2)$ for the exponential law and $(\sigma^L = 0.8)$ for

the power law. These limits also seem appropriate for relaxation but should be qualified as follows:

- for $\chi(t) > 0.5$, the exponential and power law approximations should perform adequately for $(\sigma_o > (\sigma^H = 1.2))$ and $(\sigma_o < (\sigma^L = 0.8))$ respectively,
- for $\chi(t) < 0.5$, the power law approximation may give the best overall performance regardless of the initial stress value σ_o due to the decaying nature of the stress associated with the phenomenon itself.

Conclusion

The relaxation solution associated with the strain-hardening form of the creep power law has been obtained and has been shown to be an altogether slower process than the relaxation due to the time-hardening form of the same power law. The relaxation for the hyperbolic and exponential creep have also been given and for the appropriate stress levels, the analytical forms for the power law and exponential relaxation may be sufficient for approximating hyperbolic relaxation.

Acknowledgements

The author, formerly research associate, Department of Civil Engineering, Ecole Polytechnique de Montreal, wishes to acknowledge Prof. B. Ladanyi under whom this work was initiated in conjunction with a research grant from the Office of Energy Research Development, Energy, Mines and Resources Canada.

References

ASTM (1979), Stress Relaxation Testing, ASTM STP 676, Alfred Fox, Ed., American Society for Testing and Materials, 216 pp.

Boyle, J.T. and Spence, J. (1983), Stress Analysis for Creep, Butterworths, 283 pp.

Findley, W.N., Lai, J.S. and Onaran, K. (1976), , Creep and Relaxation of Nonlinear Viscoelastic Materials, North-Holland Ser. in Appl. Math. and Mech., Vol. 18, North-Holland, 367 pp.

Garofalo, F. (1965), Fundamentals of Creep and Creep-Rupture in Metals, Macmillan Company, 258 pp.

Gradshteyn, I.S. and Ryzhik, I.M. (1965), Tables of Integrals, Series and Products, 4th Edition, Academic Press, 1086 pp.

Press, W.H., Flannery, B.P., Teukolsky, S.A., Wetterling, W.T., (1986), Numerical Recipes, The Art of Scientific Computing, Cambridge University Press, 818 pp.

Rabotnov, Y.N. (1969), Creep Problems in Structural Members, North-Holland Ser. in Appl. Math. and Mech., Vol. 7, North-Holland, 822 pp.

Spence, J. and Hult, J. (1973), Simple Approximations for Creep Relaxation, Int. J. Mech. Sci., Pergamon Press, Vol. 15, pp. 741-755.

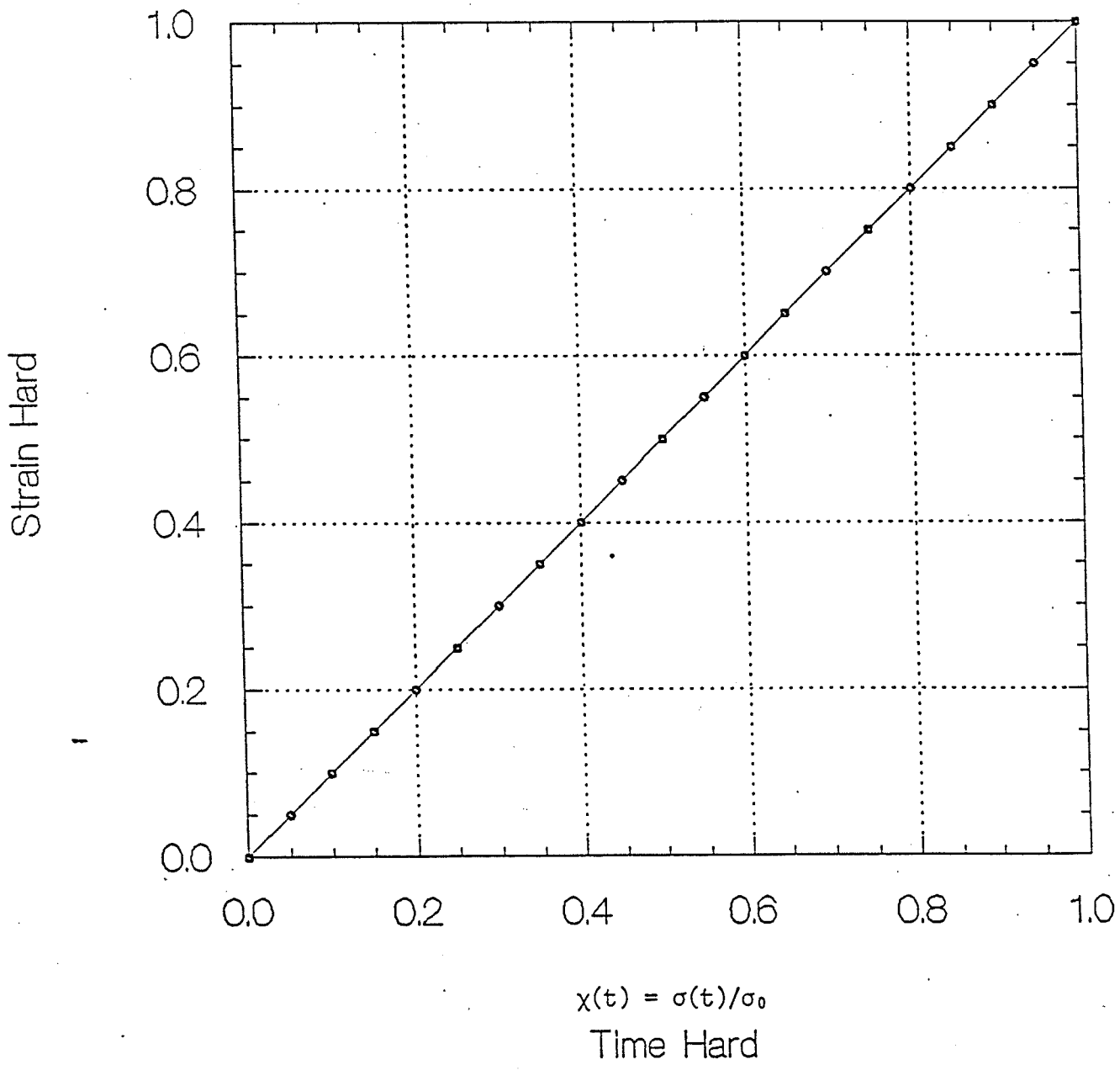

Figure 1: Time- and strain-hardening relaxation. b=1, n≥1.

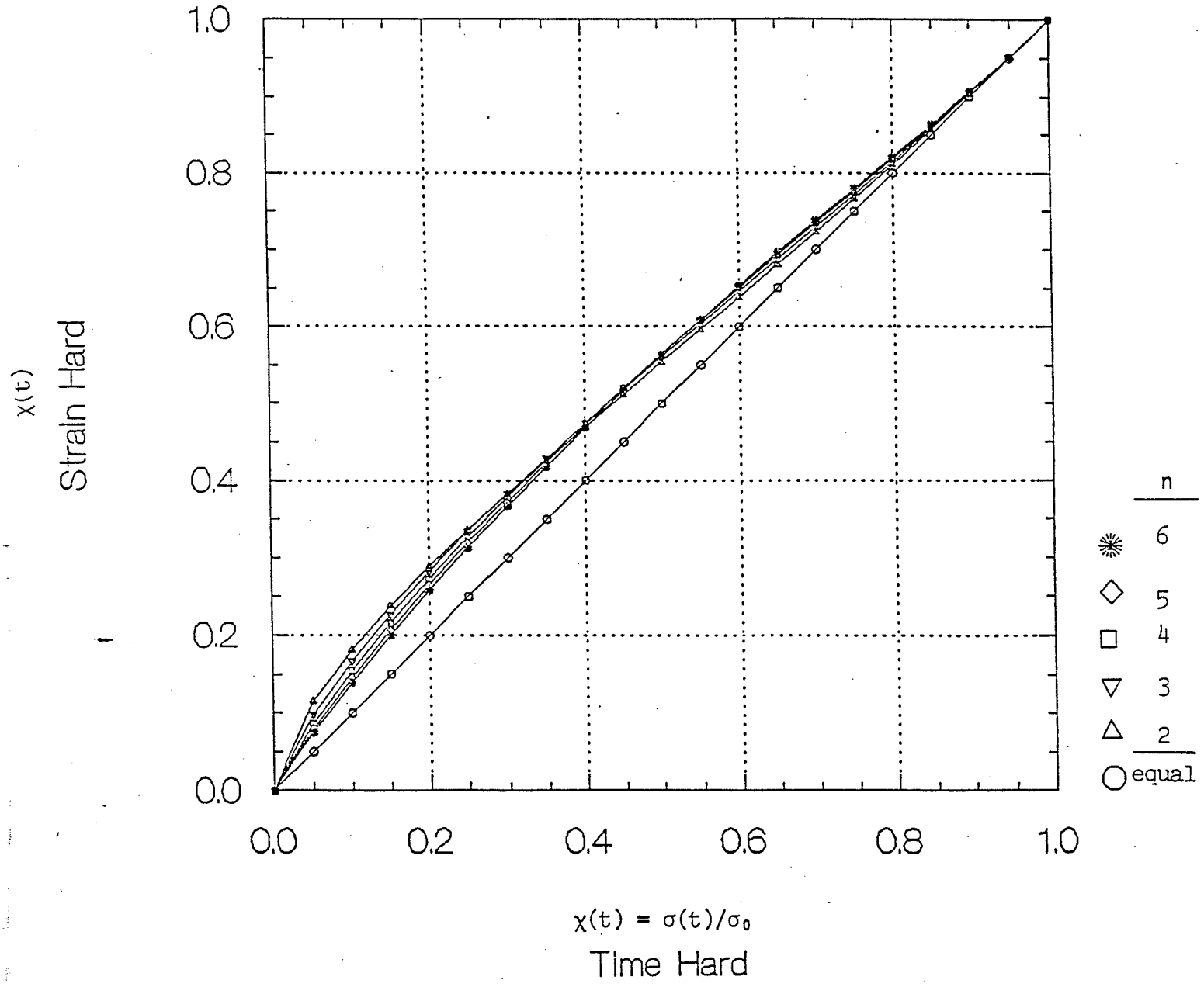

Figure 2: Time- and strain-hardening relaxation. b=1/2.

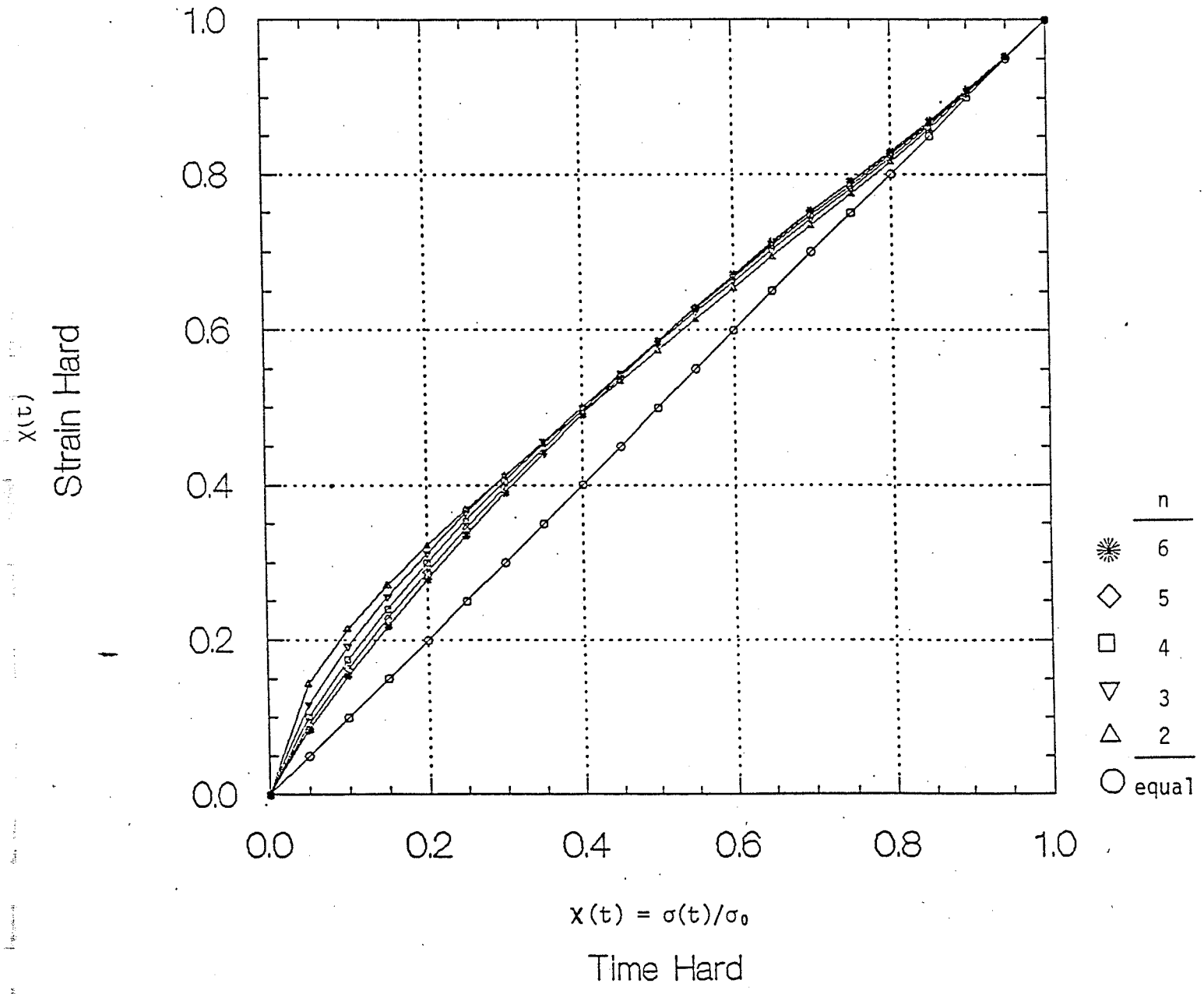

Figure 3: Time- and strain-hardening relaxation. b=1/3.

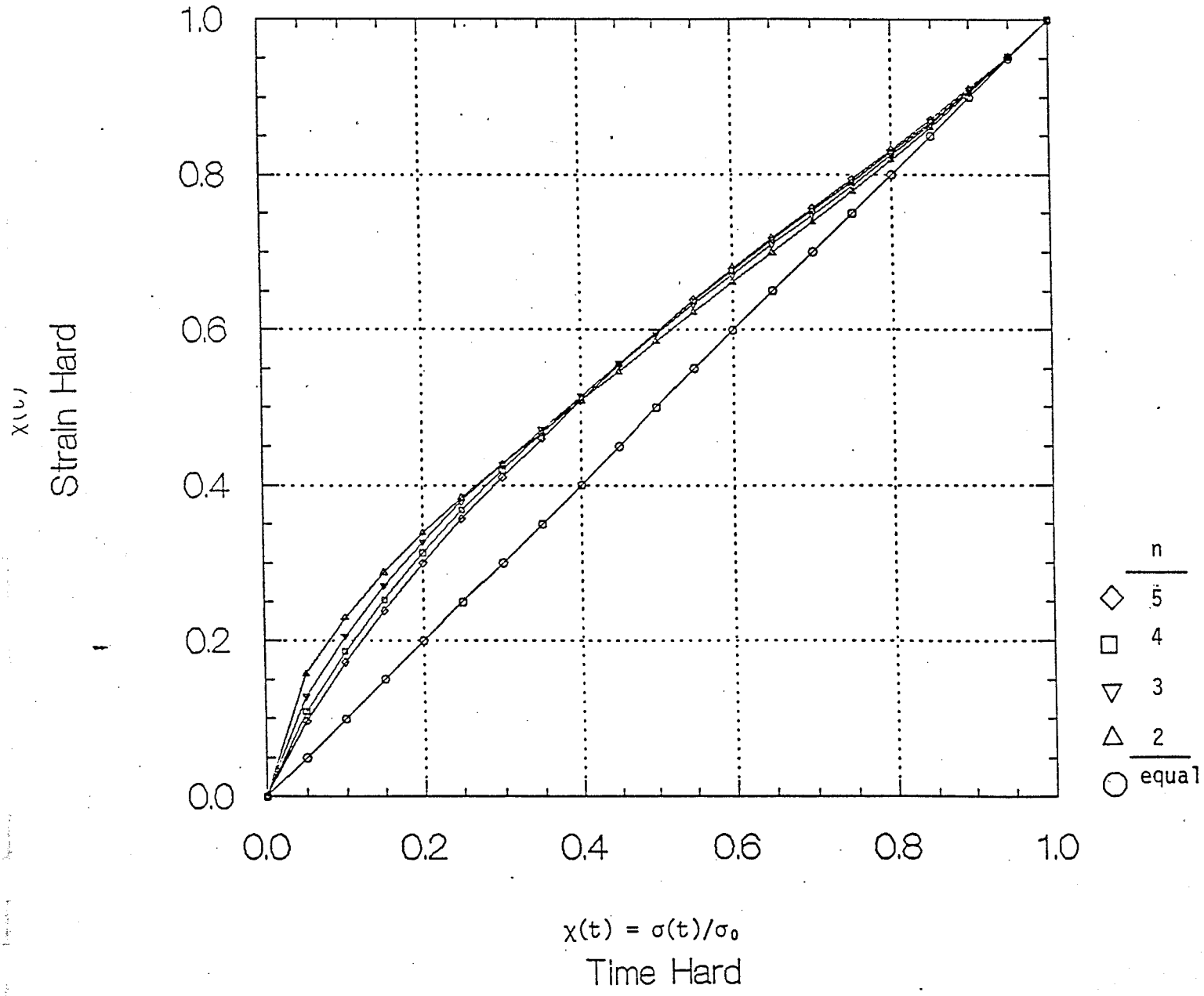

Figure 4: Time- and strain-hardening relaxation. b=1/4.

APPENDIX C

PRESSUREMETER RELAXATION TESTING IN A PERMAFROST TUNNEL

B. Ladanyi, B. Touileb and P. Huneault

1991

1991 Geotechnical Engineering Congress
Boulder, Colorado
June 9-12, 1991

PRESSUREMETER STRESS RELAXATION TESTING IN A PERMAFROST TUNNEL

B. Ladanyi*,F. ASCE, B. Touileb* and P. Huneault**

ABSTRACT: In the spring of 1988, a geotechnical testing program was carried out in the U.S. Army CRREL Permafrost Tunnel, located at Fox, near Fairbanks, Alaska. In all, some thirty cone penetrometer tests and twenty two pressuremeter tests were performed at the site. After describing the results of the load-controlled cone penetrometer tests in a previous paper (Ladanyi and Huneault, 1989), this paper covers only the results of strain-controlled pressuremeter relaxation tests and focuses on the related data processing and interpretation.

INTRODUCTION

In May of 1988, geotechnical testing was carried out over a period of two weeks in the Fox Tunnel facility excavated in permafrost and situated near the city of Fairbanks, Alaska.

Both cone penetrometer and pressuremeter tests were performed and monitored through use of a custom-designed data acquisition system. The main objectives of the tests were to obtain data for determining the various creep parameters of the frozen soil which then typically could be applied in a foundation design scheme. Very rarely have penetrometer and pressuremeter tests been carried out in parallel and in such well-controlled conditions, potentially allowing for comparisons, fundamental in nature to be undertaken. The in-situ testing also allowed fine-tuning of the experimental procedures which proved to be quite flexible, effective and cost-efficient, and of the data acquisition system, enabling practically non-stop testing over a ten day span.

The pressuremeter tests were short-term or long-term in duration. The long-term tests were either pressure controlled (creep tests) or volume controlled (relaxation tests). The cone penetrometer tests were load controlled. In all, thirty cone tests and twenty-two pressuremeter tests were performed.

* Northern Engineering Centre, Ecole Polytechnique, Montreal, Canada, Box 6079, Station A, H3C 3A7.
** Rousseau, Sauvé, Warren Inc., 500 boul. René-Lévesque W, Montréal, Canada, H2Z 1W7.

A brief report of the results of the cone penetration tests and their interpretation in terms of creep parameters of frozen soil was presented in a previous paper (Ladanyi and Huneault 1989). The present paper deals only with the pressuremeter tests, the results of which are evaluated and compared with those deduced from the cone penetrometer and some laboratory tests.

SITE DESCRIPTION AND BACKGROUND STUDIES

The Fox Tunnel Permafrost Research Station is unique to the North American continent in that it offers researchers a very well controlled and preserved natural permafrost environment. Very few other test sites similar in nature and vocation exist throughout the world. A detailed description of the site can be found in Ref. [17], [18] and [19].

The tunnel is located at a site in the town of Fox, Alaska, about 22 km North of Fairbanks, in a region of discontinuous permafrost with a normal depth of seasonal thaw of approximately 0,6m. The tunnel was originally constructed to evaluate various methods of tunneling into frozen ground, and was excavated in a near vertical 15m thick silt escarpment. Ever since, and for some twenty-five years now, the tunnel has been used as an underground laboratory for conducting experiments related to the permafrost environment. Figure 1 from [20] shows only a section of the tunnel along the inclined blind shaft ("winze"), where all the tests were made.

The tunnel passes through sections of frozen silt that are believed to have been originally deposited on the uplands by winds during the late Pleistocene or in more recent geological time. Stratification is evident as a result of included sand, gravel and in some case organic material. The silt is underlain by gold-bearing gravels. These gravels repose on bedrock, a schist, the upper portion of which is usually weathered.

Small lenses and other formations resulting from ice segregation occur in the silt, as well as more massive structures such as large ice wedges and transparent ice masses. The creep typical of permafrost is quite evident in a tunnel room where measurement poles have been twisted and deformed by creep closure. Results of in-situ creep closure measurements in the frozen silt and gravel can be found in Thompson and Sayles (1972). Analyses of laboratory unconfined uniaxial creep testing of remolded Fairbanks silt has been carried out by Thompson and Sayles (1972), Haynes (1978), Zhu and Carbee (1983) and Rein (1985) while Sayles (1985) investigated the behavior of a strip footing resting on the frozen Fairbanks silt. Huang et al. (1986) describe soil samples from the tunnel as having a 68% silt composition with a bulk unit weight ranging from 1,42 to 2,08g/cm^3 and a moisture content from 32 to 139%, leading to a dry unit weight fluctuating from 0,63 to 1,39g/cm^3, the void ratio and the porosity averaging 2,3 and 31%, respectively. The samples taken from the test location in the present study show a uniform silt without visible ice lenses with water contents varying from 96% to 130%, and dry density of less than 1g/cm^3.

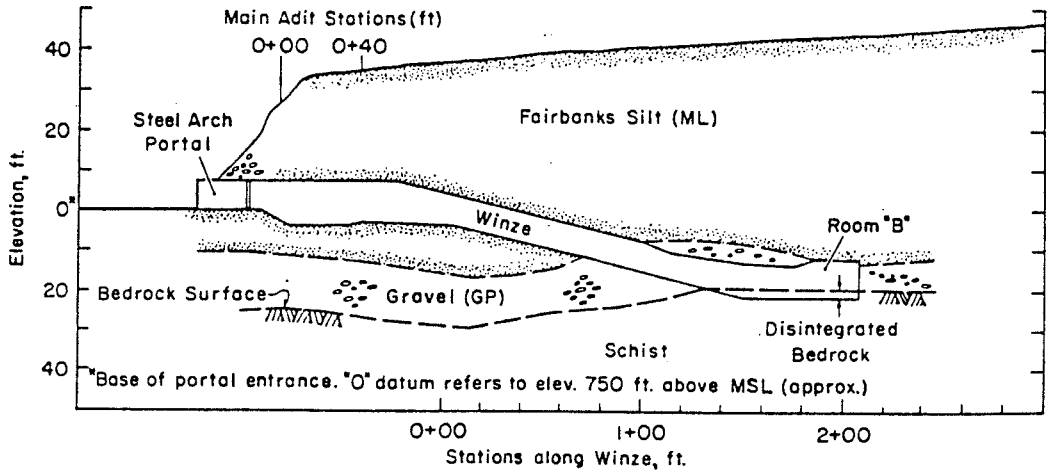

Fig. 1. The US Army CRREL Permafrost Tunnel (after Thompson and Sayles, 1972)

From thermocouple readings, the air temperature at the test site was -1,5°C ± 0,5°C whereas frozen silt temperature, 1m deep into the winze wall, was -2,3°C + 0,5°C.

TEST SET-UP AND PROCEDURE

The pressuremeter used in this investigation was the TEXAM mono-cell pressuremeter equiped with an NX-type probe. It consists of a pressure-volume control unit connected to the probe by a reinforced plastic tubing. The system has a volumetric capacity of 1200 cm^3, whereas admissible pressures range from 0 to 10 MPa.

The probe consists of a steel cylindrical core over which a rubber membrane sleeve is fitted. The membrane is protected by an extensible jacket made of overlapping metal strips. The assembly is made leakproof by 0 rings and plastic vulcolan collars which are held in place by two end nuts. The probe has a deflated diameter of approximately 7 cm and an active length of 45 cm. In a tight borehole the pressuremeter can increase the borehole radius r_o by $\Delta r/r_o$ = 40%.

For low-temperature testing, a mixture of ethylene-glycol and water for filling the probe and the hydraulic circuits is normally used.

The standard control unit has been supplemented by a pressure transducer (Data Instruments model AB-5000 psi), along with a 150 mm total stroke displacement transducer (Hewlett-Packard model 7-DCDT) for monitoring the pressuremeter piston head displacement and thus the volume of fluid injected (Note: 25.4 mm of displacement corresponds to 193 cm^3 of injected fluid).

A specially designed auger of the same diameter as that of the deflated probe and approximately 1 m in length produced boreholes with

smooth-surface walls. All the boreholes were drilled horizontally about 1.5 m into the wall of the winze.

After insertion of the probe into the borehole, fluid was injected until initial contact between the probe and the borehole wall was made. Then, depending on the nature of the test, either the pressure applied by the probe or its volume were controlled until the completion of the test. It is noted that all calibrations and volume/pressure corrections were made following the procedure described in [11].

Short-Term Tests

Pressure-controlled tests in which the pressure was applied from a compressed nitrogen gas bottle were carried out by maintaining a constant pressure over a two minute period and recording the corresponding probe volumes after the intervals of one and two minutes. Volume-controlled tests were performed by rapidly injecting a given volume of fluid and then maintaining that given volume over a two minute span. Similarly, the corresponding pressures were recorded after one and two minutes.

Creep Tests

Four stage-loaded creep tests were performed in one borehole by applying a specific pressure loading which was then maintained mostly constant with time. The expansion of the borehole due to creep can thus be associated in time with the pressuremeter probe volume recordings.

However, as membrane inertia increases slightly with the probe expansion, the true applied pressure decreases in fact slightly with time for each test.

Becauce of lack of space, the results of pressure-controlled tests, including the creep tests will not be shown in this paper but the following discussion will be limited to strain-controlled tests, and in particular the stress-relaxation tests.

RESULTS OF SHORT TERM TESTS

In most of short-term strain-controlled tests, the straining consisted in injecting into the probe an amount of 19.3 cm^3 of fluid every 2 min and taking the readings at 1 and 2 min. This corresponds to a shear strain rate of about 0.005 min^{-1}. After processing the results of four of such tests using the conventional method, described, e.g. in [9] and [10], the following typical results were found from 2 min. pressuremeter curves.

The shear modulus G, calculated by the conventional method from the tangents at the origin of pressuremeter or stress-strain curves, varied from 17 to 20 MPa.

The peak uniaxial strength, q_a, and the corresponding failure strain, ϵ_{1a}, where "a" stands for "axial symmetry" were obtained from

the calculated plane-strain stress-strain curves by using the transformation formulas:

$$q_a = (\sqrt{3}/2)\, q_{ps} \quad (1)$$

$$\epsilon_{1a} = \gamma_{ps}/\sqrt{3} \quad (2)$$

where "ps" stands for plane strain.

The values obtained in such a manner were:

$1.13 < q_a < 1.65$ MPa

$0.04 < \epsilon_{1a} < 0.05$

In particular, the test PRF6, which included the five relaxation tests described later, gave the following data:

$G_a = 17.8$ MPa, $q_a = 1.65$ MPa and $\epsilon_{1a} = 5\%$.

RELAXATION TESTS

Compared with the pressuremeter creep test, the pressuremeter relaxation test has a double advantage. First, from a practical point of view, in a relaxation test it is the strain which is controlled, while the stress variation is observed, so that the length of test time is not limited by the volume capacity of the cell, as in a pressuremeter creep test. The second advantage is related to the test interpretation. It is now generally recognized that a borehole creep test in a non-linear visco-elastic material cannot be properly interpreted without taking into account the effect of stress redistribution after each load application [6], [13]. On the other hand, in the interpretation of the borehole relaxation test, which is in fact a stress-redistribution test, this effect is taken into account normally by the underlying theory [3], [4], [7].

It is clear that the performance of pressuremeter relaxation tests requires the use of a rigid loading system, which keeps the strain level constant during each relaxation stage. The rigidity of the TEXAM cell system, measured by Murat & Lemoigne [11], fig. 18) corresponds to about 6.5 cm^3/MPa, which makes less than 1% of the volume injected at each stage and kept constant during a stress relaxation range of about 1 MPa.

RELAXATION TEST RESULTS

In all, ten relaxation tests were performed by maintaining constant at each stage a specific probe expansion, granted through fluid injection, all the while recording the decrease in probe pressure with time. The latter follows from the negative elastic strain-rates compensating for the positive creep strain-rates acting at the borehole wall in order to maintain total radial strain-rate constant and equal to zero over time.

Because of space limitations, only the results of the last five relaxation tests (R6 to R10) will be shown in the following.

Relaxation tests R6 to R10 were carried out in the same borehole RF6 and were stage-volume-incremented in steps of approximately 77 cm^3. Pressure relaxation was registered over a thirty minute period before application of the next positive volume increment, until finally test R10 was allowed to run for 21 hours before completion.

In order to illustrate the whole process of stage-strained relaxation tests, three figures are shown: Figure 2 presents for the test PRF6 several isochronous pressuremeter curves in the usual Menard plot, with the indicated levels of the five performed relaxation tests. The isochronous curves shown are those for 30 sec., and 1, 2 and 30 min. Among these, only the 2 min. curve was used for calculating the plane-strain stress-strain curve shown in Fig. 3.

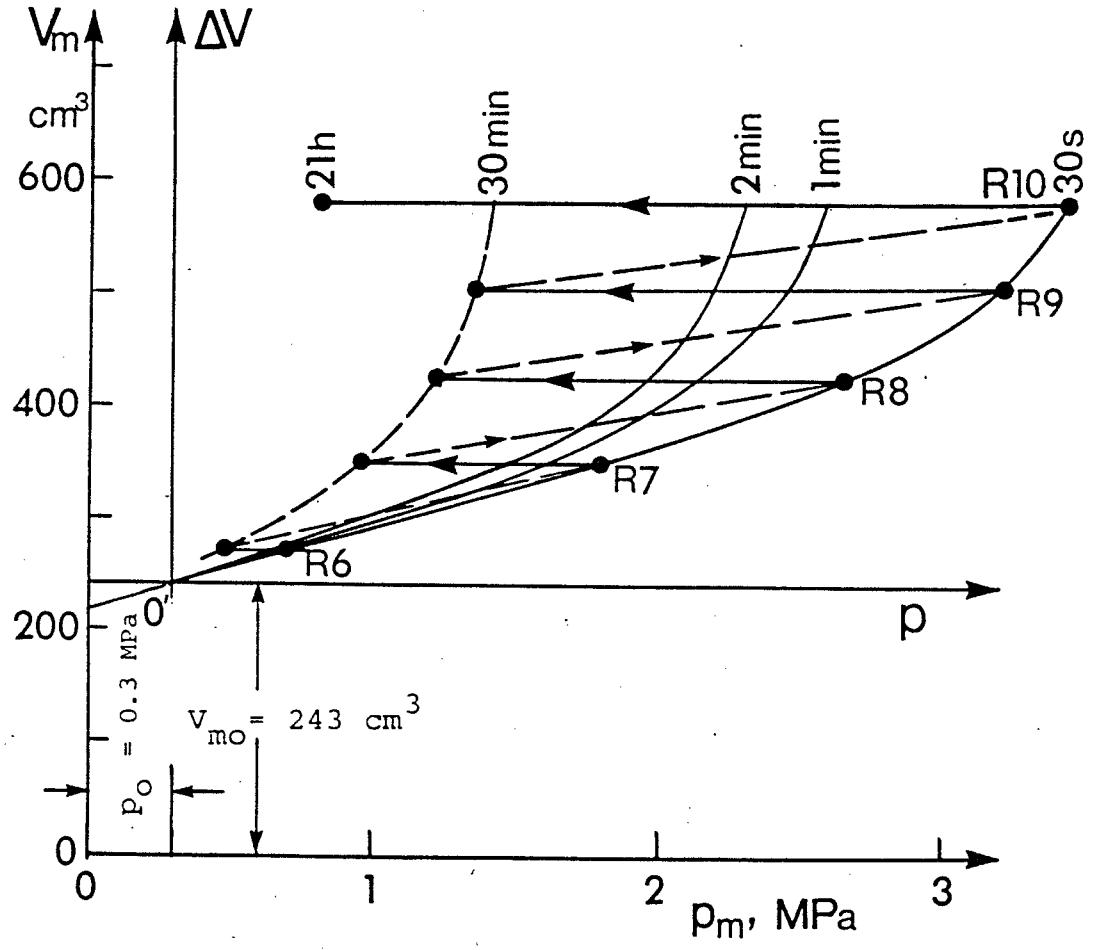

Fig. 2. Test PRF6: Isochronous pressuremeter curves and the levels of relaxation tests R6 to R10.

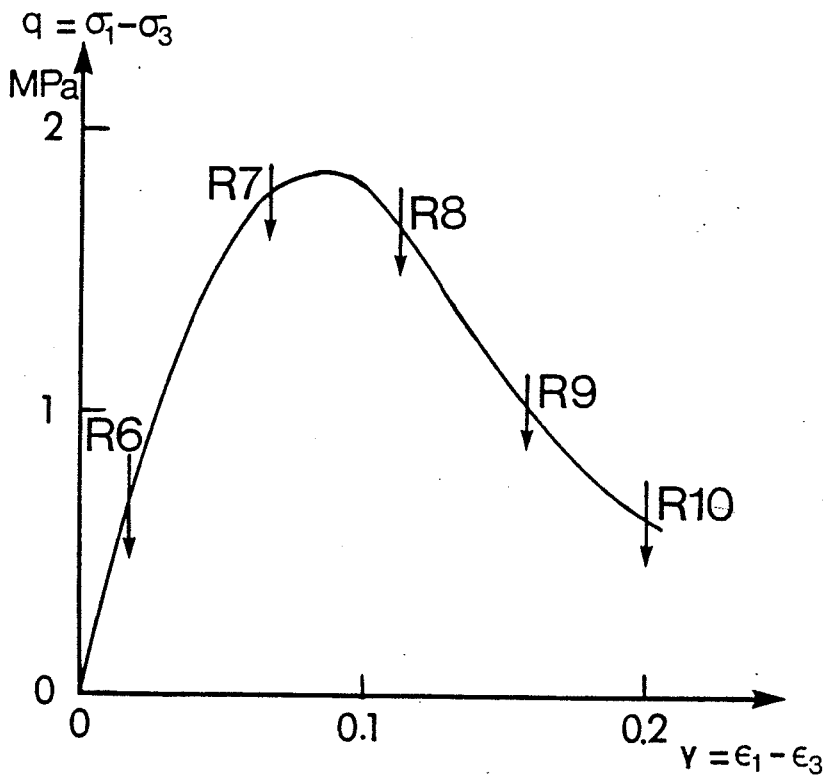

Fig. 3. Test PRF6: Plane-strain stress-strain curve from 2-min readings, with relaxation tests levels indicated.

Finally, Fig. 4 shows the five relaxation curves in log-log plot, relating the corrected pressure with time. They are seen to be remarkably regular straight lines, even up to 21 h for the last stage.

RELAXATION DATA INTERPRETATION

Although an advanced method of relaxation data interpretation exists, as described in [3] and [7], it has been found that the approximate method, described in [4] is usually quite sufficiently accurate for practical purposes. This method assumes that the basic creep equation of frozen soil is of a power-law type which for a constant stress has the following form

$$\epsilon_e^{(c)} = (\dot{\epsilon}_c/b)^b (\sigma_e/\sigma_c)^n t^b \qquad (3)$$

where (c) stands for "creep", and the subscript "e" denotes the von Mises equivalent stress and strain. The experimental parameters in this equation to be determined by the tests are the exponents b and n, and the creep modulus σ_e which corresponds to an arbitrary strain rate $\dot{\epsilon}_c$. According to the aging theory of creep and using an approximate method

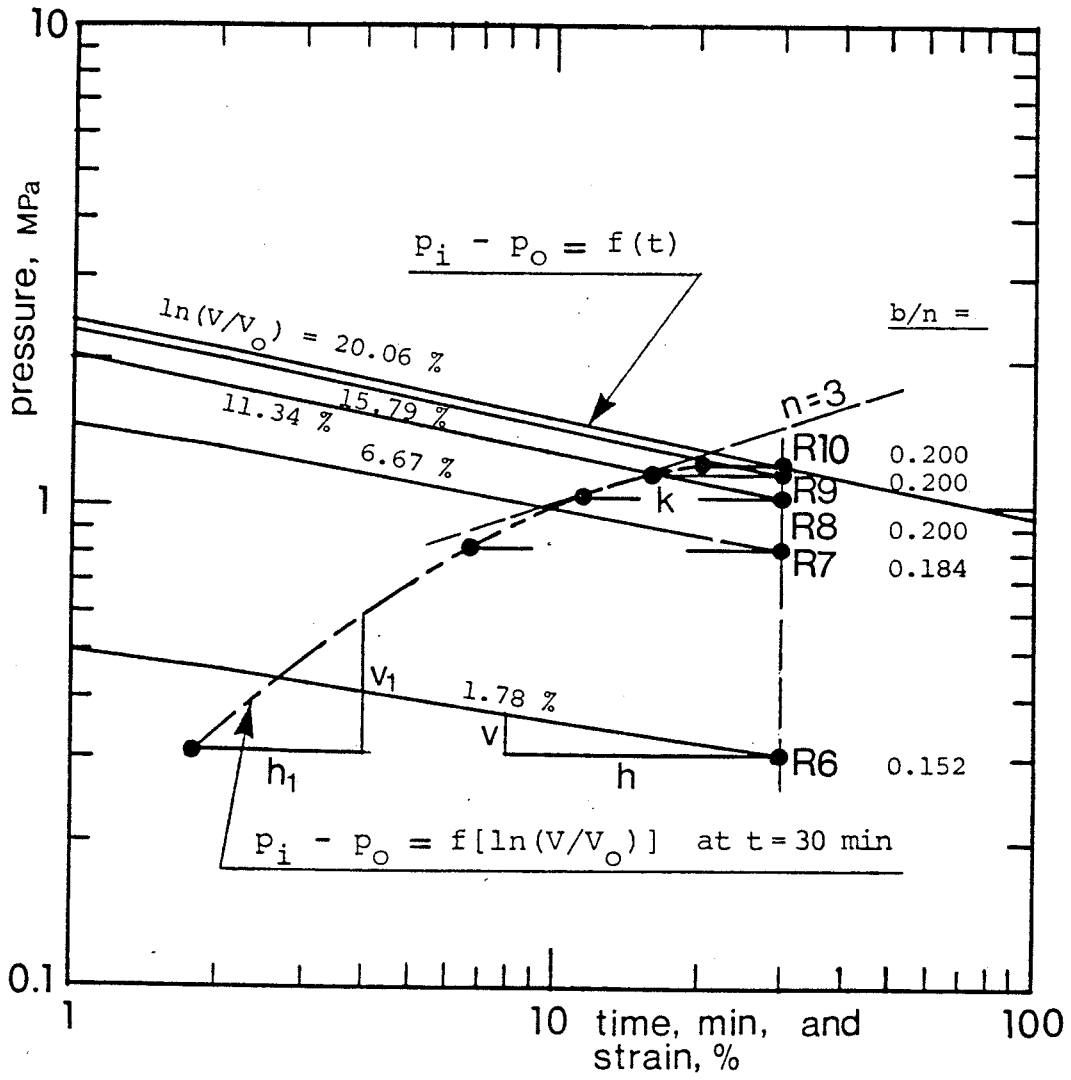

Fig. 4. Pressure relaxation curves for stage-strained tests R6 to R10, made in PRF6.

described by Rabotnov [14], a family of borehole relaxation curves can approximately be represented by the equation [4]:

$$(p_i - p_o) = \sigma_c \left[\ln(V/V_o)/M(t' + t)^b\right]^{1/n} \qquad (4)$$

where $(p_i - p_o)$ is the relaxing net pressure in the cavity, $\ln(V/V_o)$ is the shear strain, resulting from the cavity expansion from V_o to V, t', is a very short time interval during which the response of the soil is taken to be non-linear elastic (and which can be neglected for time intervals exceeding 10 to 15 min.) and M is given by

$$M = 2(\sqrt{3}/2)(\sqrt{3}/n)^n \left(\dot{\epsilon}_c/b\right)^b \qquad (5)$$

If t' is reglected, it will be seen from Eq. (4) that when such relaxation curves are plotted in a $\log(p_i - p_o)$ vs (log t) plot, as in

Fig. 4, with the strain ln (V/V_o) as the parameter, their slope gives the value of the ratio

$$b/n = - [\Delta \log(p_i - p_o)/\Delta \log t] \quad (6)$$

denoted by v/h in Fig. 4.

On the other hand, if at the same moment of the relaxation period, where $t = t_i = \text{const.}$, one plots $\log[\ln(V/V_o)]$ vs. $\log(p_i - p_o)$ (shown superimposed in Fig. 4), the slope of the line gives, theoretically, the value of n,

$$n = \Delta \log[\ln(V/V_o)]/\Delta \log(p_i - p_o) \quad (7)$$

denoted by h_1/v_1 in Fig. 4.

When b and n are known, the value of σ_c (for a selected $\dot{\epsilon}_c$) can be determined from any point k on the line $\ln(V/V_o)$ vs. $(p_i - p_o)$, by using Eq. (4):

$$\sigma_c = (p_i - p_o)_k \; [Mt_i^b/\ln(V/V_o)_k]^{1/n} \quad (8)$$

In Ladanyi (1982) it was also shown how the lateral pressure p_o could be determined from the relaxation curves. The method was used recently with success by Murat and Lemoigne [12] for determining lateral pressure variation in a sea-ice cover.

COMPUTED CREEP PARAMETERS

The relaxation curves in Fig. 4 are seen to be remarkably close to straight lines and nearly parallel to one onother, which has made it possible to determine reliable values of the b/n ratio, shown in Fig. 4. However, similarly as found in [4] for a frozen silt in Inuvik, NWT, the superimposed $\ln(V/V_o)$ vs$(p_i - p_o)$ lines show some change of slope, giving smaller n-values at low strains and larger n-values in the high strain range. This is considered to be due to the fact, clearly shown in Fig. 3, that some of the relaxation curves are in the pre-peak region, and some other in the peak- and post-peak region of the stress-strain curve. In other words, this implies that relaxations in the pre-peak region were made before the soil failed, while those in the post-peak region, were made on the soil that had already partially failed and the hole was surrounded by a plastic zone with a reduced shear strength. For this reason, it is considered appropriate to separate these two different conditions and to determine the creep parameters separately for each of them.

As a results, when tangents are drawn on the superimposed curve in Fig. 4, it is found that n varies from $n = 1.38$ at low strains, over $n = 3.0$ in the middle strain region, up to $n = 4.0$ at high strains.

Relating these n-values to the corresponding b/n ratios in Fig. 4, one gets the values of b varying from $b = 0.23$ at low strains, over

b = 0.60 in the middle region, up to b = 0.79 at high strains. It is noted that the same type of variation of the exponents b and n with strain level was found in previous studies both in frozen silt [4] and in frozen sand [5].

Taking the middle strain range to be representative, where, approximately b = 0.60 and n = 3.0, the corresponding value of σ_c can be calculated as follows:

Refering in Fig. 4 to the line R9 at t_i = 30 min, the coordinates of the point k are $(p_i - p_o)_k$ = 1183 kPa and $\ln(V/V_o)_k$ = 0.1579. Substituting these values in Eq. (8), one gets σ_c = 332 kPa for $\dot{\epsilon}_c = 10^{-5}$ min.$^{-1}$ (or σ_c = 753 kPa, for $\dot{\epsilon}_c = 10^{-5} s^{-1}$).

The creep equation (3) can now be written as

$$\epsilon_e^{(c)} = 3.716 \times 10^{-11} \sigma_e^3 t^{0.6}$$

with σ_e in kPa and t in min.

If failure occurs at axial strain $\epsilon_e = \epsilon_f$ of about 4%, as found in short-term tests, the time-dependent plane-strain uniaxial compression strength $\sigma_e = q_{u,ps}$ can be obtained by reversing Eq. (3)

$$q_{u,ps} = \sigma_c \left[\epsilon_f/(\dot{\epsilon}_c\, t/b)^b\right]^{1/n} \qquad (9)$$

giving, for plane strain,

$$q_{u,ps} = 1\,025\, t^{-2} \qquad (10)$$

and for axial symmetry case

$$q_{u,a} = (\sqrt{3}/2)\, q_{u,ps} = 887.5\, t^{-2} \qquad (11)$$

in kPa and min.

COMPARISON WITH THE DATA FOUND IN PREVIOUS TESTS

As mentioned in the introduction, the Fox Permafrost Tunnel has served for many years either as a test site for in-situ tests or for taking samples of Fairbanks silt for laboratory testing. However, to make a comparison of all published data on the creep behavior of the frozen Fairbanks silt is not an easy task, because, in varius types of field tests the test conditions differed quite substantially, while laboratory results correspond to reconstituted and refrozen samples. For that reason, only a general agreement among the determined creep parameters can be expected.

For example, comparing the results of cone penetration and pressuremeter creep or relaxation tests is always difficult, because the former records only the rate sensitivity of strength, furnishing only the values of n and σ_c in a steady-state creep equation, while the

latter yields the parameters of a primary-creep-type equation, or a time-dependent strength, containing also the time exponent b.

It is nevertheless noted that both the values of n and σ_c were similar in the two kinds of tests, with $3 < n < 4$ in the middle to high rates of strain in both tests, and with the value of σ_c of about 400 to 470 kPa in CPT tests and 750 kPa in PMT relaxation tests (with $b = 0.6$), all for $\dot{\epsilon}_c = 10^{-5} s^{-1}$.

Among some earlier investigations, it is interesting to note for comparison those by Thompson and Sayles (1972) and Haynes (1978).

Based on uniaxial compression tests on the remolded Fairbanks silt from the Fox Tunnel, carried out at - 1.7°C and at strain rates ranging from 5×10^{-7} to $8 \times 10^{-4} s^{-1}$, Thompson and Sayles (1972) found the creep parameters to be (in our notation and SI units):

$n = 4.0$ and $\sigma_c = 722$ kPa, for $\dot{\epsilon}_c = 10^{-5} s^{-1}$.

On the other hand, Haynes (1978) performed similar tests on Fairbanks silt (with bulk density of 1840 kg/m^3 and total water content of 30%) and obtained, at - 1.7°C, and at strain rates ranging from 4×10^{-3} to $4 \times 10^{-1} s^{-1}$, the creep parameters: $n = 3.06$ and $\sigma_c = 252$ kPa for $\dot{\epsilon}_c = 10^{-5} s^{-1}$.

Although all these published laboratory results on the frozen Fairbanks silt from the tunnel correspond only to remolded and reconstituted frozen samples, this comparison shown, nevertheless, that both CPT and PMT tests, as performed at the site, are able to furnish quite reasonable values of the most important creep parameters of the frozen silt, such as would be necessary for design purposes.

CONCLUSION

In the spring of 1988, two kinds of field tests were performed in the U.S. Army CRREL Permafrost Tunnel at Fox, Alaska. The first type of tests were load-controlled cone penetration tests, and the second were short- and long-term pressuremeter tests, all of them carried out in frozen silt in the wall of the tunnel, at a depth of about 15 m below the ground surface, and at a temperature of about - 2°C. After publishing the results of CPT tests in a previous paper, the present paper covers mainly the results of PMT tests, with a special reference to the stage-strained relaxation tests. It is found that, when interpreted in a conventional manner described in Ladanyi (1982), these tests yield the results comparing favorably with those deduced from CPT tests, as well as with those obtained by laboratory tests, published earlier by different authors.

REFERENCES

1. Haynes, F.D. 1978. Strength and deformation of frozen silt. Proc. 3rd Int. Permafrost Conf., Edmonton, pp. 656-661.
2. Huang, S.L., Aughenbaugh, N.B. and Wu, M.C. 1986. Stability stud of CRREL Permafrost Tunnel. J. Geotech, Eng., ASCE, 112, pp. 777-790.
3. Ladanyi, B. 1979. Borehole relaxation test as a means for determining the creep properties of ice covers. Proc. 5th POAC Conf., Trondheim, 1, pp. 757-770.
4. Ladanyi, B. 1982. Borehole creep and relaxation tests in ice-rich permafrost. Proc. 4th Canad. Permafrost Conf., Calgary, R.J.E. Brown Memorial Volume, NRCC-ACGR, Ottawa, pp. 406.415.
5. Ladanyi, B. and Eckardt, H. 1983. Dilatometer testing in thick cylinders of frozen sand. Proc. 4th Int. Conf. on Permafrost, Fairbanks, AK, Nat. Acad. Press, Washington, I, pp. 677-682.
6. Ladanyi, B. and Huneault, P. 1987a. A stress redistribution time scale for borehole creep tests in frozen soils. In "Developments in Engrg. Mechanics" (Edited by A.P.S. Selvadurai), Elsevier, Amsterdam, pp. 311-327.
7. Ladanyi, B. and Huneault, P. 1987b. Use of the borehole stress-relaxation test for determining the creep properties of ice. Proc. 6th Annual OMAE Symp., Houston TX, IV, pp. 253-259.
8. Ladanyi, B. and Huneault, 1989. Cone penetrometer tests in permafrost - The Fox Tunnel, Alaska. Proc. Int. Symp. on Mining in the Arctic, Fairbanks, AK, pp. 75-82.
9. Ladanyi, B. and Johnston, G.H. 1973. Evaluation of in situ creep properties of frozen soils with the pressuremeter. Proc. 2nd Int. Conf. on Permafrost, Yakutsk, USSR, North Amer. contr., Nat. Acad. of Sciences, Washington, pp. 310-318.
10. Ladanyi, B. and Johnston, G.H. 1978. Field investigations in frozen ground. Chap. 9 in "Geotech. Engrg. for Cold Regions (Edited by O.B. Andersland and D.M. Anderson), McGraw-Hill, pp. 459-504.
11. Murat, J.R. and Lemoigne, Y. 1988a. Improved calibration and correction techniques for pressuremeters. Geotech. Testing J., ASTM, 11, pp. 195-203.
12. Murat, J.R. and Lemoigne Y. 1988b. Study of the ice cover in Igloolik bay. Cold Regions Science and Technology, 15, pp. 239-249.
13. Murat, J.R., Ladanyi, B. and Huneault, P. 1989. In-situ determination of creep properties of sea ice with the pressuremeter. Canad. Geotech. J., 26, pp. 575-594.
14. Rabotnov, Yu. N. 1966. Creep problems in structural memebers, Transl. from Russian. North Holland Publ. Co. 1969.
15. Rein, R.G. 1985. correspondence on "Creep data and constant strain rate data for frozen silt. Cold Reg. Sci. and TEch., 11, pp. 187-194.
16. Sayles, F.H. 1985. Creep of a strip footing on ice-rich permatrost. Proc. ASCE Spring Convention, Denver, pp. 29-51.
17. Sellman, P.V. 1967. Geology of the U.S. Army CRREL Permafrost Tunnel, Fairbanks, Alaska. CRREL, Tech. Rep 199, 22 p.
18. Sellman, P.V. 1972. Geology and properties of materials exposed in the U.S. Army CRREL Permafrost Tunnel. CRREL Spec. Rep. 177, 14 p.
19. Swinzow, G.K. 1970. Permafrost tunneling by a continuous mechanical method. CRREL TEch. Rep. 221.
20. Thompson, E.G. and Sayles, F.H. 1972. In-situ creep analysis of room in frozen soil. J. Soil Mech. Found. Div., ASCE, 98, SM9, pp. 899-914.
21. Zhu, Y. and Carbee, D.L. 1983. Creep behavior of frozen silt under constant uniaxial stress. Proc. 4th Int. Conf. on Permafrost, Fairbanks, AK, pp. 1505-1512.

APPENDIX D

RESULTS OF IN SITU TESTS AT LONGYEARBYEN, SVALBARD

From the Report:

PREDICTING CREEP SETTLEMENTS FOR FOUNDATIONS IN PERMAFROST

by Branko Ladanyi, Tom Lunne and Pierre Vergobbi
1990

APPENDIX D

Permafrost Field Testing in Longyearbyen, Svalbard, August 1990

BOREHOLE SHORT-TERM AND RELAXATION TEST RESULTS

The pressuremeter used in this investigation was the TEXAM monocell pressuremeter equiped with an NX-type probe.

In the tests, all the boreholes were drilled by a compressed air drill rig, able to drill 3 inch (76 mm) diameter holes.

After insertion of the probe into the borehole, fluid was injected until initial contact between the probe and the borehole wall was established. As all the tests performed were volume (or strain) controlled, no compressed gas supply was necessary. Essentially, only two types of tests were made: Fast (or short-term) tests with equal volume injection at each stage every 2 min, and slow (or relaxation) tests in which, after an equal volume injection, the system was closed and the pressure was allowed to relax during 30 min.

In all, 7 pressuremeter tests were performed at the site at depths varying from about 3 to 5 m below the bottom of the test excavation. Of the 7 tests, 6 were successful, while the first one (SV1) had to be discarded because of the oversized and disturbed borehole. Of the remaining 6 tests, 2 were short-term tests, and 4 stage-strained relaxation tests.

Results of short-term tests

The results of short-term tests are shown in Figs. 1 to 6 and in Table 1, not only for two short-term tests, but also for the four stress relaxation tests. It is noted that all the curves and the results shown correspond to 2 min

readings. The stress-strain curves in Figs. 1 to 6 are found to have the usual shape with their peak strengths at about 5 to 7% shear strain, falling down towards the residual, which is beyond about 10% strain.

It will be seen in Table 1 that the plane-strain strength of the tested frozen soil varies between about 3 and 5 MPa, while its shear modulus is located between about 70 and 140 MPa. The tensile strength, calculated for tests SV3 and SV4, amounted to 1.63 and 2.25 MPa, respectively.

Results of borehole relaxation tests

Relaxation tests were stage-volume-incremented in steps of about 58 cm^3, in tests SV2 and SV5, and 38.6 cm^3 in tests SV6 and SV7. Pressure relaxation was registered over a 30-min period, before application of the next positive volume increment.

The results of the four stage-strained relaxation tests are shown in Figs. 7 to 10. In addition, Figs. 1, 4, 5, and 6, show the points on the stress-strain curves where each relaxation stage was made. The interpretation of relaxation tests was carried out by means of the Ging Creep Theory.

The relaxation curves in Figs. 7 to 10 are seen to be close to straight lines and nearly parallel to one another, which makes it possible to determine reliable values of the b/n ratio at the end of each 30-min relaxation stage, shown in Table 1. However, similarly as found in (2) for a frozen silt, the superimposed $\ln(V/V_o)$ vs p_i lines show some change in slope, giving smaller n-values at low strains and larger n-values in the high strain range.

This is considered to be due to the fact, clearly shown in Figs. 1, 4, 5 & 6, that some of the relaxation curves are in the pre-peak region, and some other in the peak- and post-peak region of the stress-strain curves. In other words, this implies that relaxations in the pre-peak region were made before the soil

failed, while those in the post-peak region, were made on the soil that had already partially failed and the hole was surrounded by a plastic zone with a reduced shear strength. For this reason, it was decided to separate in each test these two different conditions and to determine the creep parameters separately for each of them.

As will be seen in Table 1, for the pre-peak relaxation tests, the values of both n and b are smaller than for those in the post-peak range, with $1.01 < n < 1.35$, and $0.116 < b < 0.148$, compared to $1.64 < n < 2.75$ and $0.235 < b < 0.442$, in the post-peak range. On the other hand, the creep modulus $_c$ was found to be much higher in the pre-peak region. This means, as expected, that the frozen soil creeps less and at a slower rate when it is undisturbed than when it is disturbed by excessive deformation.

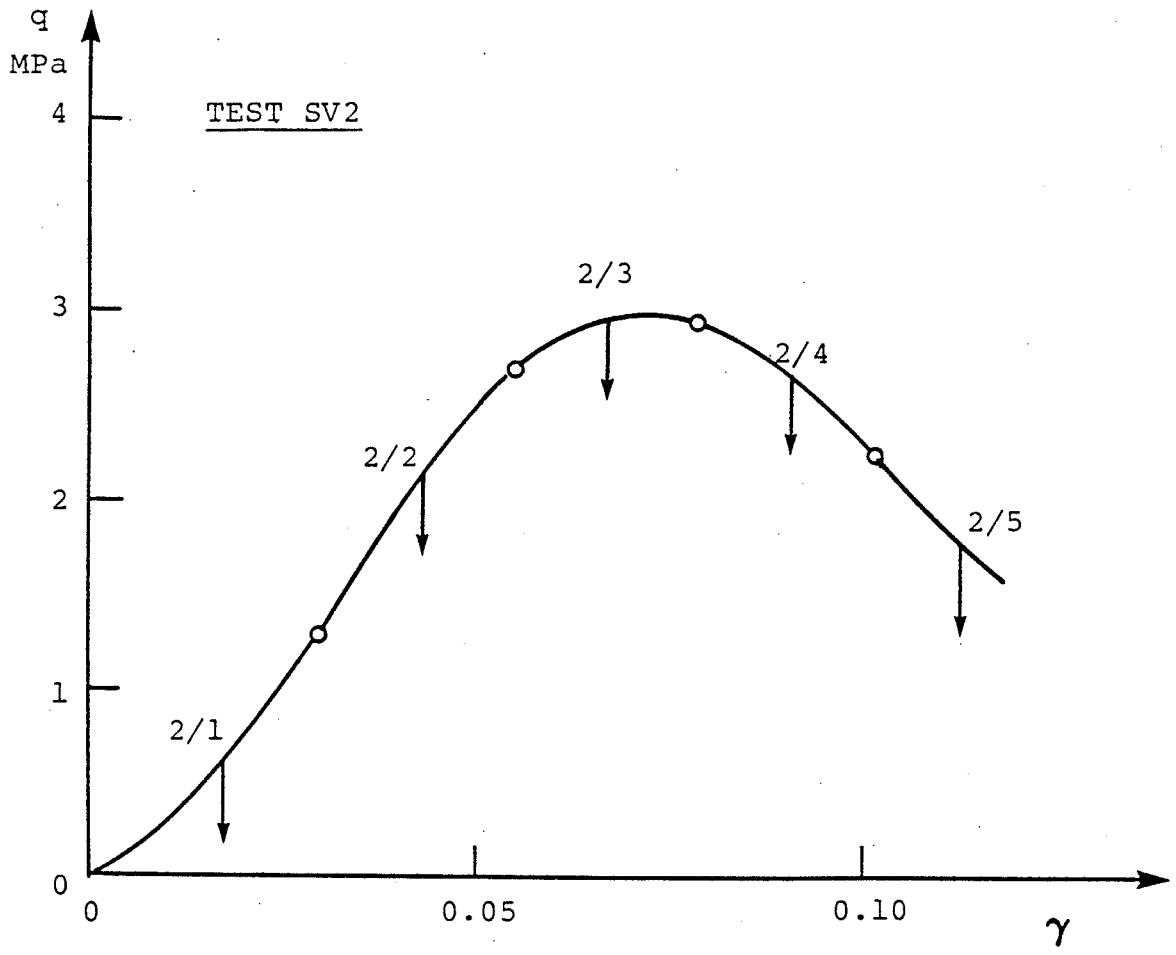

Fig.1. Stage-relaxation test SV2: 2-min stress-strain curve with relaxation stage locations indicated.

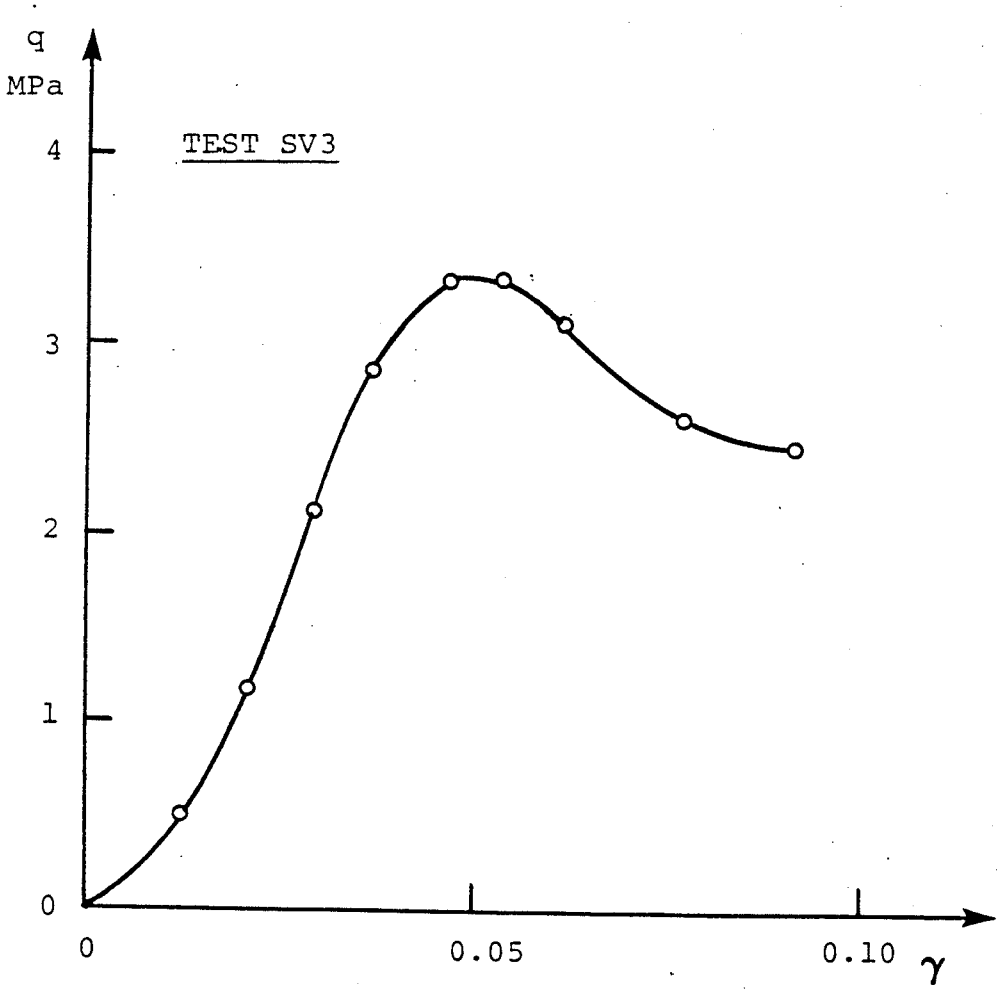

Fig.2. Short-term test SV3: 2-min stress-strain curve.

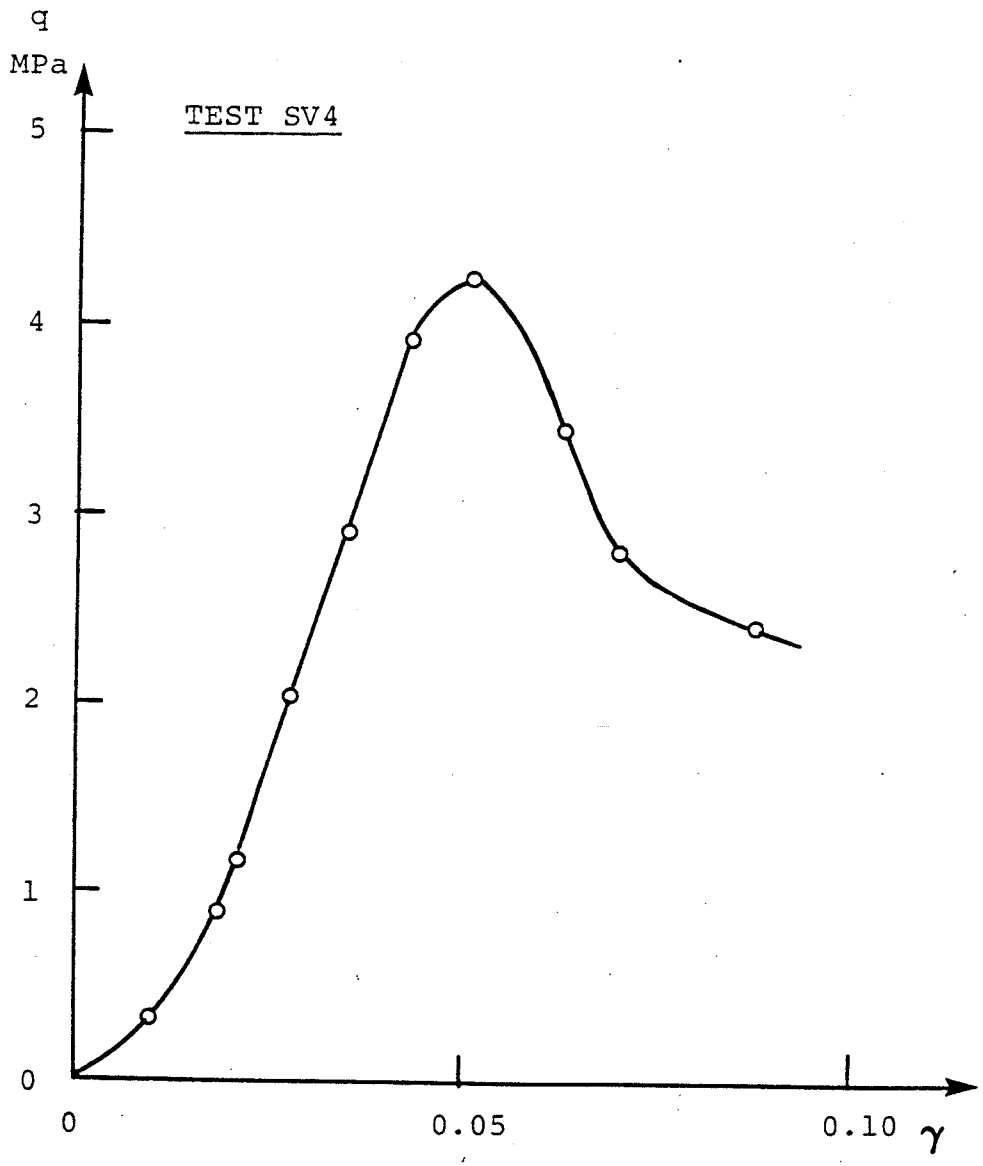

Fig.3. Short term test SV4: 2-min stress-strain curve.

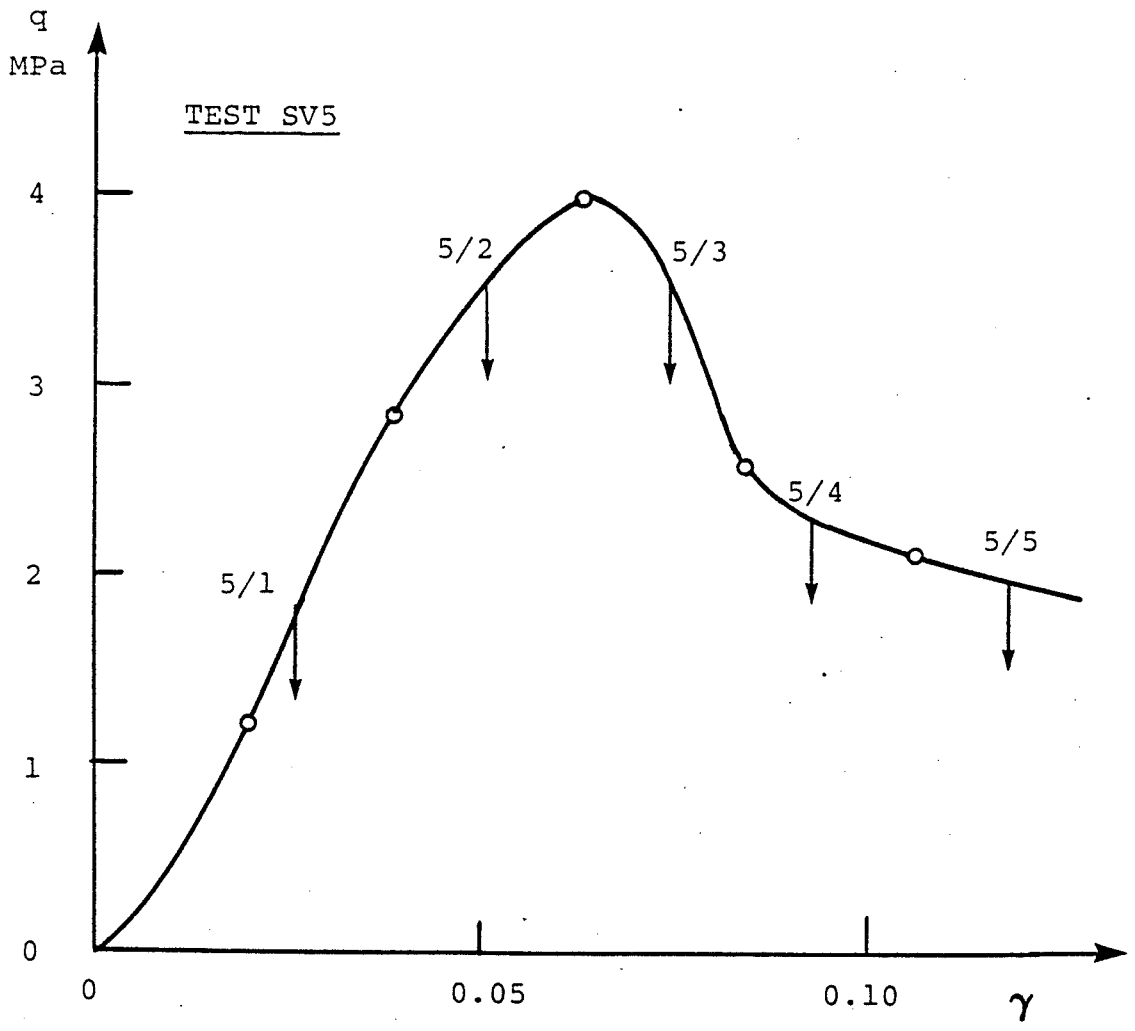

Fig.4. Stage-relaxation test SV5: 2-min stress-strain curve with relaxation stage locations indicated.

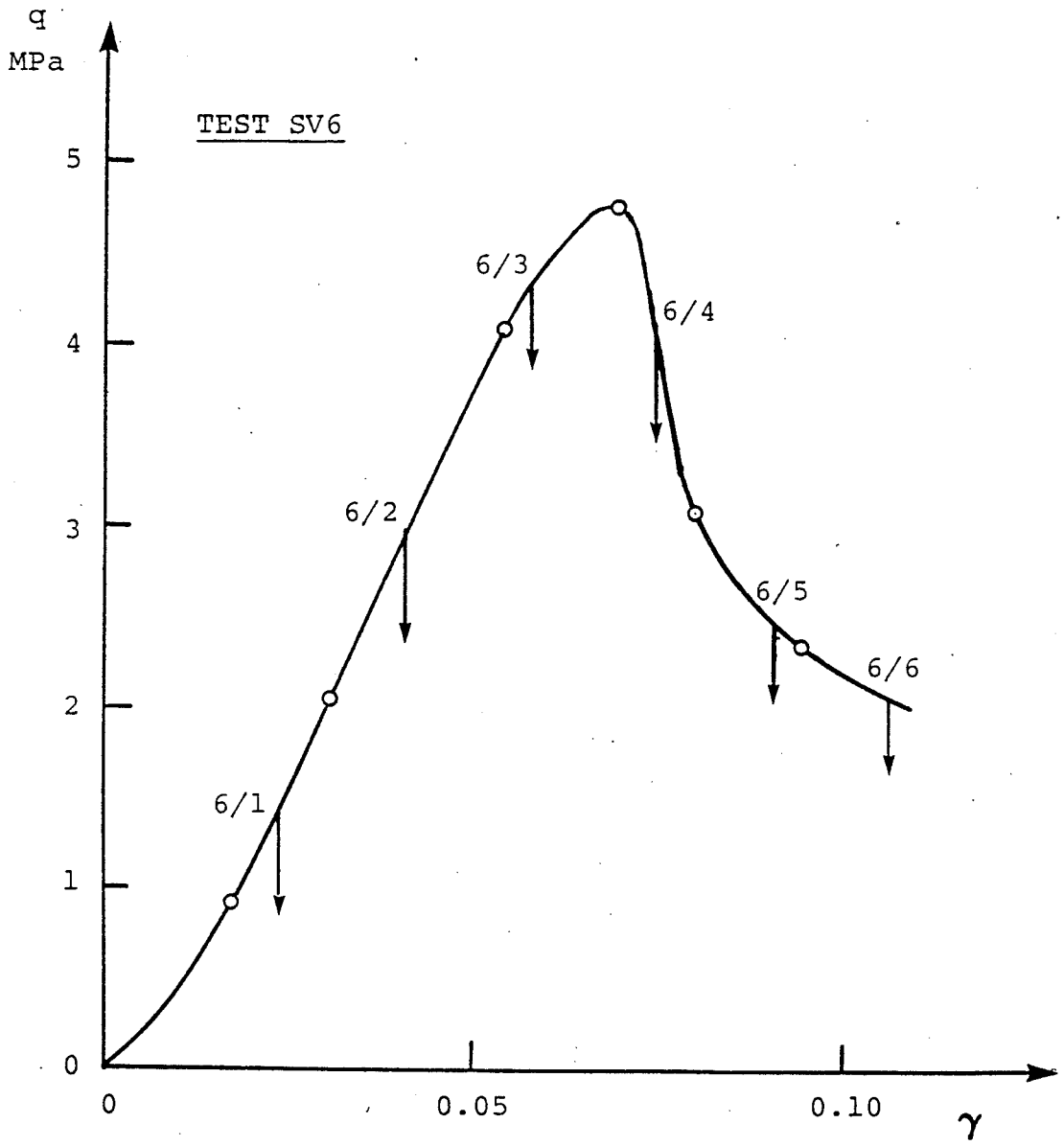

Fig.5. Stage-relaxation test SV6: 2-min stress-strain curve with relaxation stage locations indicated.

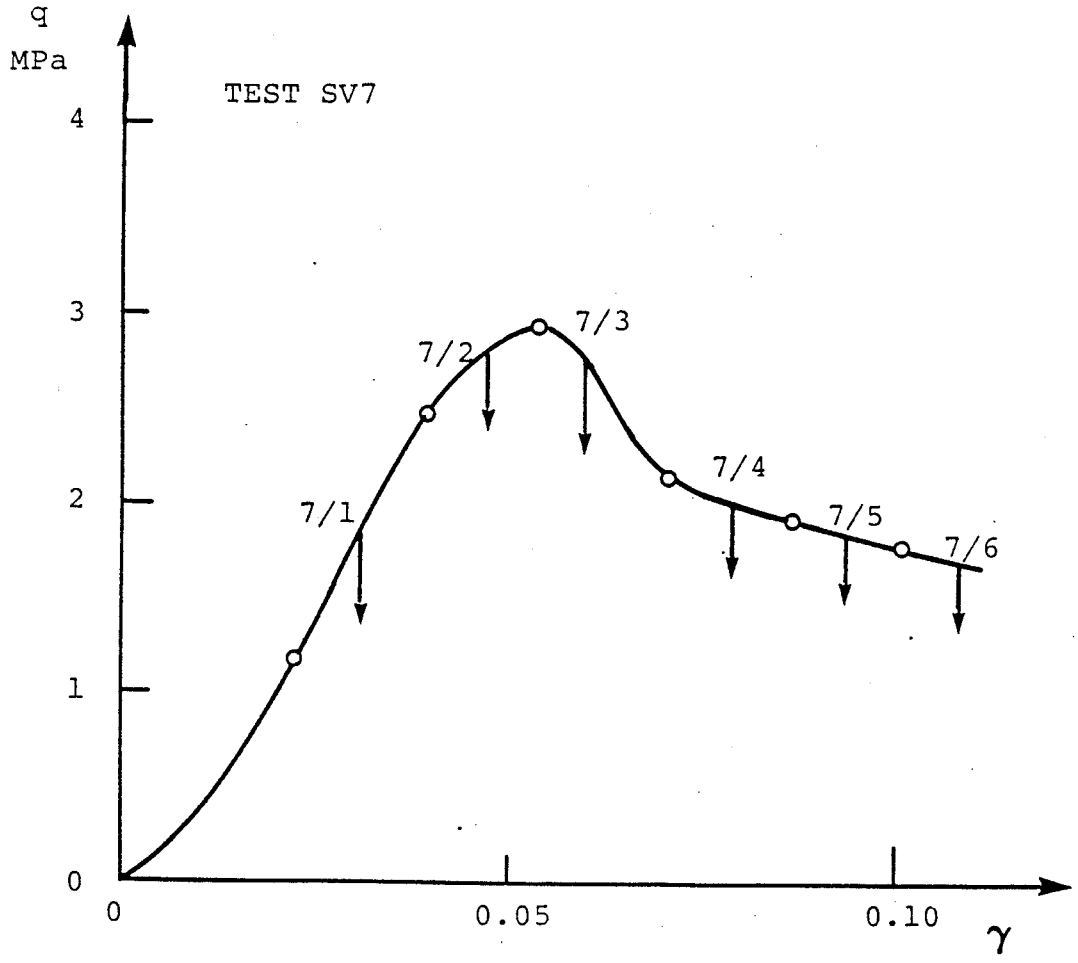

Fig.6. Stage-relaxation test SV7: 2-min stress-strain curve with relaxation stage locations indicated.

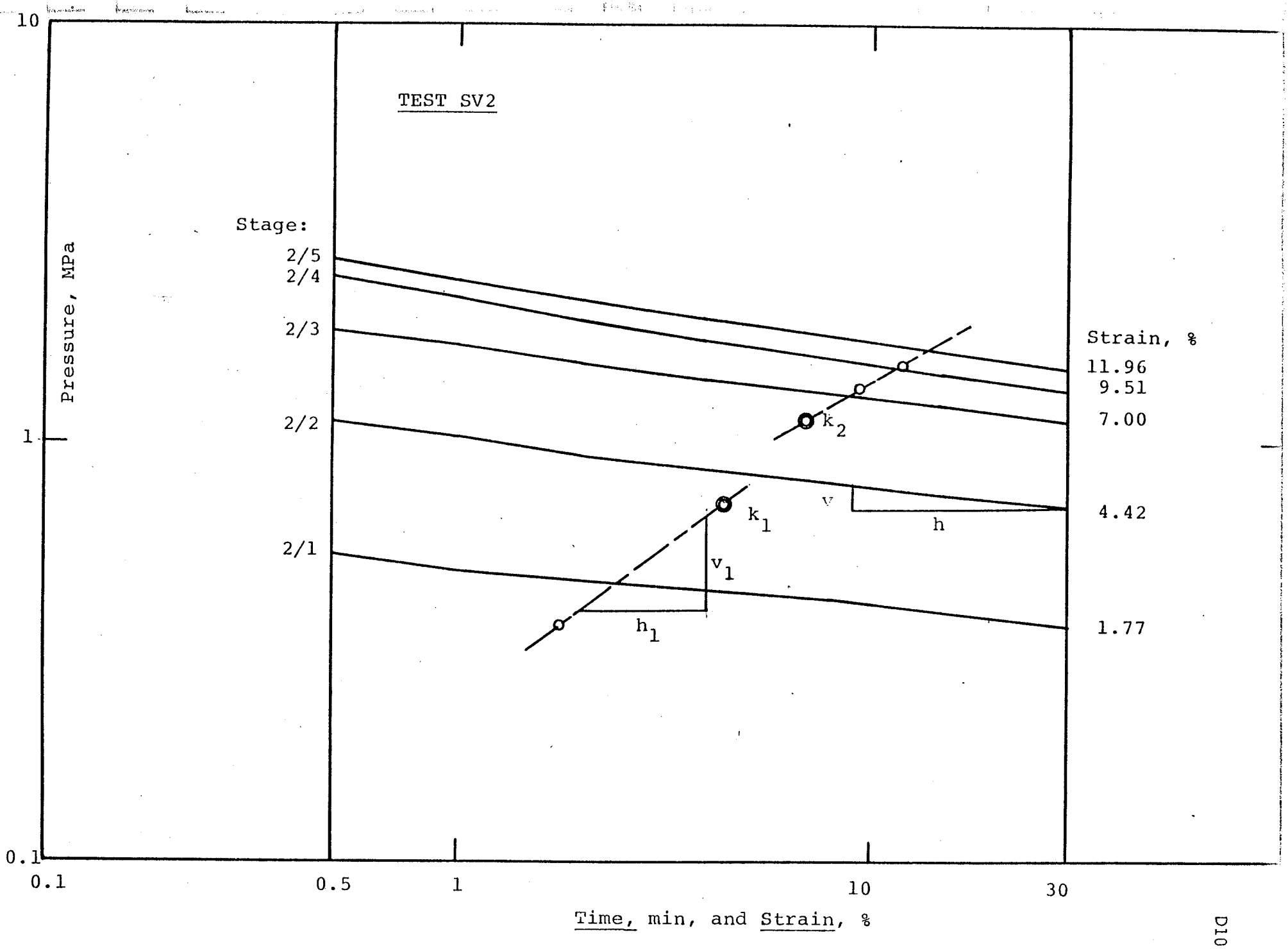

Fig.7. Test SV2: Relaxation curves.

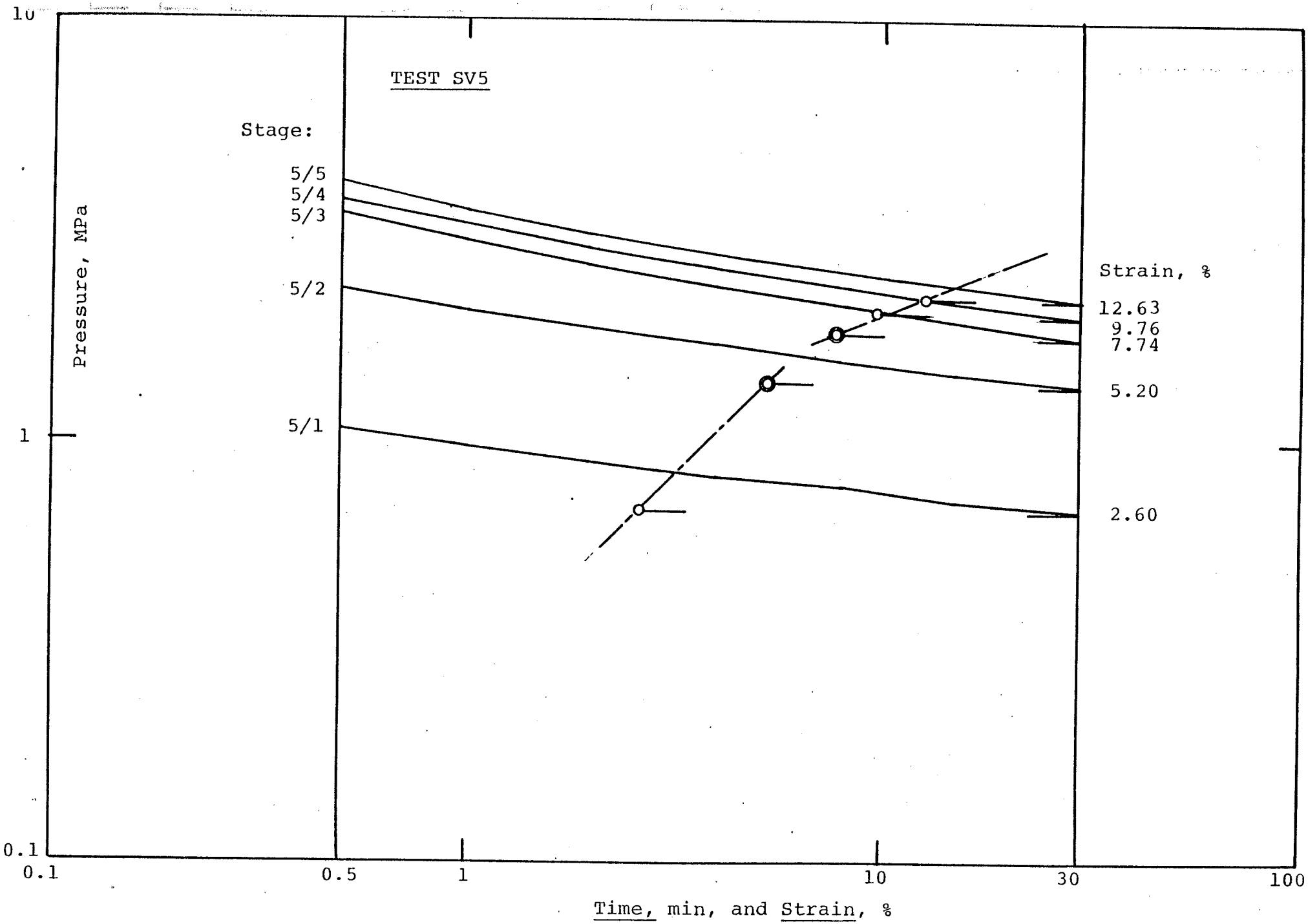

Fig.8. Test SV5: Relaxation curves.

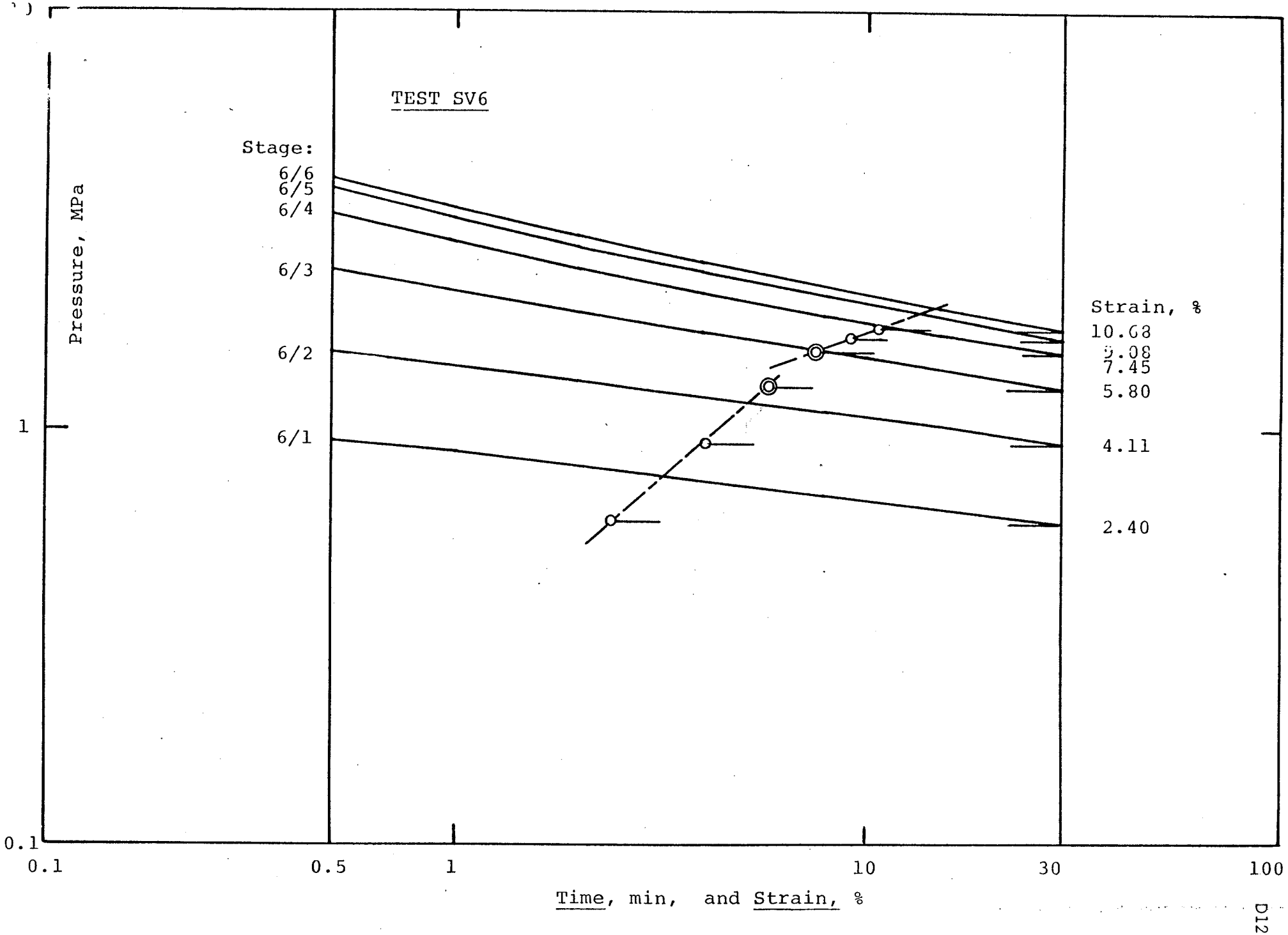

Fig.9. Test SV6: Relaxation curves.

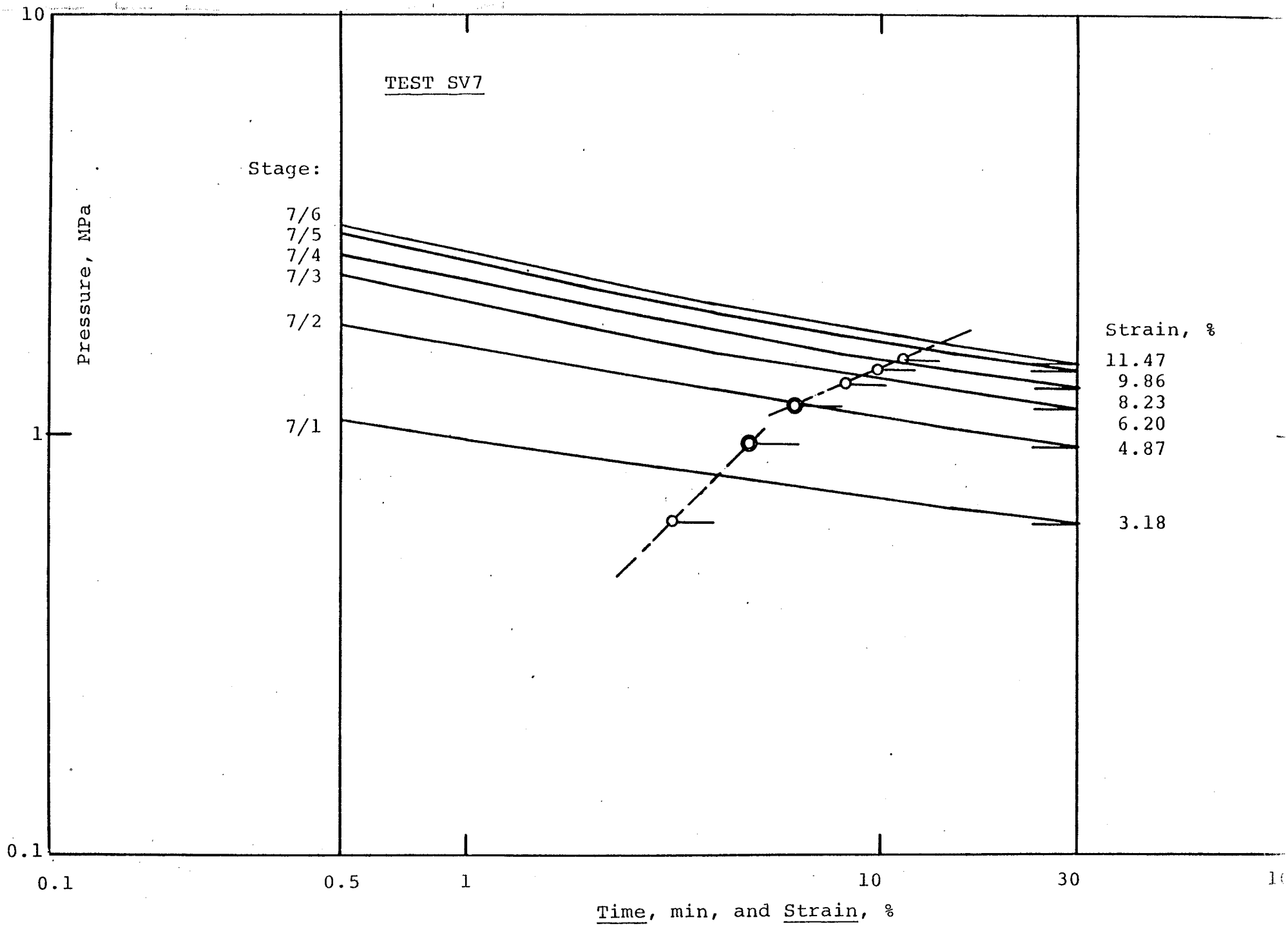

Fig.10. Test SV7: Relaxation curves.